Plasma controlled surface texturing of silver foils

Colin John Campbell

PLASMA CONTROLLED SURFACE TEXTURING OF SILVER FOILS

Colin John Campbell

Ph.D Thesis

Department of Chemistry

University of Durham

May 1999

This work is dedicated to John, Elspeth, Derek and Sarah

DECLARATION

STATEMENT OF COPYRIGHT

The work described in this thesis was carried out at the Department of Chemistry (University of Durham), between October 1993 and September 1996. It is the original work of the author unless otherwise stated or referenced.

ACKNOWLEDGEMENTS

I would like to take this opportunity to thank both my supervisors, Professor Jas Pal Badyal and Dr. Arthur Banister, for their help and enthusiasm throughout my studies.

Dr. Zdenek Hauptman, who initially started the work of this project, and designed the initial plasma reactor (even though it had to be eventually scaled down to accommodate a simple Scot).

To all the folk who I have worked with in labs 98 and 100, in particular I would like to thank Jonathan "whiiiiya" Crowther (for all his help throughout the year), Alison "I'm bored" Moyes, Christos "the dirty Greek" Spanos, Alan "Sugar" Hynes, Owen "take it easy" Dawe, and finally Iain "the cat" May.

This thesis would not have been possible if it had not been for the assistance of the technical staff who support the University, in particular Jim, Neil and Mel from the mechanical workshop, Barry, Kelvin and George in the electrical workshop, Elizabeth and Glynn who helped develop the SEM photographs and finally to Ray and Gordon for mending numerous bits of glassware. To all I would like to thank gratefully

I would also like to thank Ken Durose and Christian Lehman for all their help with the SEM and Powder diffraction machines.

Finally a very special thanks must go to my parents who helped in so many ways while at Durham, I will be eternally grateful, and also to Sarah who has been so patient and supporting throughout the grudge process of writing up, I will always remember this.

ABSTRACT

Several industrial processes involve the use of silver in one form or another, two of which there are in the use of conductive adhesives within the Personnel Computer Boards manufacturing industry and as a catalyst for the epoxidation of ethylene. Both these processes could be improved significantly if the silver surface were altered morphologically. One possible way to improve either of the aforementioned technologies would be to plasma modify the silvers surface..

The aim of the work described in this thesis is to produce a high surface area silver using a high frequency rf plasma, with the hope that with further research this technology may be used to modify silver powder for use in conductive adhesives or as a catalyst for the epoxidation of ethylene

This thesis describes the use of high frequency continuous wave (CW) oxygen plasmas for the treatment of silver foils, in particular the effects on surface morphology of changes in rf power (15-50W), gas pressure (0.2-0.8 mbar), exposure time (1min-2hrs), orientation of the foil in the reactor with respect to the gas flow (perpendicular or parallel) and distance of the foil from the live electrode (0-17cm). Scanning Electron Microscopy was used to observe these morphological changes.

Further to observing the surface topographies of the oxides under these various conditions, a brief, but no means complete, study of the structure of the various oxides produced at these various conditions was performed using X-ray powder diffraction.

Reduction of these oxidised foils using a hydrogen plasma (CW) was investigated, with particular emphasis being placed on how rf power (15-50W), gas pressure (0.2-0.8 torr) and exposure times (1min-2hrs) affected the extent of reduction of the oxidised foil

(using X-ray Crystallograhy) and its surface morphology (using Scanning Electron Microscopy).

Pulsed oxygen plasma treatments of the silver foils and CW oxygen plasma treatment of earthed silver samples were performed to try and elucidate the mechanism behind any surface modification.

From the above investigations it was found that oxygen plasma treatment of silver foils resulted in significant modification of the surfaces, and this depended on the energy density of the plasma. The optimum surface texture (in terms of apparent surface area) was observed at rf powers of 15W, gas pressures of 0.8 torr, exposure times of 30 min, and at distances of 8-9 cm from the live electrode.

The oxidised foil could be fully reduced back to silver metal using a hydrogen plasma, with little change in the optimum surface morphology.

The pulsing and earthing studies indicated that the formation of the new surface textures was either due to surface diffusion of a charged silver species or was caused by ion bombardment of the silver surface resulting in a facetted surface texture.

The oxides observed were AgO and Ag_2O, but to what extent each was present appeared to depend on the energy density of the plasma.

CONTENTS

Appendix III

CHAPTER 1

INTRODUCTION

BASIC FUNDAMENTALS OF PLASMAS

The following chapter introduces the reasons why research is needed into the modification of silver and plasmas.

1.1. Plasma Modification of Silver - Why?

There are two main industrial processes, which use silver, that could be improved if the surface of the silver could be morphologically modified. These are the use of conductive adhesives within the electronics industry [1] and secondly the epoxidation of ethylene over a silver catalyst [2].

1.1.1. Conductive Adhesives

Adhesives are used in several industrial processes to bind two or more surfaces together [3]. The adhering of materials is a complex process to optimise due to the various factors which affect adhesion such as the materials characteristics [3], surface roughness [3], contact angles [3], additives to the adhesive mixture etc [4].

The Cookson Technology Group (the part-sponsers of this research) have a particular interest in the area of conductive adhesives and especially their use within

the electronics industry [4]. In future years it is thought that the use of these materials, instead of solder, will increase due to the probability that the goverment will be forced to introduce a tax for the useage of lead (a principal component of solder) due to environmental concerns [4].

The research at Cooksons Technology has concentrated on silver filled epoxy adhesives [5]. These principally contain an epoxy resin, which when cured(hardened) forms a polymeric network, silver flake/powder filler and several additives which aid the curing reaction [5]. These resins become conductive when cured at high temperatures [1,5]. This curing process involves the forced re-orientation of the silver particles by the growing polymeric network formed by the resin during curing. By re-alignment of these silver particles a 3-D conductive network is formed throughout the resin [5,6].

Cookson Technology and scientists at the University of Durham, have proposed that it may be possible to use plasmas to modify the silver powder/flake, and thus help form a more conductive pathway by either cleaning or modifying the surface of the silver flakes. It was thought that either or both of these objectives previously mentioned could be achieved by:

(a) Cleaning of the silver - the silver used by Cookson Technology has an oxide layer and a carboxylic acid layer on the outer side of the silver flake/powder [5]. It was proposed that using alternate oxidation and reduction cycles, using oxygen and hydrogen plasmas, these two layers could be removed. This may result in better metal-metal contact between the flakes within the resin, as the only insulating layer around the particle would be the epoxy resin (**see Figure 1.1.**).

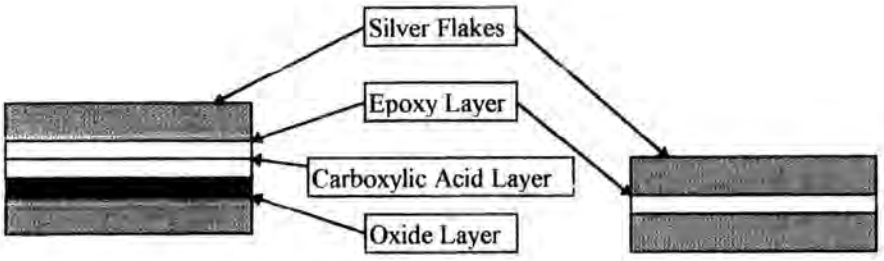

(a) Uncleaned Flakes of silver within an adhesive

(b) Plasma cleaned flakes of silver within an adhesive

Figure. 1.1. Schematic of silver particles within an adhesive for unclean and plasma cleaned silver flakes.

(b) Surface modification of the silver - it was thought that by using an oxygen plasma that the silver surface itself could be modified, in particular silver whisker formation on the flakes may occur. When this modified silver is added to a resin, it was proposed that the whiskers would establish more points of contact between particles. This would result in a conductive pathway through the adhesive and it may be possible to use lower loading of silver in adhesives and still achieve low resisitivity values.

1.1.2. Catalyst Modification

A supported silver catalyst is the most common industrial catalyst used for the epoxidation of ethylene (see Chapter 5 for further detail) [2]. However this catalyst does have its problems, such as achieving high selectivities for the production of ethylene oxide, poisoning of the catalyst and the need for chemical promoters to be added to the catalyst or into the reaction feed mixture [2,7]. Scientists at the University

of Durham proposed that by plasma treating the silver before catalytic processes were ran over the catalyst, could improve the the catalyst and help diminish or eliminate some of the aforementined problems.

Oxygen plasma treatment of the the silver catalyst was proposed followed by reduction of the resulting oxide. It was hoped that any surface modification achieved by the oxygen plasma treatment could be maintained duing the reduction process. Thus it may be possible to tailor make silver catalysts with a higher surface area. This new higher surface area catalyst could then:

(a) improve the selectivity of the catalyst for ethylene oxide production,

(b) enhance the rates of formation of ethylene oxide,

and (c) the catalytic turnover of ethylene oxide could also be increased (which would be very appealing to the manufacturer).

If the above process can be done then a new field of using plasmas to tailor make catalysts emerges.

So what are plasmas, how are they formed and what can they do and how? The next few pages aim to answer these questions.

1.2. Definition of a Plasma

The universe consists mainly of gaseous plasma (discharge), which has surrounded us for millions of years [8]. However this form of matter has only recently

been utilised by man for various chemical and physical processes, such as etching of semiconductors [9,10,11], polymer deposition [12,13] and flue gas clean-up [14,15,16].

On the macroscopic scale plasmas are quasi-neutral systems i.e. have equal numbers of positively and negatively charged species within them, and thus have no overall charge [8,17,18]. Microscopically, slight perturbations in charge exist within them, which perturbs this idea of neutrality [8,17,18]. These unbalanced charged regions affect the motion of particles within a discharge and it is this phenomenon which differentiates a plasma from an ideal gas [8,17].

When an electromagnetic field, of a certain voltage, is applied across a gas, the gas breaksdown - becomes conductive, to generate a plasma [8,17,18]. However for a plasma to exist, one further important criterion must be satisfied: the Debye length of an electron within a plasma must be smaller than the diameter of the reactor vessel [8,17]. The Debye length of an electron is defined as the distance an electron has to travel, from a point in the plasma to a region of unbalanced charge in order to stabilise this charge [8,17]. The Debye length can be obtained from **Equation 1.1.**

After ignition, a plasma can be sustained if the appropriate quantity of energy is constantly supplied to the breakdown region [8].

$$\lambda_D = \left(\frac{kT_e\varepsilon_o}{n_e e^2} \right)^{1/2}$$

λ_D = Debye length k = Boltzmans constant
T_e = electron temperature ε_o = electron permitivity coefficient
n_e = electron density e = electron charge

Equation 1.1. Debye length formula [8,17].

The constituents of a plasma are shown in **Figure 1.2.**

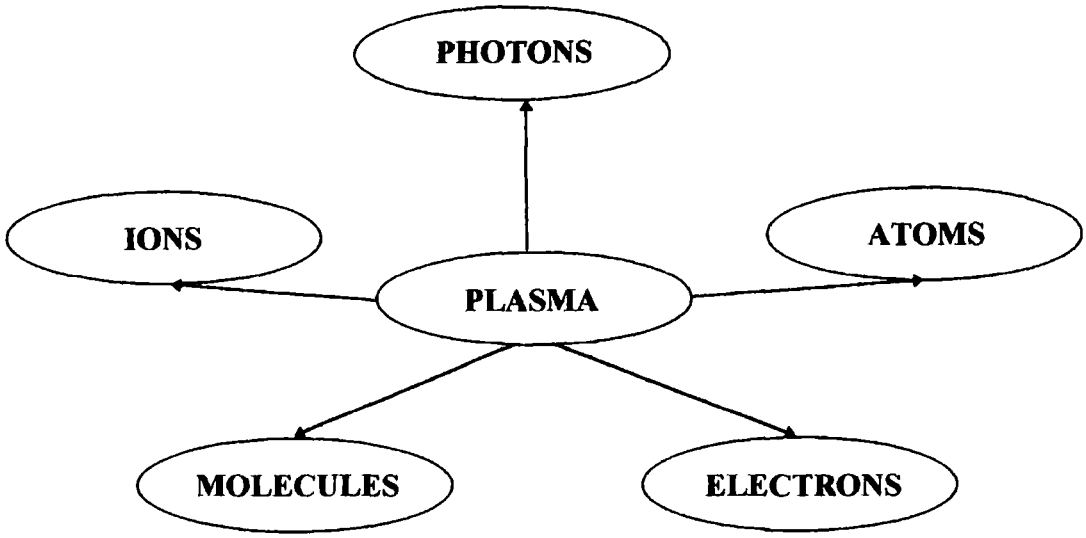

Figure. 1.2. Plasmas constituents (these are discussed in greater detail within section 1.3.)

There are two main categories of plasmas, one being low temperature [8,19], the other high temperature [8,19] :

(a) Low Temperature - also known as non-equilibrium plasmas, due to the large difference in temperature between the gaseous species and electrons [8,17]. The electrons within these systems preferentially gain energy from the applied field, due to their smaller mass, and thus shorter response times to changes in polarity of a high frequency alternating field [8]. However, the more massive gas molecules possess greater inertia and cannot respond as quickly to these polarity changes, resulting in little energy gain from the applied field [8]. So, the temperature of the electrons is significantly higher (3000°C), than that of the gas (approximately 30°C) [8].

(b) High Temperature - known as equilibrium plasmas, because of the electrons and gaseous species temperatures being similar [8]. These plasmas are

typically operated at pressures of atmospheric or above and it is this fundamental difference that results in the equilibration of the temperatures [8]. When an electron collides with a gas species, at these high pressures, a more efficient energy transfer occurs between the species [8]. This is a result of the more frequent collisions between the aforementioned species, and so any energy which the electron gains from the applied field will be readily lost to the surrounding molecules [8]. The electrons will continue to gain energy from the applied field and the electons and gaseous species will heat up gradually to the same temperatures [8]. These plasmas are commonly used in welding [20] and nuclear fusion [21] applications.

1.3. The Plasmas Constituents

The plasma species responsible for the gas phase and gas/substrate reactions which occur within a discharge are detailed below:

(a) Reactive Atoms/Radicals - are the major reactive constituents within a plasma [8,22,23]. Atomic/radical production occurs by either electron impact or photon dissociation of the background gas [24,25]. The density of these species within a plasma is dependent upon the reaction conditions and characteristics (dissociation and ionisation potentials) of the gas, and has been quoted as being 1000 times greater than the electron density for rf frequencies between 50kHz - 40MHz [26].

(b) Ions - both positive and negative ions are present within a plasma environment, but the concentrations of each depend upon the reaction conditions and the characteristics of the background gas [8,27]. Positive ions are involved in the

gas/solid interfacial chemistry, due to their attraction to the negatively charged sheath (described in detail within section **1.6.2.**) [28]. The negative ions are predominantly involved in the gas phase chemistry, due to their repulsion from the negatively biased sample [29,30]. Ions within low pressure plasmas remain at ambient temperatures due to their larger mass, and reluctance to respond to changes in the applied fields direction [8,17,19,29].

(c) Excited Species - the majority of a gas within a plasma exists in the excited state [8]. Excited species which are normally forbidden to exist under typical photochemical conditions (due to selection rules), can be present within a plasma [22]. The lifetime of an excited state is in the order of nanoseconds, however longer lived species, known as metastables, can survive up to 10^8 collisions and still be present milliseconds or even seconds after the initiating event [31,32]. The enhanced lifetimes of these molecules results from the radiative relaxation transition being forbidden [32].

(d) Radiation - photons ranging from the far infra-red to the vacuum ultraviolet are emitted from a plasma [33]. These photons can be absorbed by other species within the discharge which can result in further chemical reactions [22]. Photon emission from a plasma has also become an invaluable analytical tool, for identifying the chemical species present and the reactions occurring within a plasma [34,35].

(e) Electrons - initiate the chemical reactions occurring within the gas, due to their ease in gaining energy from the applied electric field [8,17] . The electrons energies range from 0-100eV in low pressure rf systems, with the majority being between 0-20eV [36]. The energy distribution of electrons can be shown by

Maxwellian or Druyvesteyn distribution curves (see section **1.7.1.**) [8]. Their densities within low pressure discharges are typically 10^{10} cm^{-3} [8]. The electrons within a plasma, after stabilisation, are confined mainly to the plasma volume and participate in inelastic and elastic collisions with gas molecules/atoms [8,37].

1.4. Generation of a Plasma

Plasmas are generated by applying a potential between two electrodes across a gas [8,17,38]. However in some discharges, such as direct current systems, contamination of the electrodes can occur, due to their location inside the reactor vessel. This can lead to the discharge being extinguished [8]. However rf systems eliminate this problem, by locating the coil or plates, between which the field is applied, on the outside of the reaction vessel [8,29].

At ambient temperature, free electrons are present within a gas due to the effects of cosmic rays and natural radioactivity [8,18]. Applying an electric field across the gas e.g. an alternating rf field of frequency 13.56 MHz, causes these electrons to move to and fro between the plates [8,17,38]. This motion results in the electrons gaining kinetic energy, as they are gradually accelerated by the applied field [8,38]. Collisions between these electrons and gas molecules will occur, however initially these electrons will be of low energy i.e. <1 eV, and will only undergo elastic collisions [8,38]. This results in negligible energy transfer (typically 10^{-5} eV) to the target molecules [8]. However as the electrons continue to gain energy from the applied field, the cross-section for inelastic collisions increases [8,38]. These collisions result in dissociation, electronic excitation or ionisation of the background gas [8,17,18,39].

Ionisation processes result in further electron production, which are in turn themselves accelerated by the applied field [8,17,18,38]. A summary of the above processes is given in **Figure 1.3.**

The above section has concentrated on the initiation of the discharge, however Paschen's Law determines at what voltage plasma formation will occur [8,27,38]. Here the breakdown voltage can be determined, if the gas nature, pressure and inter-electrode spacing are known [8,27,38]. The breakdown voltage(V_b) is given by Paschen's equation (see **equation 1.2.**) [8,27,38]:

$$V_b = \frac{C_1(pd)}{C_2 + \ln(pd)}$$

p = potential difference
d = distance between electrodes
C_1 and C_2 = constants that change with nature of gas.

Equation 1.2 Paschen's equation

Radio frequency plasmas of 13.56 MHz are used within this study. As has been stated previously, electrons are able to respond to such high frequency alternating fields and thus possess a very high critical electron frequency (f_{ce}) [8,38]. This is given by the following equation [8]:

$$f_{ce} = \frac{\langle v \rangle_{de}}{2L}$$

$\langle v \rangle_{de}$ = average drift velocity of electrons
L = distance between two electrodes

Equation 1.3. Critical electron frequency.

As for the ions, with their larger masses, they are unable to respond to such changes in field, and thus remain relatively stationary throughout an rf cycle [8,17,38].

This means that the ions gain little energy from the applied field and thus remain predominantly at ambient temperatures [8,17,29]. This smaller response time is determined by the critical ion frequency (f_{ci}), which is given below [8]:

$$f_{ci} = \frac{\langle v \rangle_{di}}{2L}$$

$\langle v \rangle_{di}$ = average drift velocity of an ion
L = length between two electrodes

Equation 1.4. Critical Ion Frequency

These two equations are characteristic of non-equilibrium low pressure plasmas and explains why the electron temperature is far higher than the gas temperature.

1.5. Types of Plasmas

There are several other types of plasmas besides rf, which can be used for a variety of processes, such as:

(a) Direct Current - consists of a pair of electrodes within a reactor vessel; however this can be a disadvantage when treating certain materials due to contamination [8,17,38]. The discharge itself has various dark and glowing regions between the electrodes, such as the Faraday Dark Space, Negative Glow etc [8,17,38]. D.C. plasmas are generally used for lighting applications [8,17,38].

(a)

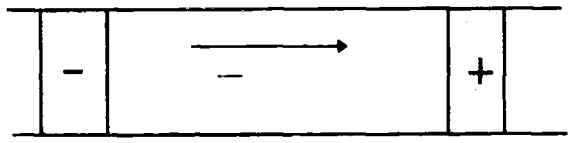

The applied electric field accelerates the electrons.

(b)

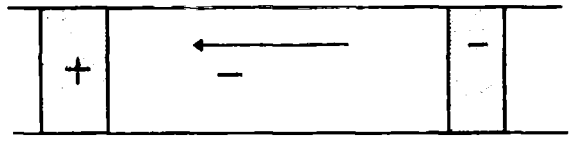

Electrodes' polarity changes and so to does the electrons' direction of travel.

(c)

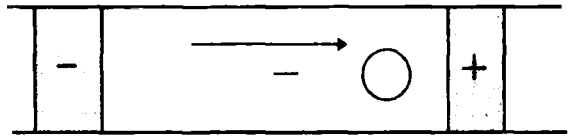

The electron has gained enough energy from the applied field to undergo an inelastic collision with a gaseous species.

(d)

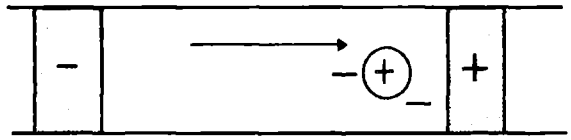

An inelastic collision occurs generating an ion and an electron. This increases the density of electrons within the plasma and these electrons are themselves accelerated by the applied field.

Figure. 1.3. Schematic of the generation of a plasma and further electron production.

(b) Silent Discharge - uses rf power as the main energy source, but in this type of discharge one of the electrodes or sometimes both is covered with a dielectric . The dielectric allows charge to build up on it and once it reaches a certain potential, breakdown of the dielectric occurs. This gives rise to a microdischarge filament between the electrodes. These microdischarges are occurring randomly with respect to time and positon on the dielectric [39,40]. These plasmas operate at atmospheric conditions and are used to generate large quantities of ozone for industrial purposes [30].

(c) Microwave Discharges - MW energy is used to generate the plasmas at pressures of 1 torr or above [8]. They are typically produced within electrode or electrodeless reactor configurations [41,42,43]. They are generally higher in temperature than rf systems, however similar plasma processes can occur within them [8]. These systems can be used to generate diamond-like films for various coating applications [8,44].

(d) Electron Cyclotron Resonance - are also MW generated plasmas, but with one fundamental difference in that an external magnetic field is present, to increase the ionisation cross-section of the electrons [8,45]. These systems operate at pressures typically of 10^{-4} torr and are finding more use within the semiconductor industry for etching applications [46].

1.6. Plasma Fundamentals

1.6.1. Electron Energy Distribution Function

The energy of the electrons is one of the most important parameters within a plasma, as it is this which determines the chemistry occurring within them [8,17,18,38]. The electron energy is dependent upon the strength of the applied field, and also on the loss processes, such as collisions, which the electron undergoes [8,17,38]. The electron energy distribution can be shown by Maxwellian or Druyvesteyn distribution curves (see **Figure 1.4.**) [8,17].

Maxwellian distribution makes the assumption that all species are in thermodynamic equilibrium within a plasma, which is not the case with non-equilibrium systems. The Druyvesteyn distribution is probably a better model to use for non-equilibrium systems.

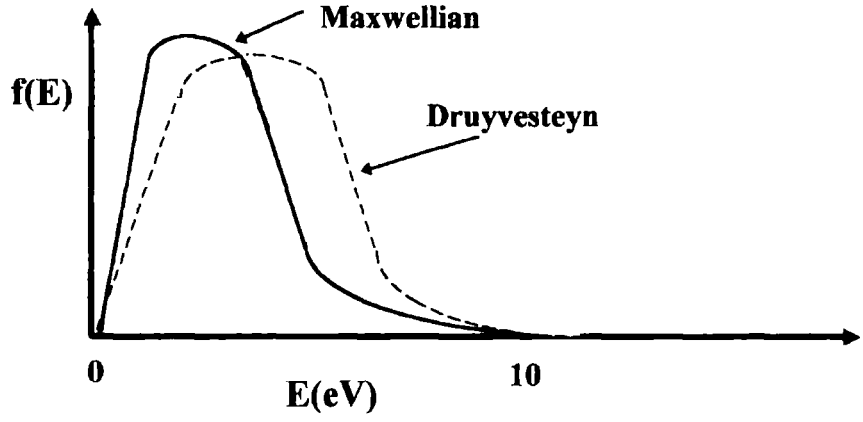

Figure. 1.4. Maxwellian and Druyvesteyn electron energy distributions.

1.6.2. Floating and Sheath Potentials

When an isolated substrate is placed within a plasma the sample accumulates negative charge (see **Figure 1.5.**) [8,38,47]. This is because after plasma ignition, the electrons gain energy from the applied field and rapidly move to all surfaces in contact with the plasma [8,17,38]. The negative charge which accumulates on the substrate is termed the floating potential (v_f) [8,17,38]. This negative bias repels further electrons from the sample except those of high energy, and attracts positive ions to the surface [8,17,38]. These positive ions are accelerated towards the sample, due to the marked potential drop just in front of the sample [8,17]. This drop occurs between the bulk plasma which is electrically neutral (plasma potential (v_p)) and the negative sample [8,17,47]. This region is termed the sheath and the voltage across this gap the sheath potential (v_{sh}) [8,17,29,38,47].

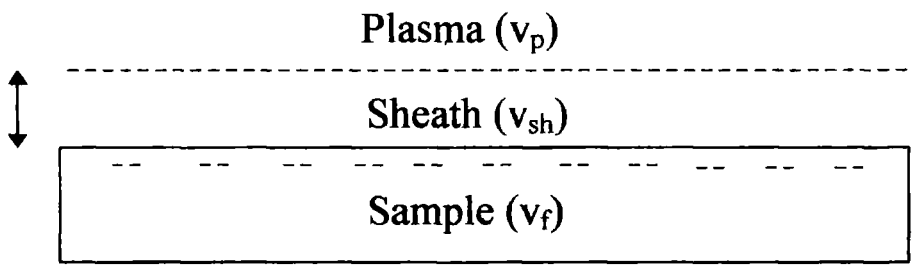

Figure. 1.5. Location of floating, sheath and plasma potentials location (schematic).

1.7. Non-equilibrium Discharge Chemistry

After igniting a discharge a complex series of chemical reactions occurs. Several reaction pathways which are not available under normal chemical conditions,

may occur within a plasma, thus leading to the production of some unusual chemical species [8]. These species may be important in chemical processes occurring within the discharge and also in the properties of the plasma modified product. Typical reactions occurring within the gas phase are listed below:

(a) Electron - Molecule Interactions

These are the main class of reactions which occur within low pressure, high frequency plasmas [8,42,49].

The excited species can be rotationally, vibrationally or electronically excited [8].

Dissociation occurs when an electron undergoes an inelastic collision with a molecule [8,48,49].

Occurs readily within electronegative gases and usually arises when electrons have very little energy (< 1 eV) [8,27].

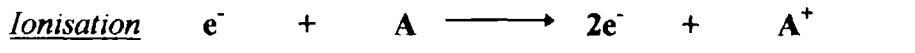

This usually involves electrons at the high energy tail of the distribution curves [8,17]. *The ions formed are responsible for ion bombardment of the sample* [8].

Here the recombined state will be in an excited level, and thus photon emission must occur [8].

Other typical reactions which occur within a discharge are ion-molecule, ion-ion, and radical-molecule [8,17,38]. Examples of these are given below:

(b) Ion-Molecule Reactions [8]

Charge Transfer $A^+ + A_2 \longrightarrow A + A_2^+$

New Species $A^+ + BC \longrightarrow AB^+ + C$

Associative Attachment $A^- + BC \longrightarrow ABC + e^-$

(c) Ion-Ion Reactions [8]

Recombination $A^+ + B^- \longrightarrow AB$

(d) Radical-Molecule Reactions [8]

Electron Transfer $A + B \longrightarrow A^+ + B^-$

Ionisation $A + B \longrightarrow A^+ + B + e^-$

Recombination $A + A \longrightarrow A_2$

The above examples are only some of the reactions that may occur within a plasma.

1.8. Applications of Plasmas

Plasmas have recently been developed for use in many industrial and non-industrial applications, due to their ease of use, environmental friendliness and energy efficiency [50]. However, plasmas have the added advantage in that novel products can be produced, which are unable to be formed under typical thermal conditions [8]. Several of these processes are listed below:

(a) Plasma Polymerisation - involves flowing a polymer monomer into a plasma to produce radicals and reactive species [8,51]. These species then polymerise on a substrate and within the gas to produce a polymeric film [8]. An example of this is the deposition of fluorocarbon films from various monomers [52,53,54,55].

(b) Surface Modification - modification of a substrate can be achieved due to the interaction of the chemically reactive ions and atoms produced within a discharge with the substrate [8,38]. This process can be used to treat materials in order to improve their biocompatibility [56,57], or to produce various modified coatings [58,59,60].

(c) Surface Cleaning - plasmas can be used to remove contaminants, such as hydrocarbons, from the surface of a material [8]. This is achieved by exposing the surface of the material to a reactive gas for short periods of time, to produce

volatile components such as CO and CO_2 [8,61]. An example of this is the cleaning of aluminium surfaces for adhesion applications [62].

(d) Surface Hardening - materials are treated with specific reactive gases, to produce hardened surface coatings, an example of which is steel reacted with nitrogen atoms to form hardened steel [63,64,65].

(e) Toxic Waste Destruction - plasmas have also been used to destroy toxic contaminants emitted from power stacks, to meet EEC limits [66,67]. Such contaminants as benzene, toluene and various hydrochlorocarbons have been destroyed using plasmas [68,69,70].

Two other plasma processes used very much within industry are etching and sputtering [8]. These two processes are described in greater detail within the following sections.

1.8.1. Etching of Materials

Etching processes are used within the semiconductor manufacturing industry to produce fabricated microchips [8,17,70]. This process involves transferring the pattern of a substrate mask to a microchip's surface [8,17,70]. This used to be achieved using wet etching techniques, however significant problems were associated with it, such as it being environmentally unfriendly due to vast amounts of solvent; also adhesion between the substrate and the patterned mask often became weak [8,70]. Plasmas have now replaced the wet processes and have eradicated these problems. Thus plasmas

are now seen as the way of the future, due to the ever present requirements to obtain smaller and smaller chips [8,17,70].

The process of etching can occur in two ways, the first being chemical the second physical (this will be discussed within section **1.8.2.**) [8]. Chemical etching involves reactions between atoms, which have been produced within the plasma, and the substrate which has to be etched [8,17,70,71]. The first stage of the reaction is for the adsorption of the atoms onto the substrate's surface and the subsequent reaction between them, to form a volatile compound [8,70,71,72]. This volatile species then departs from the surface, leaving behind an etched layer [8,71,72]. This process can be seen in **Figure 1.6.**

There are two main etching profiles which can be obtained using plasmas, the first being isotropic the second anisotropic [8,70]. Isotropic etching occurs when the vertical and horizontal etch rates of the film are similar [8]. This means that if a mask with a pattern is placed upon a substrate, the material under the mask will also be etched [8]. However as for anisotropic etching the vertical etch rate is far greater than the horizontal component and thus the material under the mask will be largely untouched [8]. This is shown within **Figure 1.7.**

Etching using a plasma can lead to damage of the substrate due to ion bombardment, however this depends upon the reactor set-up and also the type of etching used [8,70]. There are two main types [8]:

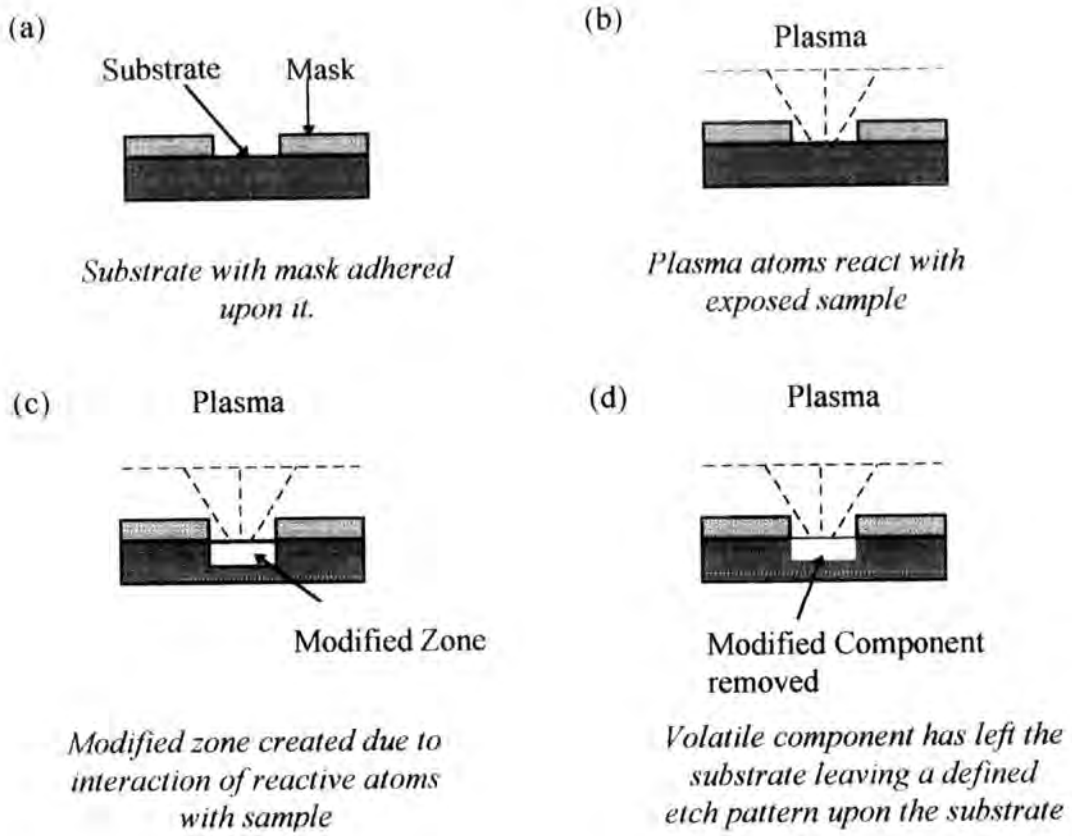

Figure 1.6. Etching mechanism

Figure 1.7. Isotropic and anisotropic etch profiles.

(a) **Plasma Etching** - where the interacting ions have a low energy

and (b) **Reactive Ion Etching**- where the ions have a far greater energy and can cause considerable damage to the sample.

During etching an etch resistant layer can also form, if an organic component is present. This layer can restrict etching along the horizontal axis of the sample and enhance the vertical etching component [8,70].

1.8.2. Sputtering (Physical Etching)

Sputtering processes are used within a variety of fields such as in the etching of materials or in the deposition of thin films [8,17,73]. Sputtering involves bombarding a solid surface (target) with either energetic ionic or neutral species [8,17,74]. This bombardment process can result in the ejection of atoms from the surface, leaving a pitted structure behind [8,17,74].

The most commonly encountered processes involve using ions as the incident particles, rather than neutrals due to their ease at being accelerated by applied electric fields [17,74]. Thus ions can gain significant amounts of energy from the applied field before impacting upon the target [17,74].

When an ion interacts with a surface, several processes can occur. These are: [17,74,75]

(a) Ion Reflection - here the ion is reflected from the target and is usually neutralised in the process. This phenomenon is utilised in the technique of Ion Scattering Spectroscopy [17,75].

(b) Secondary Electron Ejection - the impacting ion causes a secondary electron to be emitted from the sample [17].

(c) Ion Implantation - impacting ions may be implanted into the sample surface. This phenomenon is used to selectively modify certain materials and alter their properties [17].

(d) Structural Rearrangements - the energy from the impinging ion can be transferred throughout the sub surface lattice and create a variety of defects such as dislocations, point defects, interstitial defects etc [17].

(e) Sputtering - the impinging ion transfers most of its energy to a surface atom which causes it to break bonds with its neighbouring atoms, and leave the target's surface. This is the phenomenon which will be described in slightly more detail below [17].

When an impinging ion strikes a surface, the energy of the ion is dissipated throughout the lattice via several secondary collision processes [17,75]. This energy can spread into the surface, sub-surface and bulk lattice of the target material [17,75]. Which one of these phenomena will occurs preferentially will be difficult to predict, however it would be expected that the majority of the energy will be expended into the bulk lattice, and that only a small fraction of energy will be possessed by any ejected surface atoms [17]. In fact approximately 1% of the energy is transferred to the

sputtered atom [17]. The energy transfer to the surface is dependent upon the masses of the impinging ions and target material and also on the energy and angle with which the ion impacts into the materials surface [17].

The two main processes for which sputtering is used are etching and deposition, however sputtering is often too slow for certain applications within these fields [31,76,77,78]. Typical deposition and etching rates for these two processes, using sputtering, are 50-500Å and 50-10000Å respectively [31].

A summary of the sputtering process is shown in **Figure1.8.**

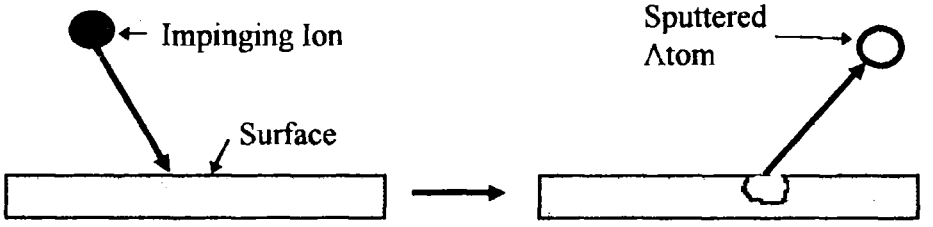

Figure 1.8. Summary of sputtering process

REFERENCES

1. Nguyen, G.P.; Williams, J.R.; Gibson, F.W.; **Albestik Internal Report,** 1993.
2. Bond, G.C.; **Heterogeneous Catalysis: Principles and Applications 2nd Edition;** Clarendon Press: New York, 1990.
3. **Shaw's Book**
4. Nriagu, J.O.; Pacyna, J.M.; **Nature, 1988;** Vol. 333, 134.
5. ***Private Communication*** with Matthew Holloway **(Cookson Technology Centre, Sandy Lane, Yarnton, Oxfordshire.)**
6. Lovinger, A.J.; **J. Adhesion, 1979;** Vol. 10, 1.
7. Jorgensen, J.A.; Hoffmann, R.; **J. Phys. Chem., 1990;** Vol. 94, 3046.
8. Grill, A.; **Cold Plasma in Materials Fabrication**; IEEE Press: New York, 1994.
9. Manos, D.M.; Flamm, D.L.; **Plasma Etching, an Introduction**; Academic Press: New York, 1989.
10. Goldstein, I.S.; Kalk, F.; **J. Vac. Sci. Technol., 1981**; Vol. 19(3), 743.
11. van Roosmalen, A.J.; van den Hoek, W.G.M.; Kalter, H.; **J. Appl. Phys., 1985**; Vol. 58(2), 653.
12. Inagaki, N.; Yamazaki, H.; **J. Appl. Polym. Sci., 1984**; Vol. 29, 1369.
13. Yasuda, H.; Hsu, T.; **J. Polym. Sci. Polym. Chem. Ed., 1977**; Vol. 15, 81.
14. Evans, D.; Rosocha, L.A.; Anderson, G.K.; Coogan, J.J.; Kushner, M.J.; **J. Appl. Phys., 1993**; Vol. 74(9), 5378.
15. Nunez, C.M.; Ramsey, G.H.; Ponder, W.H.; Abbott, J.H.; Hamel, L.E.; Kariher, P.H.; **Air & Waste, 1993**; Vol. 43, 242.
16. Han, Q.Y.; Zhuang, Q.D.; Herberlein, J.V.R.; Tormanen, W.; **ACS Sympos. Ser., 1995**; Vol. 607, 135.
17. Chapman, B.; **Glow Discharge Processes**; Wiley: New York, 1980.

18. Penning, F.; **Electrical Discharges in Gases**; Cleaver Hume Press: London, 1957.

19. Friedel, P.; Gourrier, S.; **J. Phys. Chem. Solids, 1983**; Vol. 44(5), 353.

20. Uman, M.; **Introduction to Plasma Physics**; Mcgraw-Hill: New York, 1964.

21. Longmire, C.L.; Tuck, J.L.; Thompson, W.B.; **Plasma Physics & Thermonuclear Research Vol. 2**; Pergammon Press: London, 1963.

22. Holohan, J.R.; Bell, A.T.; **Techniques and Applications of Plasma Chemistry**; Wiley: New York, 1974.

23. Gordillo-Vazquez, F.J.; Kune, J.A.; **Phys. Rev. E, 1995**; Vol. 51(6), 6010.

24. Collart, E.J.H.; Baggerman, J.A.G.; Visser, R.J.; **J. Appl. Phys., 1991**; Vol. 70(10), 5278.

25. Filseth, S.V.; Welge, K.H.; **J. Chem. Phys. 1969**; Vol. 51, 839.

26. Hess, D.W.; **J. Vac. Sci. Technol., 1990**; Vol. A8(3), 1677.

27. Von Angel, A.; **Ionised Gases**; Clarendon Press: Oxford, 1955.

28. Wild, C.; Koidl, P.; **J.Appl. Phys., 1991**; Vol. 69(5), 2909.

29. Vossen, J.L.; Kern, W.; **Thin Film Processes II**; Boston Acad. Press: Boston, 1991.

30. Stoffels, E.; Stoffels, W.W.; Vender, D.; Kando, M.; Kroesen, G.M.W.; de Hoog, F.J.; **Phys. Rev. E, 1995**; Vol. 51(3), 2425.

31. Coburn, J.W.; **IEEE Trans. Plasma Sci., 1991**; Vol. 19(6), 1048.

32. Wayne, R.P.; **Principles and Applications of Photochemistry**; O.U.P.; Oxford, 1988.

33. Samson, J.A.R.; **Techniques of Vacuum Ultraviolet Spectroscopy**; John Wiley & Sons; New York, 1967.

34. Coburn, J.W.; Chen, M.; **J. Appl. Phys., 1980**; Vol. 51(6), 3134.

35. Curtis, B.J.; Brunner, H.J.; **J. Electrochem. Soc., 1978**; Vol. 125, 829.

36. Godyak, V.A.; Piejak, R.B.; **Phys. Rev. Lett., 1990**; Vol. 65, 996.

37. Shibata, M.; Nakano, N.; Makabe, T.; **J. Phys. D: Appl. Phys., 1997**; Vol. 30, 1219.

38. Howatson, P.M.; **Introduction to Gas Discharges**; Pergammon Press; 1976.

39. Eliasson, B.; Hirth, M.; Kogelschatz, U.; **J. Phys. D: Appl. Phys., 1987**; Vol. 20, 1421.

40. Yamamoto, T.; Kumar, R.; Lawless, P.A.; Ensor, D.S.; Newsome, J.R.; Plaks, N.; Ramsey, G.H.; **IEEE Trans. Ind. Appli., 1992**; Vol. 28(3), 528.

41. McTaggart, F.K.; **Plasma Chemistry in Electrical Discharges**; Elsevier: New York, 1967.

42. Wertheimer, M.R.; Moisan, M.; **J. Vac. Sci. Technol. 1985**; Vol. A3, 2643.

43. MacDonald, A.D.; **Microwave Breakdown in Gases**; John Wiley & Sons: New York, 1966.

44. Gruen, D.M.; Liu, S.Z.; Krauss, A.R.; Pan, X.Z.; **J. Appl. Phys., 1994**; Vol. 75(3), 1758.

45. Matsuo, S.; Kiuchi, M.; **Jap. J. Appl. Phys., 1983**; Vol. 22, L210.

46. Cahn, R.W.; Haasen, P.; Kramer, E.J.; **Materials Science & Technology: Processing of Semiconductors**; VCH: Weinheim, 1996.

47. Flender, U.; Wiesemann, K.; **J.Phys. D: Appl. Phys., 1994**; Vol. 27, 509.

48. Sommerer, T.J.; Kushner, M.J.; **J. Appl. Phys., 1992**; Vol. 71(4), 1654.

49. Feoktistov, V.A.; Mukhovatova, A.V.; Popov, A.M.; Rakhimova, T.V.; **J. Phys. D: Appl. Phys., 1995**; Vol. 28, 1995.

50. Boenig, H.V.; **Advances in Low Temperature Plasma Chemistry, Technology, Applications - Volume 1**; Technomic: Pennsylvania, 1984.

51. Yasuda, H.; **Plasma Polymerisation**; Academic Press: Orlando, 1985.

52. Kogoma, M.; Kasai, H.; Takahashi, K.; Moriwaki, T.; Okazaki, S.; **J. Phys. D: Appl. Phys., 1987**; Vol. 20, 147.

53. Savage, C.R.; Timmons, R.B.; Lin, J.W.; **Chem. Mater., 1991**; Vol. 3, 575.

54. Hynes, A.M.; Shenton, M.J.; Badyal, J.P.S.; **Macromolecules, 1996**; Vol. 29, 4220.

55. Yamada, Y.; Yamada, T.; Tasaka, S.; Inagaki, N.; **Macromolecules, 1996**; Vol. 29, 4331.

56. Ward, T.L.; Jung, H.Z.; Hinojosa, O.; Benerito, R.R.; **Surf. Sci., 1978**; Vol. 76(1), 257.

57. Hollohan, J.R.; Stafford, B.B.; Fall, R.D.; Payne, S.T.; **J. Appl. Polym. Sci., 1969**; Vol. 13, 807.

58. Maa, J.S.; Meyerhofer, D.; O'Neill, J.J.; White, L.; Zanzucchi, P.J.; **J. Vac. Sci. Technol., 1989**; Vol. B7(2), 145.

59. Makino, T.; Nakamura, H.; Nakashita, T.; **J. Appl. Phys., 1980**; Vol. 51(11), 5868.

60. Conrad, J.R.; Radke, J.L.; Dodd, R.A.; Worzala, F.J.; Tran, N.C.; **J. Appl. Phys., 1987**; Vol. 62(11), 4591.

61. Steffen, H.; Schwarz, J.; Kersten, H.; Behnke, J.F.; Eggs, C.; **Thin Solid Films, 1996**; Vol. 283, 158.

62. Dylla, H.F.; **J. Vac. Sci. Technol., 1988**; Vol. A6(3), 1276.

63. Jurcik Rajman, M.; Veprek, S.; **Surf. Sci., 1987**; Vol. 189, 221.

64. Kuppusami, P.; Terrance, A.L.; Sundararaman, D.; Raghunathan, V.S.; **Surf. Eng.; 1993**; Vol. 9(2), 142.

65. Wang, C.J.; Duh, J.G.; **J. Mater. Sci., 1988**; Vol. 23, 769.

66. Boulous, M.I.; **Pure & Appl. Chem., 1996**; Vol. 68(5), 1007.

67. **EH40/97 Occupational Exposure Limits;** HMSO, London, 1997.

68. Nunez, C.M.; Ramsey, G.H.; Ponder, W.H.; Abbott, J.H.; Hamel, L.E.; Kariher, P.H.; **Air & Waste, 1993**; Vol. 43, 242.

69. Haverlag, M.; Stoffels, W.W.; Stoffels, E.; Kroesen, G.M.W.; de Hoog, F.J.; **J. Vac. Sci. Technol., 1996**; Vol. A14(2), 384.

70. Sugiyama, L.; **Plasma Science and the Environment**; 1997.

71. Flamm, D.L.; Manos, D.M.; **Plasma Etching: An Introduction**; Academic Press: New York, 1989.

72. Goldstein, I.S.; Kalk, F.; **J. Vac. Sci. Technol., 1981**; Vol. 19(3), 743.

73. Mogab, C.J. ; Adams, A.C.; Flamm, D.L. ; **J. Appl. Phys., 1978 ;** 49(7), 3796.

74. Veprek, S.; Venugopalan, M.; **Elementary Processes at Solid Surface Immersed in Low Pressure Plasmas, Plasma Chemistry III**; Verlag: Berlin, 1980.

75. Briggs, D.; Seah, M.P.; **Auger & X-ray Photoelectron Spectroscopy (Vol. 1)**; John Wiley & Sons: New York, 1990

76. Wehner, G.K.; Kim, Y.H.; Kim, D.H.; Goldman, A.M.; **Appl. Phys. Lett., 1988**; 52(14), 1187.

77. Hirasawa, M.; Shirakawa, H.; Hamamura, Y.; Egashira, Y.; Komiyama, H.; **J. Appl. Phys., 1997;** 82(3), 1404.

78. Greiner, R.H.; **J. Appl. Phys., 1974;** 45(1), 32.

CHAPTER 2

EXPERIMENTAL CHAPTER

The following chapter describes the various analytical techniques used in this study.

2.1. Microscopy

The field of microscopy deals with the phenomenon of increasing the dimensions of an object's image [1]. This magnification is achieved using either light (optical microscopy) [1] or high energy electrons (electron microscopy) [1,2,3]. There are several versions of electron microscopy which can be used to obtain different information on a material's composition or morphology, for example [1,2,3]:

(a) **Transmission Electron Microscopy** - gives detail on the internal structure of a material.

(b) **Scanning Electron Microscopy/Elemental Dispersive Analysis by X-rays** - gives detail on the surface morphology of material, or its chemical composition.

(c) **Scanning Transmission Electron Microscopy** - gives a combination of both of the above.

However, within this study, the technique of choice was Scanning Electron Microscopy (SEM) and it is this technique that will be described in further detail.

SEM is particularly useful for investigating surface morphologies because of its large depth of field and high resolution [1,2]. However, disadvantages of this technique are that damage to the sample can occur and also the sample must be conductive for it to be analysed unless a conductive coating is deposited on the sample [1,2]. In particular, this technique has been used to investigate several silver/silver oxide systems, where morphological changes have occurred such as in catalytic reactions [4] and the plasma [5,6] or electrochemical treatment of silver

2.1.1. Scanning Electron Microscopy

Scanning Electron Microscopy, is used to look at the surface morphology of given materials [1,2,3]. This is achieved by bombarding the surface of a material with high energy electrons and analysing the emitted signals [1,2,3].

The primary electron beam, which bombards the surface, is generated by thermionic emission from a tungsten/lanthanum hexaborate filament, or by field emission from an emission gun (see (**1**) of **Figure 2.1.**) [1,2]. The emitted electrons are then accelerated to a desired energy whilst traversing an electrostatic field, which exists between the cathodic filament and the anode (**2**) [1,2,3]. Emerging from the field, they then pass into either a single or pair of electromagnetic lenses (**3**), which focuses the electrons to a beam with a crossover point of several hundred nanometers (**4**) [1,2,3]. The electrons then pass through a condenser lens, (**5**) containing a stigmator (used for correcting any distortion within the beam) and a final aperture, which helps produce a well focused, distortion-free beam, used for probing surfaces (**6**) [1,2,3].

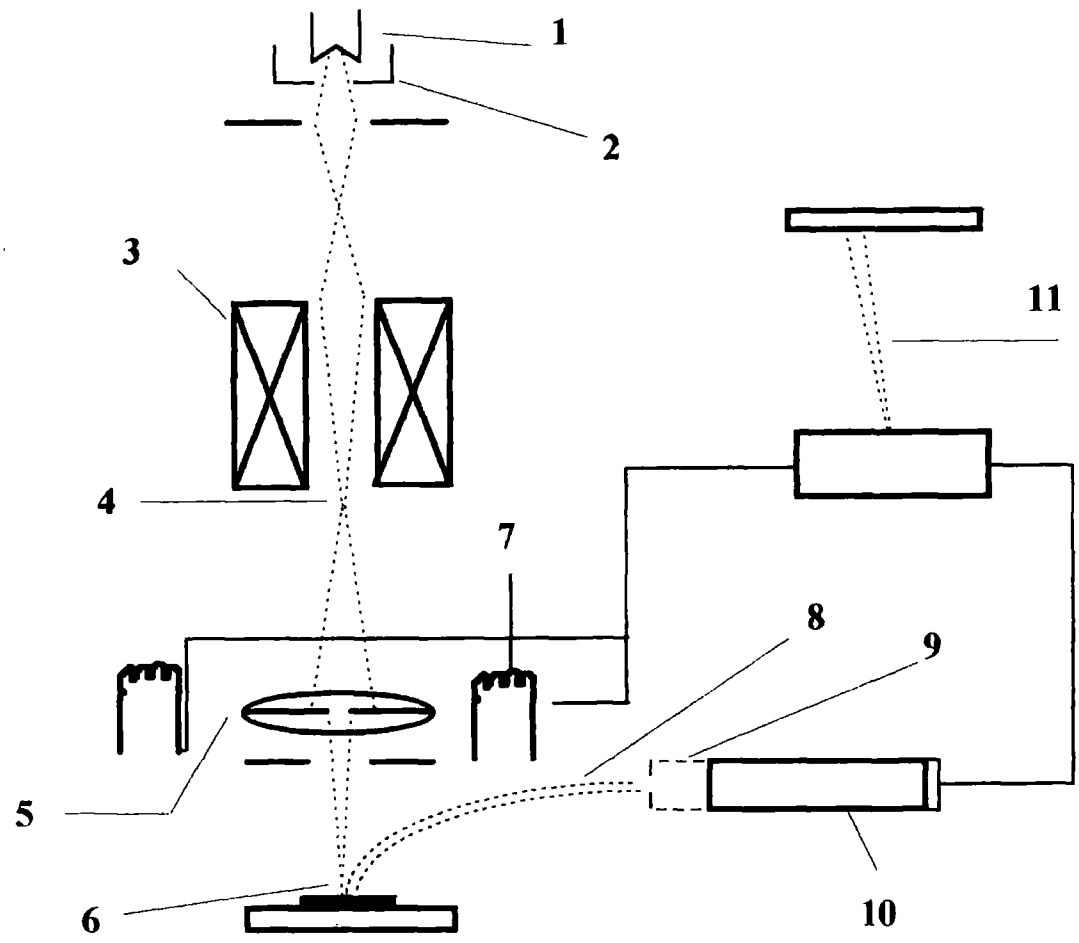

Figure. 2.1. A schematic of a Scanning Electron Microscope [2]

The beam is then raster scanned across the surface using a set of scan coils. This allows the beam to spend a specific amount of time at each point upon the surface (7) [1,2]. These small areas, which the beam bombards, are termed pixels (picture elements) and are several hundreds of nanometers in diameter [1]. From these pixels, secondary and backscattered electrons are emitted, along with a range of wavelengths of electromagnetic radiation (**8**) [1]. For imaging a sample's surface, the signals of utmost importance are the secondary and backscattered electrons [1,2]. These electrons are collected within an electron capture detector e.g. a Faraday Collector

(9), and strike a photoluminescent material, which results in the emission of light, which then passes along a lightguide (**10**) [1,2]. It is the intensity of this signal that is used to build up an image of the surface [1,2]. Analysing the radiation emitted from the sample can give information about the chemical composition information of the material [1,2].

While the electron beam is being raster scanned over the surface, a cathode ray oscilloscope (CRT) beam is simultaneously raster scanned over a CRT screen (**11**) [1,2,3]. The only difference between the two scanning beams is in the size of the pixels which they scan. The CRT's pixels are far larger than those which the electron beam scans [1,2]. This is a very important phenomenon, as it is this property which allows magnification of a surface to be achieved. For example, if the electron beam scans a pixel of length 2 mm, then the CRT beam correspondingly scans a length of 20 mm. This means that everything within the samples pixel will be magnified 10 times upon the CRT screen (see **Figure 2.2.**). Thus the magnification is given by [1] :

$$\textbf{Magnification} = \frac{\textbf{size of pixel on the CRT}}{\textbf{size of pixel on the sample surface}}$$

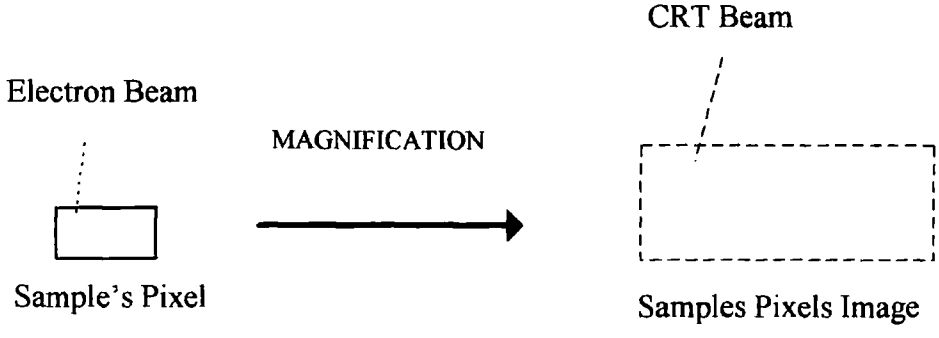

Figure. 2.2. Sample pixel magnification of approximately 3 times

2.2. Photoelectron Spectroscopy

Photoelectron spectroscopy entails bombarding a material's surface with high energy radiation, resulting in the ejection of electrons from either the valence or core levels of an atom [9,10,11,12]. However, the energy of the radiation used can determine which electrons are ejected and thus two branches of photoelectron spectroscopy have developed[4,5]:

(a) Ultra-Violet (UV) Photoelectron Spectroscopy (UPS) - the incident radiation (UV) has sufficient energy to eject electrons from the valence levels of the surface atoms [4,5].

(b) X-Ray Photoelectron Spectroscopy (XPS) - here the incident X-rays have sufficient energy to eject electrons from the core levels of the atoms [9,10,11,12].

UPS was not used within this study and thus will be discussed no further. XPS is the tool of choice for analysis of silver, within this work, and has been used previously to study silver catalysts [13]. However as for studying the oxides of silver this is far more difficult due to the small separation in Ag binding energy between AgO and Ag_2O [14,15].

2.2.1. X-Ray Photoelectron Spectroscopy (XPS)

XPS, as has been stated above, is an elemental analytical technique and involves the use of X-rays [9,10,11,12].

Similar to SEM, electrons are accelerated by a high potential located between the cathodic filament and an anode [9]. These high energy electrons then strike an anode, which can be coated with a variety of different materials [9,10,11]. The materials

often encountered are magnesium and aluminium [9,10]. Electron bombardment of these films results in the emission of a broad continuum of radiation, which has superimposed upon it some strong emission lines, characteristic of the coating [9,10]. For aluminium and magnesium, the major X-rays produced are the $K\alpha_{1,2}$ which have energies of 1486 eV (linewidth = 0.8 eV) and 1253 eV (linewidth = 0.7 eV) respectively [9]. Switching between these materials can be useful in distinguishing between Auger and photoelectron peaks, both of which are present within a spectrum [9]. However, during the bombardment process, a $K\alpha_{3,4}$ X-ray is also emitted which is half of the intensity of the $K\alpha_{1,2}$ [9]. The emission of this line may complicate the spectra obtained. The X-rays produced pass through an aluminium window, of approximately 2μm in thickness, and then irradiate the sample [9] (see **Figure 2.3.**).

Irradiating the sample results in a photoelectric effect, where the energies of the X-rays are absorbed by the surface atoms electrons within the sample. If this energy is greater than the binding energy of a certain electron, then the electron is ejected from the atom [9,10,11]. This electron will possess a characteristic kinetic energy, which will be indicative of the element from which it came [9,10,11]. The kinetic energy of the ejected photoelectron is given by the following relationship [9,10]:

$$E_K = h\upsilon - E_B - \Phi$$

E_K = kinetic energy of the photoelectron

$h\upsilon$ = energy of the exciting source

E_B = binding energy of the ejected electron

Φ = work function of the material

The flux of these photoelectrons is determined by [9] :

(a) the energy of the exciting source,

(b) the atomic number of the element from which the ejected electron came from,

(c) photon incidence angle and emission angle.

The ejected electrons are then usually analysed by a concentric or cylindrical hemispherical analyser, which separates the electrons according to their differences in kinetic energies [9,10].

2.2.2. Typical Features of Photoelectron Spectra

The XPS spectrum, is a plot of the number of photoelectrons versus kinetic energy. The features often observed for such a spectrum are [9]:

(a) ***Auger Electrons*** - electrons emitted due to the relaxation process that occurs after photo-ionisation.

(b) ***X-ray Satellites*** - formed due to the ejection of a core electron by a weaker X-ray emission line e.g. $K\alpha_{3,4}$.

(c) ***Ghosts*** - X-rays produced by contaminants on the anode surface e.g. copper and oxygen.

(d) ***Shake-up/Shake off satellites*** - are produced due to the ejected photoelectron having less energy than expected due to an intra-atomic energy transfer process.

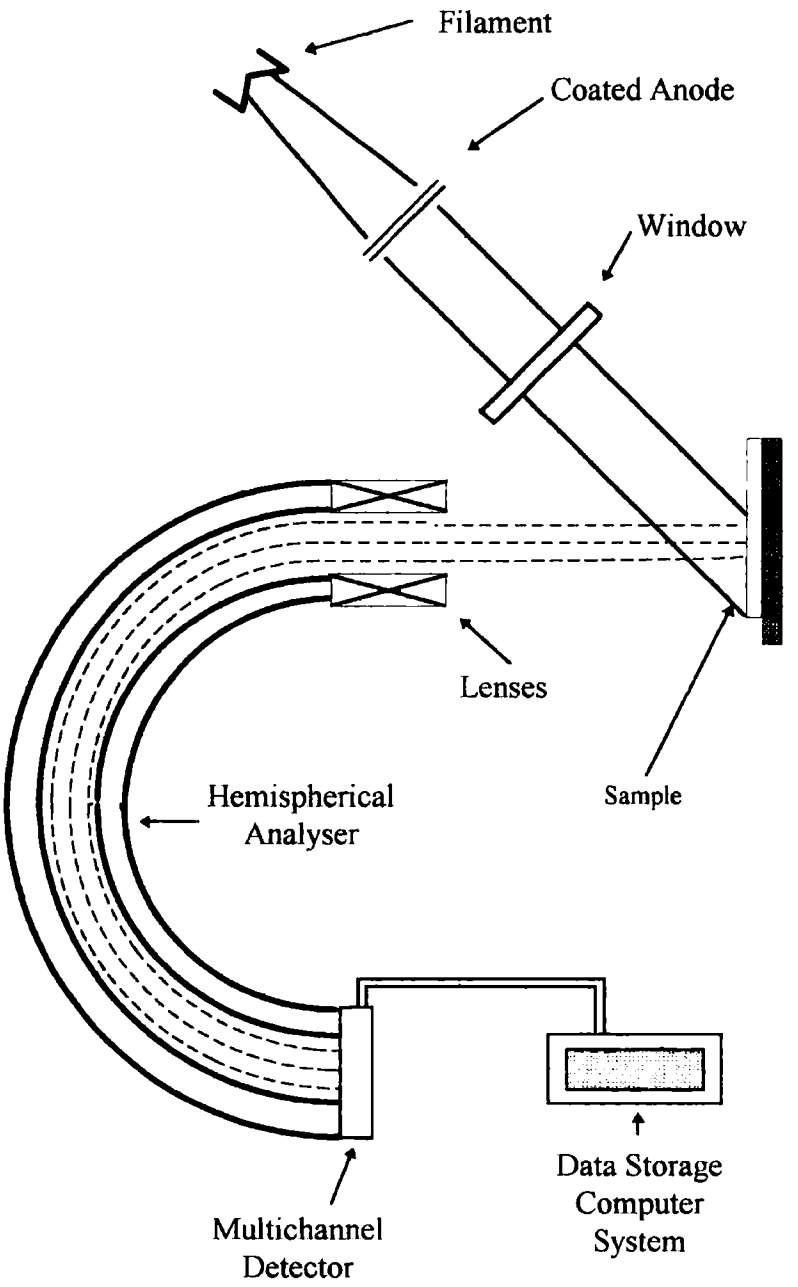

Figure. 2.3. Typical XPS spectrometer

2.3. Diffraction

There are three primary types of radiation, that can be used to obtain structural information about a sample, utilising the phenomenon of diffraction. These are [16,17]:

(a) electrons

(b) neutrons

(c) X-rays

The technique used within this study was powder X-ray diffraction, and thus electron and neutron processes will be discussed no further.

2.3.1. X-ray Diffraction

In 1913 Wilhelm Röntgen and Max von Laue were the first to postulate that X-rays could be diffracted by materials [16,17]. Crystals are ideal for diffracting X-rays, since the regular 3-D periodic array of lattice planes are separated by a distance similar to that of the wavelength of X-rays (a condition for diffraction) [16,17].

However, it is not true to say that if X-rays irradiate a crystal, then diffraction will occur. X-rays entering a crystal may encounter a crystallographic plane of atoms and thus can be diffracted, however they may be diffracted so that either destructive or constructive interference occurs [16,17]. If destructive interference occurs then the beams are out of phase and no or a very weak diffraction spot will be observed [16]. Rotating the crystal so that constructive interference occurs gives rise to a pronounced diffraction spot. This interference occurs, because the angle with which the incident beam has encountered the lattice plane has changed, and it now satisfies Braggs Law (see **Figure 2.4.**) [16,17].

Braggs Law is stated as follows [16,17] :

$$n\lambda = 2d \sin\theta$$

λ = wavelength of X-rays

θ = Bragg Angle

d = lattice spacing

n = integer plane

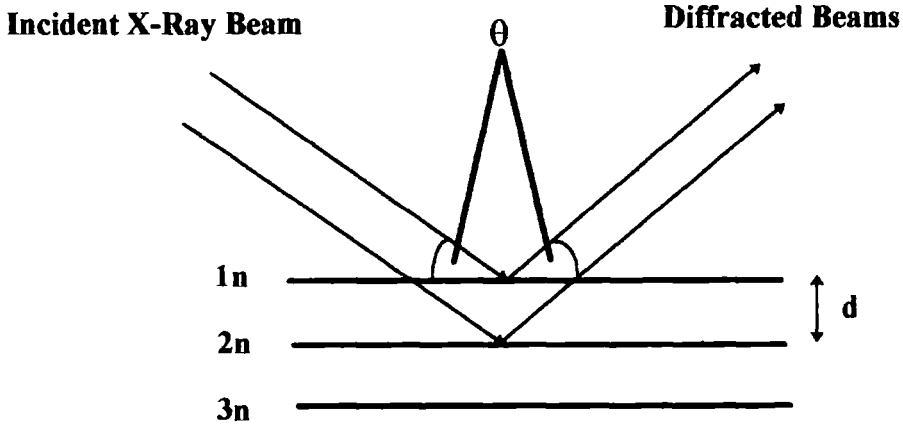

Figure. 2.4. Diffraction of X-rays by a series of lattice planes [8]

Lattice planes which give rise to diffraction, are labeled according to their intersection with axes of the unit cell, and are assigned values of (a,b,c) [16,17]. However, sometimes this is inconvenient and so the reciprocals of these intercepts are used. These reciprocals are termed Miller Indices and are given values of (h,k,l)[16,17]. For example the intersection may be given by ($^1/_2$,$^1/_2$,1), then the Miller Indices will be (2,2,1).

There are two main classes of materials which can be studied by x-ray diffraction. These are [16,17] :

(a) **single crystals,**

and (b) **amorphous/powder materials**

The first method involves rotating a single crystal around an axis so that all planes within the crystal are able to diffract at some instant in time [16]. The second does not involve such a procedure, and will be described in more detail within the following section.

2.2.2. Powder Diffraction

Powder samples consist of thousands of crystallites, which are randomly orientated [16,17]. This means that when a sample is irradiated by X-rays, some of the planes present within certain crystallites will satisfy Braggs Law and thus diffract incoming X-rays [16]. However the same planes in other crystallites will not, because Braggs Law is not satisfied [16]. Thus, rotation of powdered samples is not necessary. It is this technique that is the one of choice for studying the composition of silver oxides. Powder diffraction is useful for studying oxides due to the well defined lines of silver oxides and the difference in patterns with changes in phases [18]. Also the technique is sensitive to impurities that may be present within the sample [18]. Possible disadvantages with this technique are that the radiation may alter the composition of the material being investigated, and secondly it is not very useful for quantitative analysis [18]. Many researchers have used powder diffraction to analyse compositional changes in silver oxides [19,20].

Two of the most common powder methods utilised are [16] :

(a) **Debye-Scherrer Method** - Here the camera film lies on the surface of the cylindrical chamber, while the specimen is positioned on the axis of the cylinder [16]. Typical cameras used have a range of resolving powers (R) for various diffracting planes. This is given by the equation [16]

$$d/\Delta d = -(2R/\Delta S) \tan \theta$$

d = mean spacing of 2 sets of planes
Δd = difference in their spacing
ΔS = separation between diffracting planes
θ = diffracting angle

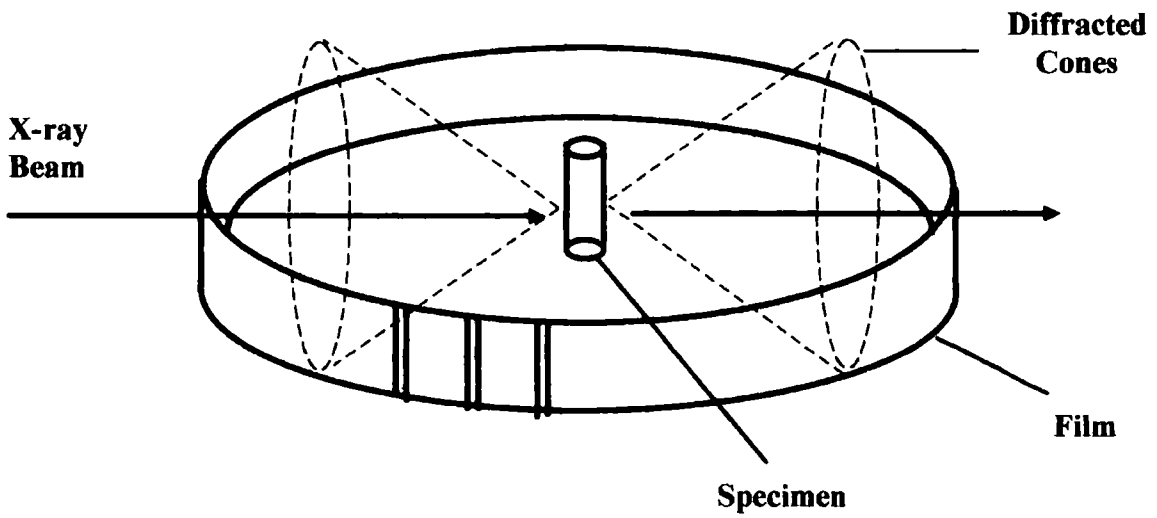

Figure. 2.5. Diagram of the Debye-Scherrer camera.

(b) **Focusing Camera** - Here the camera film, specimen and the X-ray source are all placed upon the surface of the cylinder [16]. A typical camera is theSeeman-Bohlin type which has a range of resolving power (R) for the different diffracting planes. This is given by [16]

$$d/\Delta d = -(4R/d) \tan \theta$$

(refer to previous equation for labels)

A typical camera is shown in **Figure 2.6.**

As more and more computer technology becomes available, photographic films will be become more and more obsolete. Thus, in a computer generated spectrum intensity is plotted against 2θ.[16,17]. A typical spectrum is shown in **Figure 2.7.**.

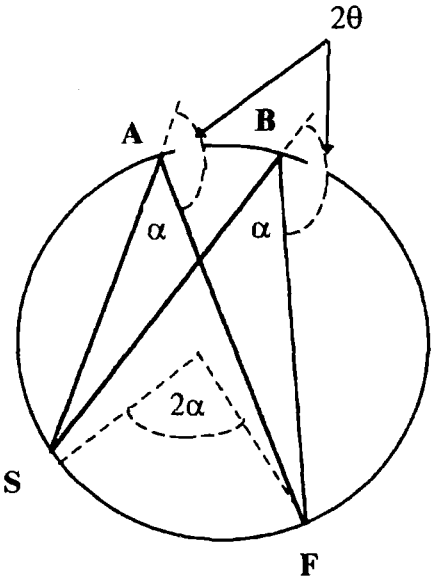

Figure. 2.6. Focusing camera

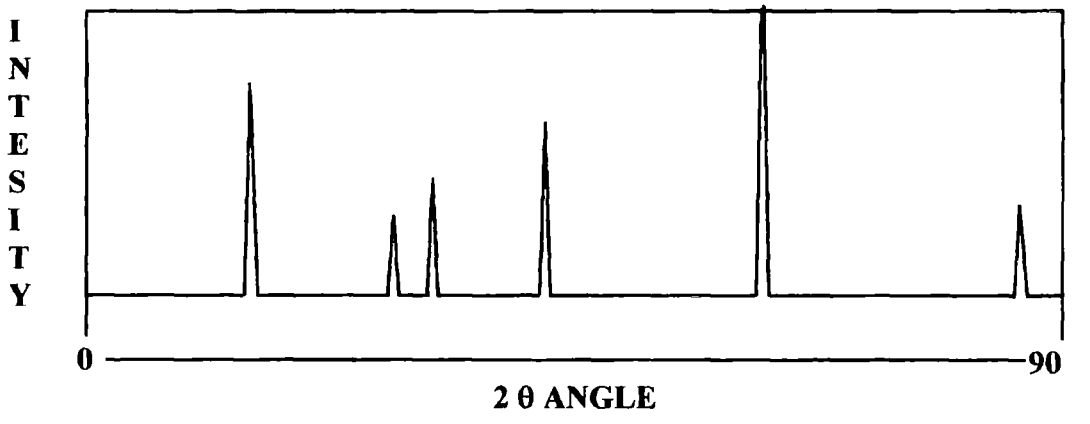

Figure. 2.7. Computer displayed diffraction spectrum

REFERENCES

1. Goodhew, P.J.; Humphreys, F.J.; **Electron Microscopy & Analysis**, Taylor & Francis: 1988.
2. Goldstein, J.I.;Newbury, D.E.; Echlin, P.; Joy, D.C.; Fiori, C.; Lifshin, E. **Scanning Electron Microscopy & X-ray Microanalysis**, Plenum Press: New York, 1981.
3. Wells, O.C.; **Scanning Electron Microscopy**, McGraw-Hill: New York, 1974.
4. Bao, X.; Barth, J.V.; Lehmpfuhl, G.; Schuster, R.; Uchida, Y.; Schlogl, R.; Ertl, G.; **Surf. Sci. 1993**, 284, 14.
5. Chou, C.H.; Phillips, J.; **J. Vac. Sci. Technol. 1991**, A9(5), 2727.
6. Bhan, M.K.; Nag, P.K.; Miller, G.P.; Gregory, J.C.; **J. Vac. Sci. Technol. 1994**, A12(3), 699.
7. Corish, J.; O'Briain, C.D.; **J. Mater. Sci. 1971**, 6, 252.
8. Mayer, S.T.; Muller,R.H.; **J. Electrochem. Soc. 1988**, 135(9), 2133.
9. Briggs, D.; Seah, M.P.; **Auger and X-Ray Photoelectron Spectroscopy** Volume 1; John Wiley & Sons: New York, 1990.
10. O'Connor, D.J.; Sexton, B.A.; Smart, R.St.C; **Surface Analysis Methods in Materials Science;** Springer Verlag: 1992.
11. Willard, H.H.; Merritt(Jr), L.L.; Dean, J.A.; Settle, F.A.; **Instrumental Methods of Analysis**; Wadsworth: California, 1988; 7th Edition.
12. West, A.;. **Solid State Chemistry and Its Applications**; John Wiley & Sons.: New York, 1992.
13. Bukhtiyarov, V.I.; Boronin, I.P.; Prosvirin, P. Savchenko, V.I.; **J. Catal. 1994**, 150, 268.
14. Weaver, J.F.; Hoflund, G.B.; **Chem. Mater. 1994**, 6, 1693.
15. Weaver, J.F.; Hoflund, G.B.; **J. Phys. Chem. 1994**, 98, 8519.
16. Cullity B.D.; **Elements of X-ray Diffraction**; Addison-Wesley: London, 1991.
17. Atkins, P.W.; **Physical Chemistry** Oxford University Press: Oxford, 1990, 4th Edition.
18. ***Private Discussion*** with Dr. C. Lehman.

19. Dallenbach, R.; Painot, J.; Tissot, P. **Polyhedron 1982**, 1(2), 183.

20. McMillan, J.A. **Chem. Rev. 1962**, 62, 65.

CHAPTER 3

PLASMA OXIDATION OF SILVER FOILS

3.1. Introduction

The aim of this chapter is to describe the morphological changes that occur during the plasma oxidation of silver foils. Parameters such as rf power, gas pressure, time of reaction and the position and orientation of the foil within the reactor were studied. The main goal of this work was to produce a high aspect ratio silver oxide layer (highly faceted surface texture).

3.1.1. Surface Modification of Materials

A vast research area, investigating the morphologies of surfaces and their alteration, has developed over recent years [1]. The importance of this area in the advancement of industrially related disciplines, such as thin film processing[1,2], heterogeneous catalysis[3], adhesion[4] etc. cannot be over estimated. This area encompasses the modification of materials such as polymers [1,2,5], rubbers [6], metals and their salts [7,8].

Treatment of polymeric materials in order to obtain certain desired surface properties has been achieved using ultraviolet radiation, lasers, X-rays, electron and ion beams [9]. An example of such surface modification is the photo-oxidation of polypropylene, where improvements in wettability, adhesion and antistatic properties are obtained [9]. However this thesis will place emphasis mainly on the modification

of metals/metal salt materials and so the alteration of polymeric materials will be discussed no further.

Surface modification of metals can be achieved in similar ways to those of polymers [1]. Three main techniques used are ion bombardment [10,11], thermal/plasma evaporation [3,12,13,14] and the deposition of thin metal films onto various substrates [1,15]. Ion bombardment of metal surfaces often produces cone-like structures upon the surface [10,11]. This phenomenon has been observed on seeded metal substrates e.g. aluminium seeded with gold [16], copper seeded with aluminium [16], and also on non-seeded metals such as tin[16]. The ion beams normally used to induce such structural phenomenon are composed of positively charged inert gas ions [10,11].

Alternative topographical features observed on modified metal surfaces are whiskers [17,18], faceted structures [19] and crystallites [3]. These modified structures are normally produced when a metallic substrate has been subjected to a reactive gaseous atmosphere [17].

Metallic whiskers have been produced on platinum [20], copper [20], nickel [20], and cobalt [20] by reducing a halogenated salt (except the fluoride), in an atmosphere of hydrogen, at very high temperatures (typically 800 °C) [20]. Reasonings behind the formation of these whiskers are:

(1) the presence of screw dislocations within the material which could possess areas where high metallic atom/ion diffusion may occur[21],

(2) a chemical concentration gradient existing between the treated surface and the gaseous species within the plasma[22]

and **(3)** finally the very high temperatures could give atoms sufficient energy to become mobile within the lattice [17].

Whisker formation (see **Figure 3.1.**) is associated with either a migrating, diffusive or volatile component which can then re-deposit, and agglomerate on the surface forming the desiredstructures[17].

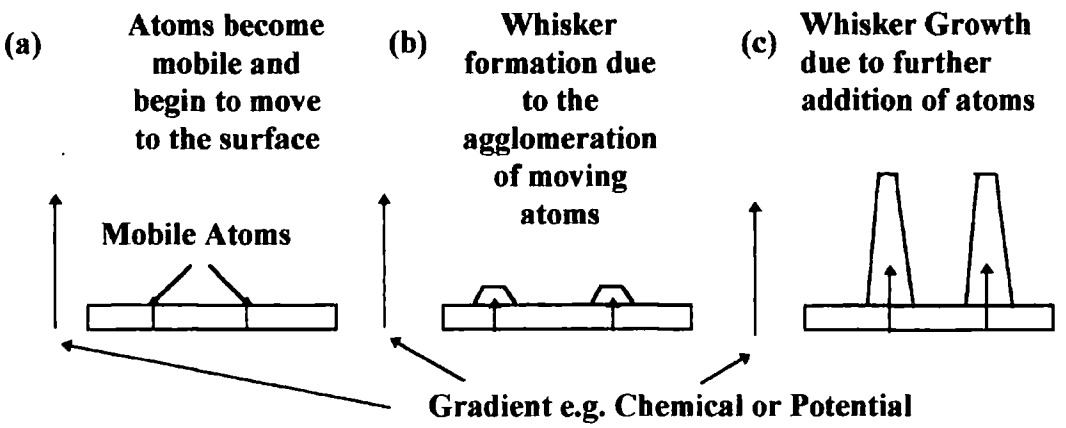

Figure. 3.1. Whisker formation - **(a)** Atoms become mobile within the lattice due to field, concentration or temperature gradients and move in direction of the gradient **(b)** Nucleation begins and gradually the whiskers begin to grow **(c)** Whiskers continue to grow with end furthest from whisker base remaining the same width as initially, suggesting the growth occurs from the base.

Crystallites and faceted structures are normally produced by two inter-related phenomena - etching and facetting [3,19]. The formation of crystallites and facets can normally be observed on the surface of catalysts, where severe structural rearrangement has occurred due to the effects of the reactive gaseous environment in which they operate [19,23]. Examples of catalytic systems where the aforementioned phenomena occurs, are in the oxidation of ammonia over a platinum catalyst [24] and the oxidation of methanol to formaldehyde over a silver catalyst [23].

Restructuring of metals also occurs when platinum and tin are treated within an oxygen [3] and hydrogen discharge [25] respectively. Small crystallites appear upon the platinum surface, whereas pits form upon the tins [3,25]. In both cases the rearrangements are produced due to the formation of a volatile component, which leaves the surface, resulting in the eroded textures [3,25].

Thin film deposition of copper and titanium onto various substrates can produce a variety of surface textures, which depends upon the substrate temperature (during deposition) and deposition rate [26].

As this chapter is concerned with silver/silver oxide, the question arises as to whether these materials can also form similar surface textures. Different textures have been achieved on silver/silver salts by :

(a) **deposition (e.g. silver selenide films)** [27]

(b) **etching within a reactive atmosphere (air or oxygen at high temperatures)** - by reacting a metal substrate with a specific gas can lead to the formation of a volatile component, which can then leave the surface giving rise to the formation of an etched surface [14, 28].

(c) **reduction of metal salts (e.g. silver halides or sulphides) -** silver halide salts can be reduced using hydrogen gas, resulting in reduction of the salt back to silver metal [17,18,20].

(d) **exposure to electric fields on growth (electrochemical formation of silver oxides and sulphides) -** electrochemically forming a silver sulphide layer, with significant modification of the surface, can occur wihin an electrochemical cell. The extent of modification is dependent upon the electrodes potential. [29, 30]

(e) **plasma treatment of surfaces (plasma formation of silver oxides)** - structure modification of silver oxides can be achieved using oxygen plasmas [13,31]

The aim of the following work was to concentrate on using plasma for thin film growth, and in particular to study the effects of a variety o plasma parameters on the formation of silver oxides within a capacitively coupled rf plasma.

3.2. Experimental

Silver foil (99.99% purity: Goodfellows) was initially cleaned with Brasso (Household Products) as this was found to give the cleanest surface when analysed by X-ray Photoelectron Spectroscopy. The foil was treated using ultrasound in a 20 ml, 0.1 molar nitric acid solution (General Purpose Reagent (GPR) from BDH) for a period of 5 min. Subsequent rinsing in 2 x 10 ml of de-ionised water , and one aliquot of a 1:1 mixture of isopropyl alcohol (AnalaR from BDH) and cyclohexane (GPR from BDH) followed. A further 15 min. period of ultrasonication within a second aliquot of the 1:1 mixture was carried out. The foil was then dried in an oven (50°C) for a period of 8 min..

Plasma treatments using a 13.56MHz, rf capacitively coupled non-equilibrium system, were performed within a Pyrex tube (59 cm length, 4.5 cm diameter). Two copper capacitor plates, one earthed, the other fluctuating between a positive and negative potential at 13.56 MHz (separated by a distance of 18 cm), encapsulated the outer diameter of the reactor (see **Figure 3.2**.). Power from an ENI 13.56MHz

generator, was coupled to the plates via an ENI matching network. This allowed the maximum amount of energy to be transferred into the plasma medium.

The reactor base pressure of 5 x 10^{-3} mbar measured using an Edwards PRE 10K Pirani gauge, was achieved using an Edwards E2M5 Fomblin rotary pump (82.5 dm^3h^{-1}). The gas inlet system was pumped to a base pressure of 6 x 10^{-3} mbar using an Edwards E2M5 mineral oil rotary pump (82.5 dm^3h^{-1}), measured using an Edwards Barocell (see **Figure 3.2**).

The oxidation of the silver foils was performed using oxygen gas (BOC: 99.9% purity). The gas was flushed through the reactor for 5 minutes before ignition of the plasma occurred.

X-ray photoelectron spectroscopy analysis of the cleaned silver foils was carried out using a Kratos ES2000 spectrometer (typical base pressure of < 1 x 10^{-7} torr) which was equipped with a Mg ($K\alpha_{1,2}$ = 1253.6 eV) [32] X-ray source. A concentric hemispherical analyser system was used to separate the electrons of different energies, which was operated in the fixed retard ratio mode (FRR 22:1). All samples appear to the naked eye to be undamaged by X-ray irradiation. The main elements analysed for were O (1s), C (1s) and the Ag ($3d_{5/2}$) (see **Tables 3.1. and 3.2.**).

Surface morphological images were obtained using a Cambridge Instruments S600 scanning electron microscope. The samples were fixed to the sample stage using Silver Conductive Paint (Adhesion Colloids). The stage was inserted into the column which was then evacuated to a base pressure of <1 x 10^{-6} torr. Images were obtained by bombarding the surface with high energy electrons generated from a tungsten filament which was at 2800 K [33]. The typical voltage used to accelerate the electrons

to their desired energies was 25 kV. A camera was used to obtain a photographic image of the surface.

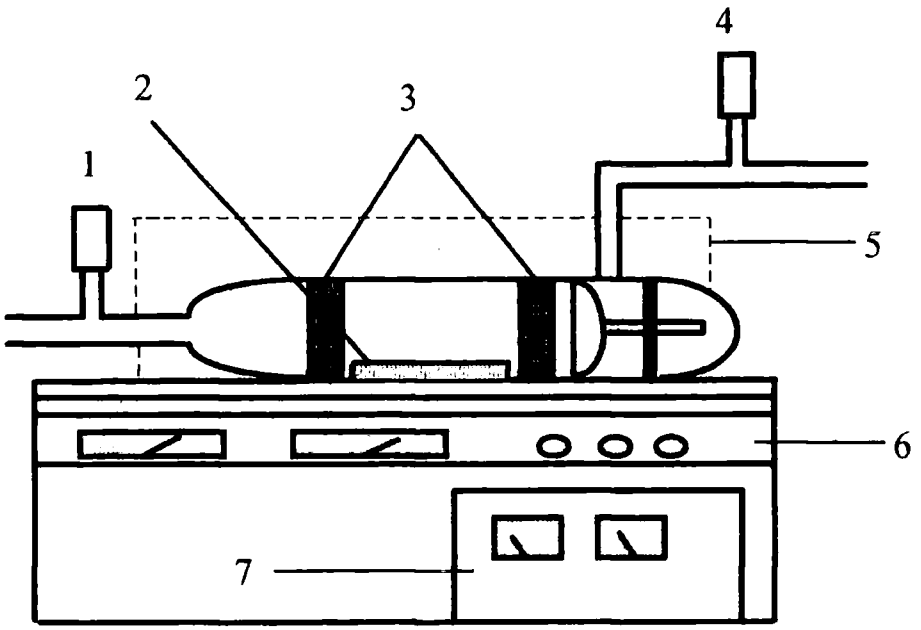

1. Pirani Pressure Gauge
2. Sample Tile
3. Earth (LHS) & Live (RHS) Electrodes
4. Barocell Pressure Gauge
5. Faraday Cage
6. Matching Network
7. 13.56 MHz rf Generator

Figure 3.2. Plasma system used to produce the oxidised silver foils.

3.3. Results

A table showing the difference in surface elemental analysis composition between the non-clean and clean silver foils is shown below:

Sample	Silver (Ag) %	Carbon (C) %	Oxygen (O) %
Non-clean Silver	6 ± 5	78 ± 5	16 ± 5
Cleaned Silver	45 ± 5	41 ± 5	14 ± 5

Table 3.1. Data from XPS analysis of silver foils.

The clean silver foil was also subjected to depth profiling and analysed after each subsequent argon bombardment. The data is tabulated below:

Profile Time (Seconds)	Silver (Ag) %	Carbon (C) %	Oxygen (O) %
0	45 ± 5	41 ± 5	14 ± 5
30	85 ± 5	15 ± 5	0
60	100	0	0

Table 3.2. Depth profile data of surface elemental composition

The parameters varied were: rf power, gaseous pressure, time of reaction, position of foil and orientation of foil with respect to the gas flow. Power input was investigated first, due to its strong influence on the chemistry occurring within the plasma.

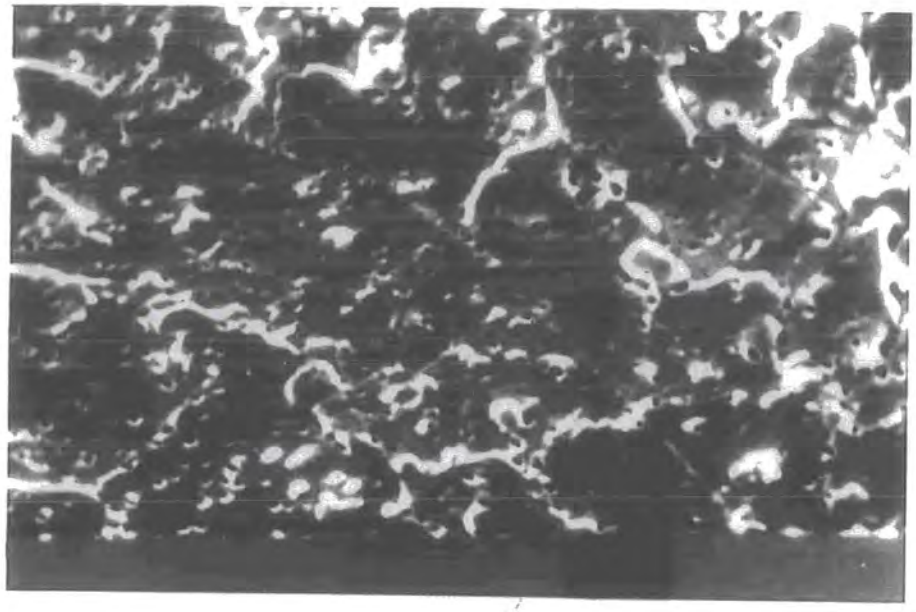

HYDROGEN CLEAN Ag (scale 10μm = 1.5cm)

INPUT POWER = 15 W (scale 10μm = 1.5cm)

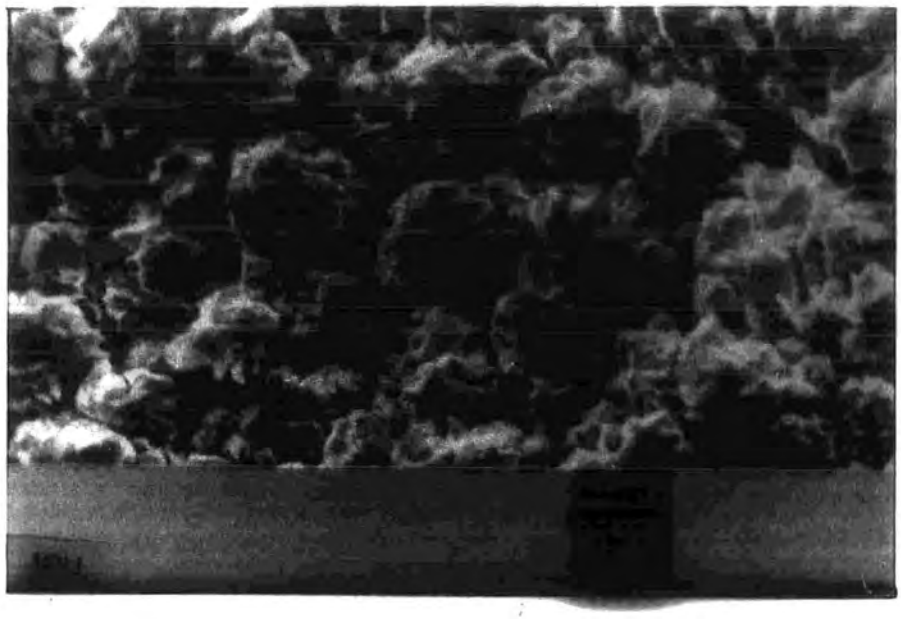

INPUT POWER = 20 W (scale 10μm = 1.5cm)

INPUT POWER = 25 W (scale 10μm = 1.5cm)

INPUT POWER = 30 W (scale 10μm = 1.5cm)

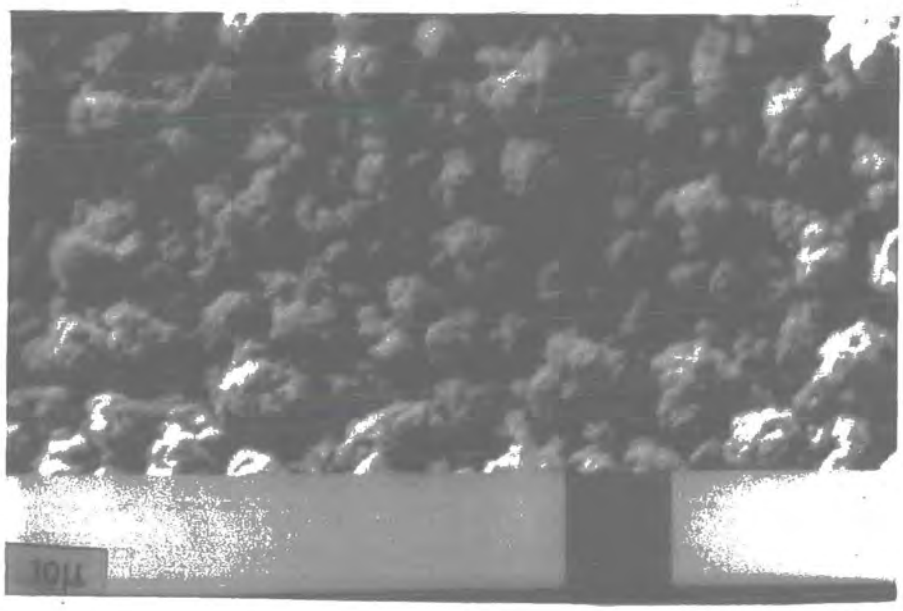

INPUT POWER = 50 W (scale 10μm = 1.5cm)

Treatment at 15 W, (the lowest power at which the plasma could be ignited) produced a roughened surface, with plate-like structures projecting from it. These platelets were approximately 4-10 μm in length with a cross-section of several hundred nanometers.

Increasing the power to 20 W leads to agglomeration of the plates, producing clusters (diameters approximately 10-15 μm). Further increases in rf power produced a far more regular cluster arrangement.

Considering that the main aim of the project was to produce high aspect ratio silver, the optimum power appeared to be 15 W.

All results above were able to be reproduced and were checked at various stages throughout the study.

3.3. 2. Gaseous Pressure

The gas pressures studied were between 0.2 and 0.8 mbar. All other parameters were held constant i.e. power = 15 W, time of reaction = 1 hr and centre of the foil = situated at 8.5 cm from the live electrode.

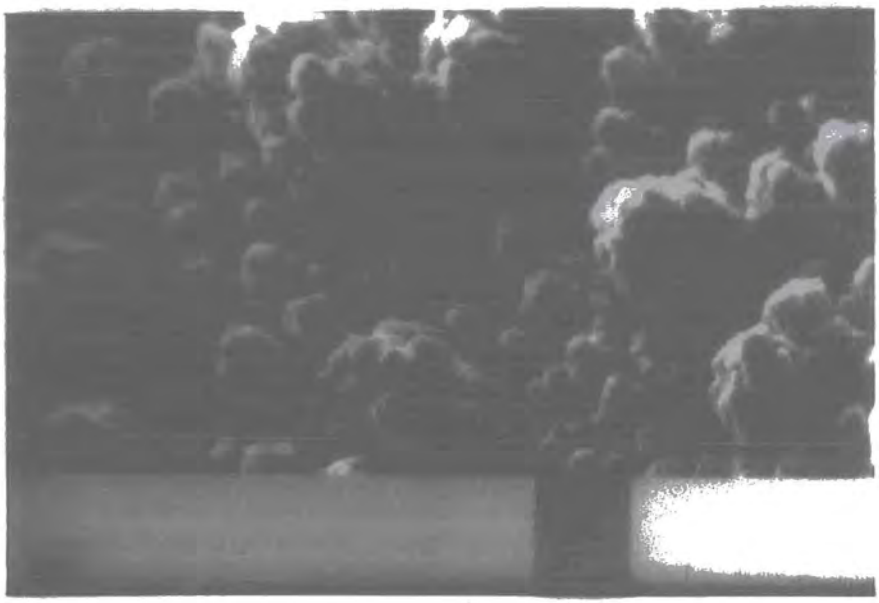

GAS PRESSURE = 0.2 mbar (scale 10μm = 1.5cm)

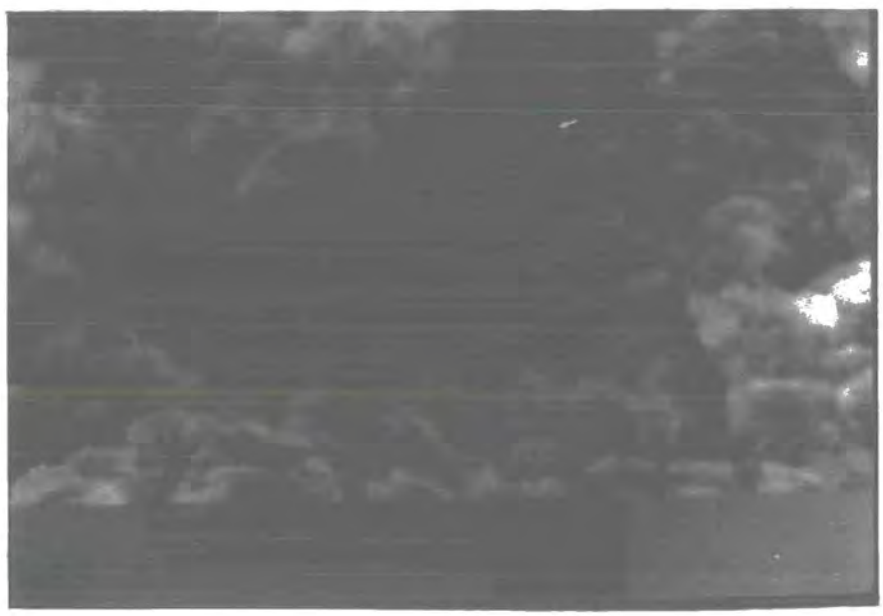

GAS PRESSURE = 0.4 mbar (scale 10μm = 1.5cm)

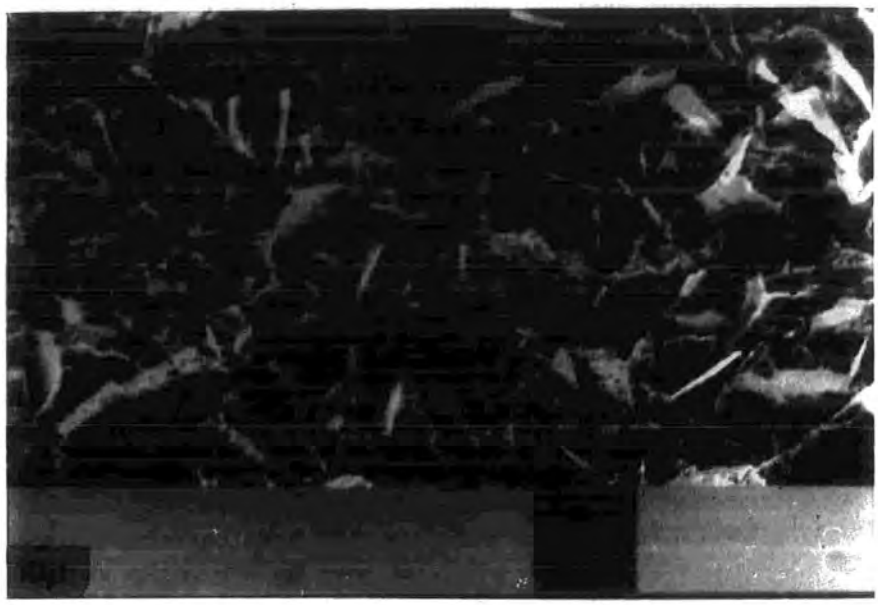

GAS PRESSURE = 0.6 mbar (scale 10μm = 1.5cm)

GAS PRESSURE = 0.8 mbar (scale 10μm = 1.5cm)

At 0.2 mbar, globular clusters formed on the surface which are analogous to those produced for the 30 W power treatments (see Input Power section 3.3.1.).

The globular structures were still present after treatments at 0.4 mbar, however at 0.6 mbar the microplatelet structures began to grow. Eventually at 0.8 mbar the microplatelet structure was the dominant feature of the oxide film.

3.3.3. Time of Reaction

The oxidation reaction times studied ranged from 1 min to 2 hrs. The parameters held constant throughout this study were rf power = 15 W, pressure = 0.8 mbar and position of the foil = 8-9 cm from the live electrode.

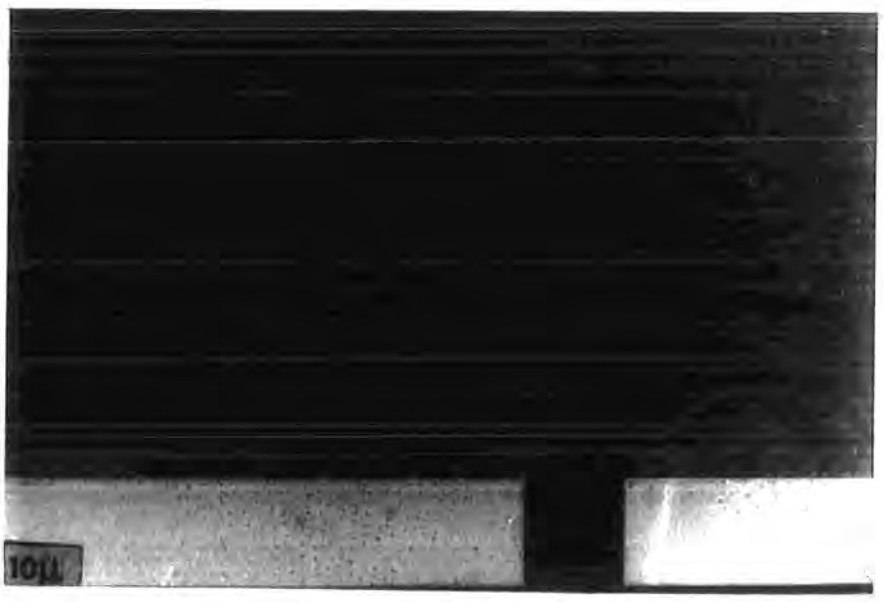

TIME OF REACTION = 1 min (scale 10µm = 1.5cm)

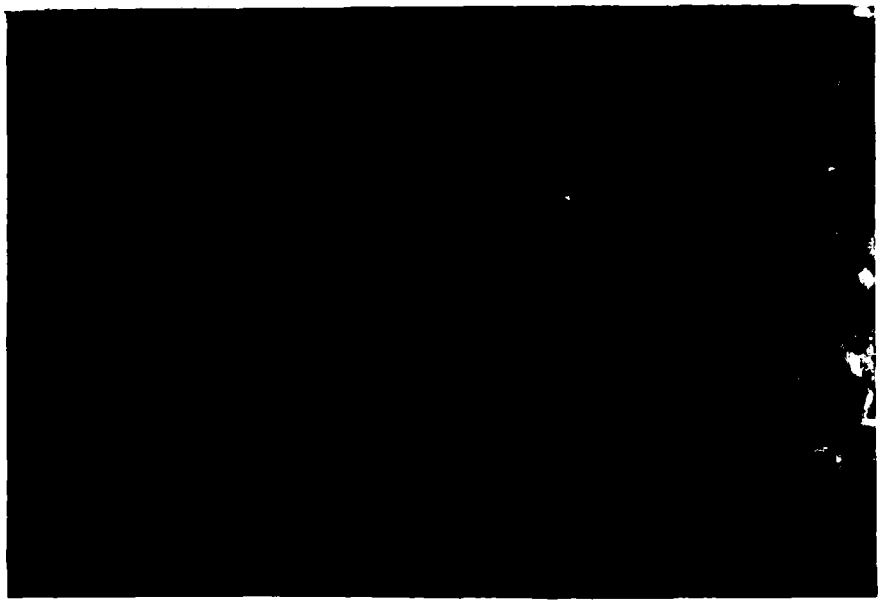

TIME OF REACTION = 30 min (scale 10μm = 1.5cm)

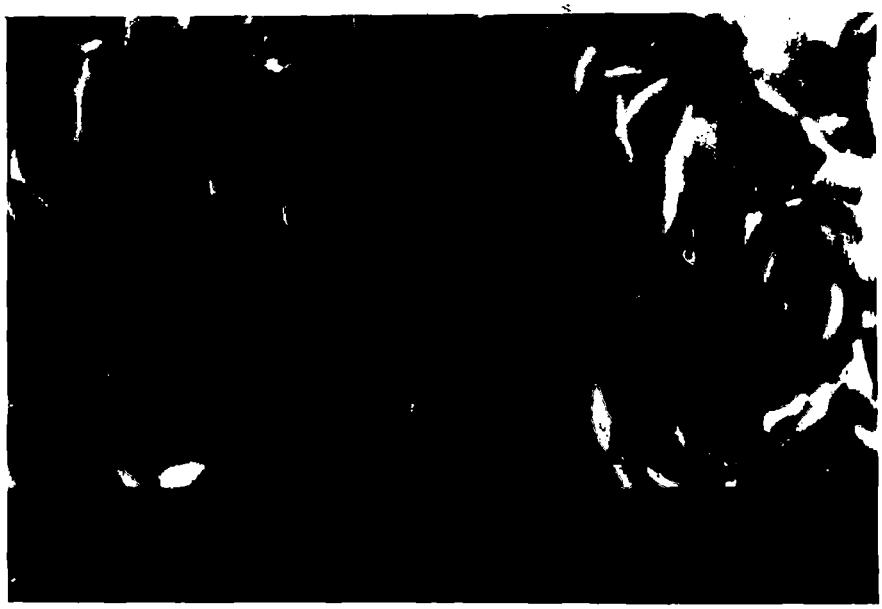

TIME OF REACTION = 1 hr (scale 10μm = 1.5cm)

TIME OF REACTION = 2 hr (scale 10μm = 1.5cm)

Oxidation treatment (1 min.) of the foil, produced a relatively smooth oxide surface. The only significant new surface features were small cracks apparent within the oxide film.

Gradual nucleation and enhanced growth of the microplatelets occurred between 15 min. and 1 hr. Longer exposure times led to sintering of the microplatelets and thus a loss of potential surface area.

All the above results checked for reproducibilty at least twice.

3.3.4. Position of the Foil with Respect to the Live Electrode

The foil positions studied were between zero and 17 cm from the live electrode. All other parameters were held constant i.e. power = 15 W, pressure = 0.8 mbar, time of reaction = 30 min.

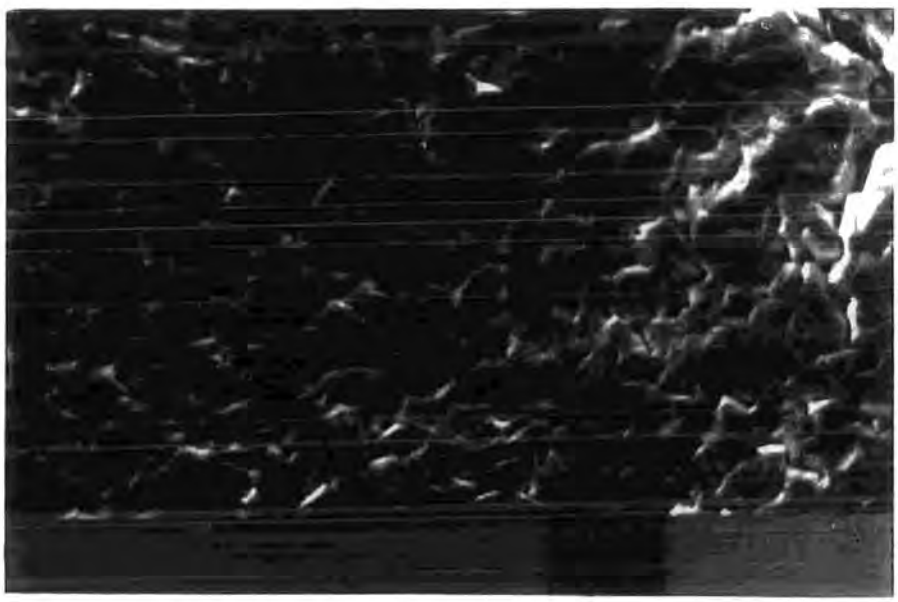

POSITION OF THE FOIL = 0-1 cm (scale 10μm = 1.5cm)

POSITION OF FOIL = 4-5 cm (scale 10μm = 1.5cm)

POSITION OF FOIL = 8-9 cm (scale 10μm = 1.5cm)

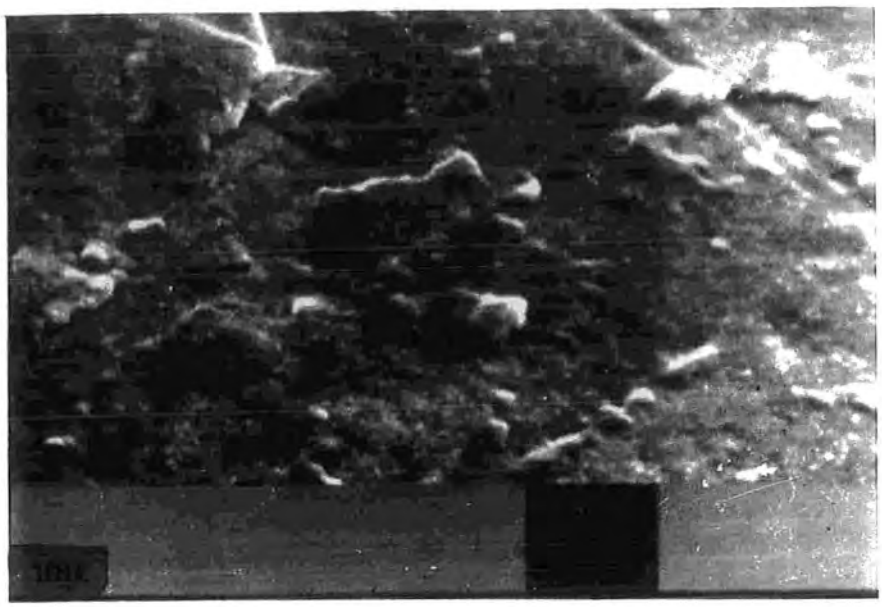

POSITION OF FOIL = 12-13 cm (scale 10μm = 1.5cm)

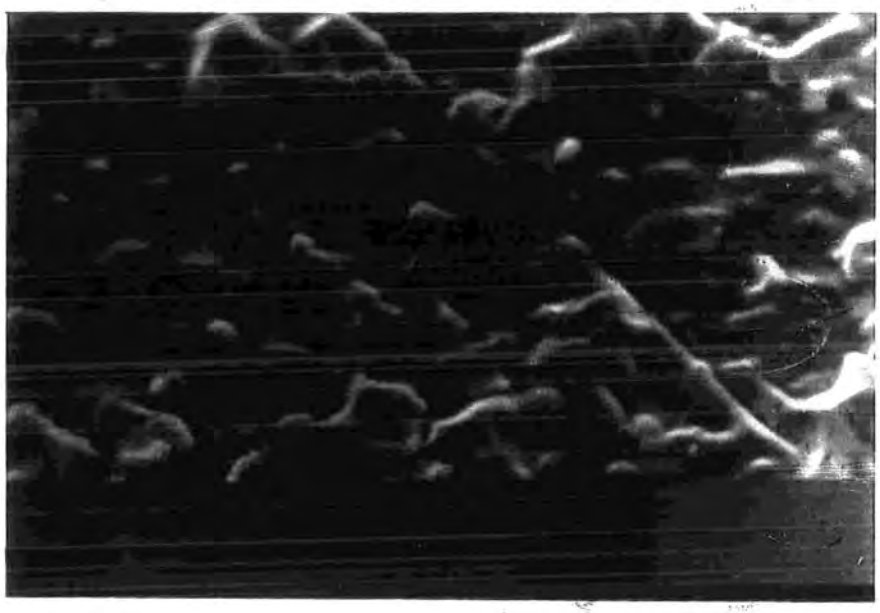

POSITION OF FOIL = 16-17 cm (scale 10μm = 1.5cm)

At distances of 0-5 cm from the live electrode, the surface was composed of globular structures, suggesting again that extensive sintering had occurred.

Increasing the distance further leads to growth of the more favored microplatelets. However at distances greater than 12 cm the surface appears to be relatively smooth with only small mounds present.

All the above results were checked for reproducibilty at least twice.

3.3. 5. Orientation of the Foil

The orientations of the foil sample studied were :

(a) perpendicular to the gas flow (both sides analysed)

and **(b) parallel to the gas flow (both sides analysed).**

A pyrex holder was used to mount the silver vertically (see page 63):

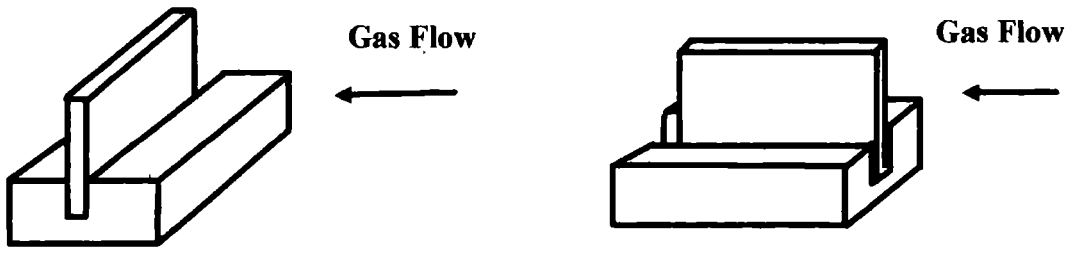

Perpendicular To Gas Flow

Parallel to Gas Flow

Figure 3.3. Orientation of silver foils with respect to the gas flow.

DISTANCE FURTHEST FROM BASE (scale 10μm = 1.5cm)

SECOND FURTHEST DISTANCE (scale 10μm = 1.5cm)

3.4. Discussion

Low pressure, non-equilibrium oxygen plasmas consist of molecular oxygen, ozone, atomic oxygen, ions, electrons and a broad continuum of electromagnetic radiation [15, 34]. The most abundant species is the background gas in the excited state[35], predominantly O_2 ($a^1\Delta_g$) [36] and ($b^1\Sigma_g$) [37]. Their energies lie approximately 0.98 eV above that of ground state molecular oxygen [36,37]. However atomic oxygen is thought to be the most abundant reactive component [34,38]. Altering the plasma parameters (stated within the results section) can induce changes in the concentration of all the species present within an oxygen plasma [34].

The atomic oxygen species present within rf. discharges are ^3P, ^1D and ^1S (**see (1)**) [39, 40, 41]. The ground state atomic oxygen can be produced by electron impact dissociation at approximately 4.5 eV, which corresponds to the dissociation energy of molecular oxygen [38].

(1) $O_2 + e^- \longrightarrow O(^3P) + O(^3P)$ **λ = < 244 nm (via a forbidden absorption to the $^3\Sigma_u^-$)**

$\longrightarrow$ $O(^3P) + O(^1D)$ **λ = <175.9 nm (via absorption in the Schumann Runge continuum)**

$\longrightarrow$ $O(^3P) + O(^1S)$ **λ = 134.2 nm (via absorption in the Rydeberg Series)**

One important emission line from atomic oxygen is the 777 nm emission, produced from the ^3P to ^3S transition, which is used in Laser Induced Fluorescence (LIF) studies [42]. The concentration of atomic species depends upon the extent of homogeneous and heterogeneous recombination occurring within the discharge [43]. Both of these depletion reactions lead to the formation of molecular oxygen and become more prevelant as the atomic oxygen concentration rises [43]. Photon absorption by ground state molecular oxygen can also result in atomic species [44].

The major charged component, though quite small in concentration when compared to that of atomic oxygen, is the O_2^+ molecular ion [37]. The production of this ion is the result of either electron or photon induced molecular ionisation reactions (**see (2)**) [34].

(2) $O_2 + e^- \longrightarrow O_2^+ + 2e^-$

The molecular ion is the most abundant positively charged species, due to its lower ionisation energy of 12.2eV, when compared to that for atomic oxygen which is 13.5 eV [45]. This ion is thought to be responsible for ion bombardment of substrates placed within an oxygen plasma [29]. However, the concentration of this species is again dependent upon the plasma conditions chosen [34, 29].

Due to oxygen being an electronegative molecule, the abundance of negative ions, within an oxygen plasma, can often be quite high and may even exceed the number of electrons [46]. The negative ion species often encountered are O^- (E_a = 1.46 eV)[47], O_2^- (0.44 eV)[47] and O_3^- (E_a = 2.10 eV)[47]. However, the involvement of

these reagents in plasma/surface chemistry will be negligible due to their repulsion from the negatively biased substrate [15].

Ozone, another reactive constituent found within oxygen plasmas, is produced by reaction of an atomic species with the background gas (**see (3)**) [37].

(3) $O + O_2 + M \longrightarrow O_3 + M$

(**M** = 3rd body component)

However ozone concentrations are thought to be relatively small (0.3%), within low pressure rf oxygen discharges [35].

Other reactions can also produce the components stated within the previous few paragraphs, such as ion-ion recombination [34], ion neutralisation [34], electron-ion neutralisation etc.

The other major component within a plasma are the electrons, and these are responsible for most of the gaseous chemistry occurring within such an environment. They possess energies typically within the range of 1-20 eV and are present in concentrations of approximately 10^9 - 10^{11} cm^{-3} [48].

Graph 3.1 summarises the energies associated with the production of the discharge species.

As for the optical properties of the oxygen plasma and how these are effected by changing the plasma parameters, it was observed that as the pressure was increased or the rf power was decreased the plasma became smaller. In fact the plasma would shrink towards the live electrode. As for decreasing the gas pressure or increasing the rf power the plasma glow would grow from the live electrode to the earthed. It was

observed that the plasma would extend from the live to the earthed electrode at powers of 50W at 0.6 mbar. Thus for the optimum plasma conditions for growth of the microplatelets the plasma glow extended to approximately 10-11 cm form the live electrode.

It was also noted that within the oxygen plasma there appeared to be different glow regions with a white glow being present near the live electrode of approximate dimensions of 0-3 cm depending on the plasma conditions. Extending form this white region was a pink glow which would encompass the rest of the plasma glow for the conditions chosen e.g. the whole plasma glow may be 11 cm, the white region may be 0-2 cm and the pink region would then appear to cover the distances of 2-11 cm and would become dimmer towards the 11 cm mark.

Placement of a metallic substrate within a plasma environment, results in the surface biasing negatively, due to the greater mobility of the less massive electrons [2, 15, 34]. A plasma sheath is thus formed, which can possess voltages ranging from 0-50 eV.

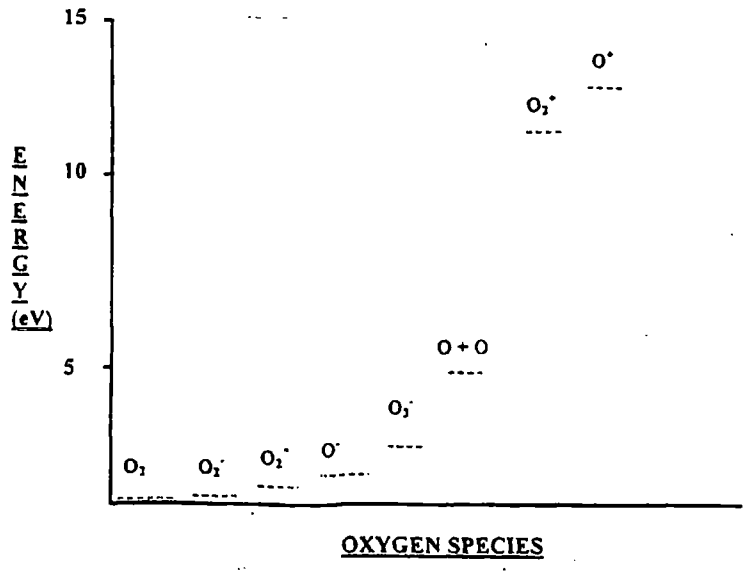

Graph 3.1. Energies at which oxygen species are produced within an rf plasma.

Increasing the rf power or decreasing the gas pressure, leads to several changes within the plasma. These are [34,35]:

(a) increase in the average electron energy,

(b) increase in the ionisation rate,

(c) increase in the dissociation rate,

(d) the sheath potential becomes larger,

(e) more ion bombardment of the substrate,

(f) greater photon flux within the plasma and to the sample (a 50 W plasma is more luminescent than a 15 W).

The different morphologies obtained by decreasing the gas pressure, or increasing the rf power, can be linked to changes in these parameters.

Increasing the time of the plasma treatment leads to the growth of microplatelets due to the longer exposure of the substrate to the reactive component(s). A typical microplatelet size distribution of the length of the microplatelets for 30 minute oxidation treatment is shown below:

In moving the substrate away from the live electrode the trend is as follows:

cluster growth ⟶ *microplatelet formation* ⟶ *no microplatelet growth.*

Varying the orientation of the foil with respect to the gas flow, produced no change in the surface morphology. However, on descending the foil's surface, a

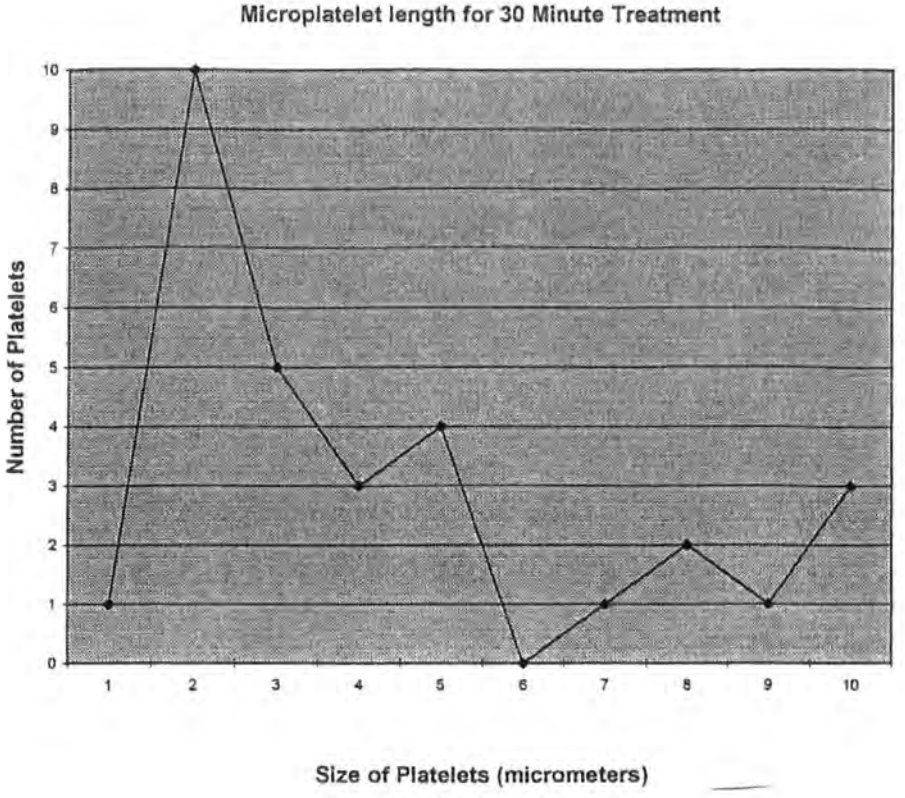

transformation from the high aspect ratio microplatelets to a relatively smooth surface occurs. This suggests that there maybe a link between the surface textures obtained and the concentration of a reactive component or fluctuations in the sheath potential.

There are three possible mechanisms that explain the formation of such structures when the plasma parameters, stated within the experimental section, are changed. They are as follows:

(a) chemical or physical etching [49],

(b) plasma induced facetting [19]

and (c) plasma induced thin film growth [26].

The etching phenomena can possibly be ruled out, as it would be expected from the time study, that the structures would continue to grow with time, as ion

assisted etching continued [49]. This is not the case, as can be seen from the two hour study (see time section 3.3.3.) where the nanoplatelet structures begin to collapse.

Plasma induced facetting involves preferential erosion of a specific crystallographic face within the silver oxide, by either ion bombardment or reaction with atomic oxygen, to produce a volatile component [14]. It differs from etching in this last respect and thus is a more specific process. However again this appears to be unlikely as the sides of the platelets are randomly orientated suggesting no direct link with the erosion of certain faces [31].

The more probable mechanism appears to be a form of plasma induced thin film growth. This film will be produced predominantly by reaction of the polycrystalline silver with atomic oxygen (generated by the plasma) and resulting in the probable formation of Ag_2O and AgO [31]

$$4\,Ag + O_2 \longrightarrow 2\,Ag_2O \quad (13)$$

$$2Ag + O_2 \longrightarrow 2\,AgO \quad (13)$$

As has been stated previously when a substrate is placed within an oxygen plasma, a negative bias forms on it [15]. The formation of this bias means that a field gradient will exist across the growing oxide film [50]. From the postulated mechanisms stated, the thin film formation and consequent structural formation, may be due to the migration of either neutral or charged silver atoms. If the species were charged then it would be expected that the negative bias upon the samples surface would attract any Ag^{n+} species (present within the oxide or produced by vacuum UV ionisation) [51]. These positive ions would migrate through the layer to the surface [52,53], where they will encounter more atomic oxygen and be oxidised. Neutral migration is also

possible, but this process would not be facilitated to the same extent by the charge accumulation upon the surface [51]. Ion bombardment of the oxide layer will assist the diffusion of either of these aforementioned species, by possibly forming point defects and dislocations within the oxide layer resulting in diffusion pathways of low activation energies [2]. This diffusion process may result in the formation of the roughened surfaces observed. The above explanation seems to confirm the results observed whereby increasing the rf input power (i.e. enhancing the sheath potential) causes the surface to take on a clustered appearance. However at lower rf powers the diffusion process appears to be more selective, thus the reasoning for the formation of the microplatelets.

Increasing the reaction time would allow significantly more of the diffusing species to reach the surface and thus explains why the microplatelets grow gradually for longer treatment times.

Moving the foil further away from the live electrode would also indicate that the sheath potential plays an important role in the structural growth. This may be due to lower electron energies present at 8-9 cm from the live electrode, compared with those at distances of 1-5 cm where cluster formation is observed on the foils surface. The electrons present beyond 8-9 cm have little energy (indicated by the decay in the glow luminosity and finally extinguishing). Thus, the potential that could possibly build-up on the materials surface will be dependent on the electron energy and hence will decrease in moving away from the electrode. Thus it would be expected, and is indeed observed that microplatelet formation occurs as the silver foil is treated at areas further away from the live electrode (see **Figure. 3.2.**).

The reasoning why a cluster or microplatelet texture may be produced at certain rf powers, can possibly be related to the rate of growth of certain planes within the oxide [54]. Another possible reason for cluster formation is that surface heating of the oxide layer may be occurring as more energy is transferred to the samples surface form the bombarding ions. This would lead to severe sintering of the surface (similar to an icicle melting to form a puddle).

Summary of the Diffusion Mechanism

When a silver substrate is placed within a plasma a negative bias accumulates.

(A)

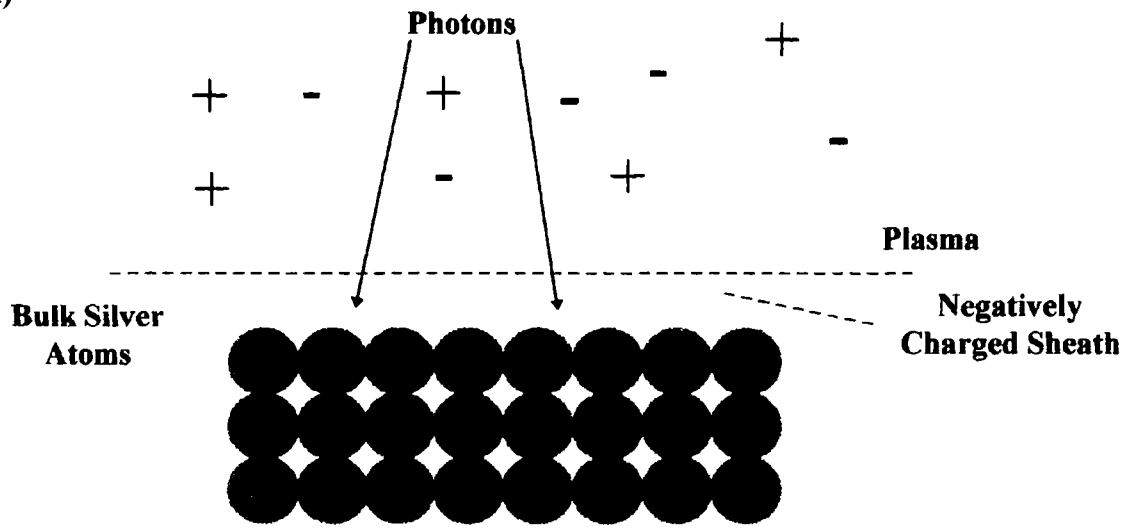

Positive ions (+) are attracted to the sheath, electrons (-) are repelled from it. Neutral radicals react with the silver surface atoms forming an oxide layer. Photons initiate ionisation of silver atoms within the silver oxide layer or within subsurface layers.

(B)

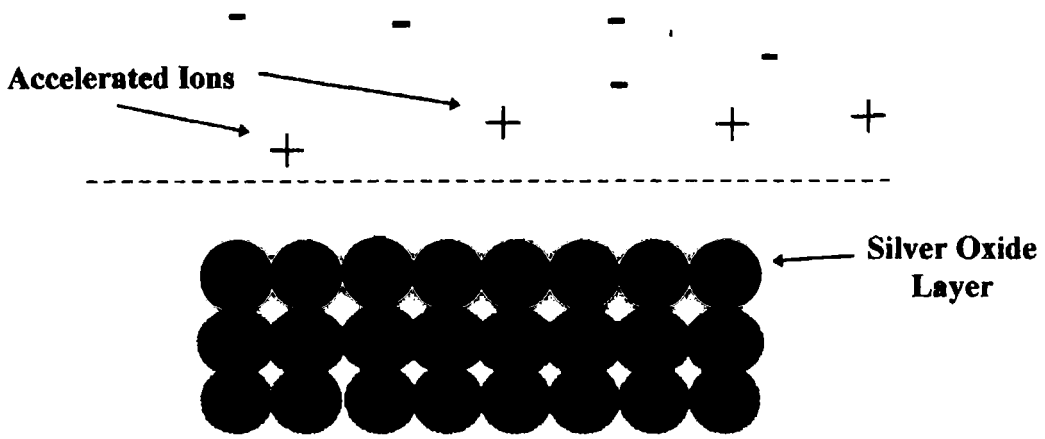

Accelerated ions bombard the surface while simultaneous diffusion of some form of silver charged species occurs within the oxide layer. The diffusing species migrate towards the sheath.

(C)

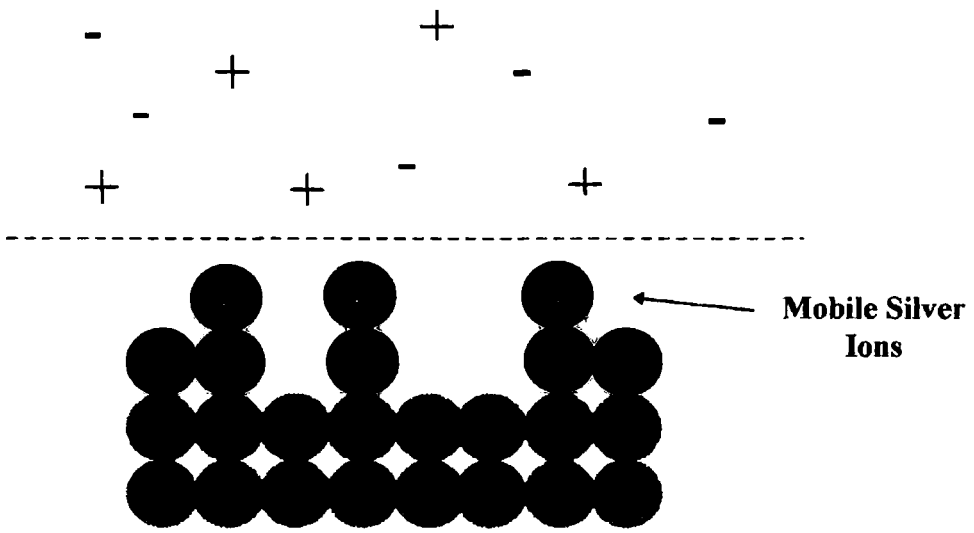

Figure. 3.4. Schematic representation of silver ion/atom diffusion process shown on pages 76 and 78)

3.5. Conclusion

Oxygen plasma treatment of silver foils leads to the formation of a thin mixed silver oxide layer upon it. By varying such parameters as rf input power, gas pressure, time of oxidation reaction, position of foil with respect to the live electrode and orientation of the foil with respect to the gas flow can give rise to a variety of surface textures (microplatelets and clusters). Three mechanisms are suggested as to why these structures are formed, with the more likely being that of thin film growth. A diffusion mechanism is suggested where the active species is thought to be a particular charged silver ion. As to the actual shapes of the structures it is suggested that these are related to the crystallographic properties of the film and are dependent on the growth rate of the planes. From this study it was concluded that the optimum conditions were rf input power of 15W, gas pressure = 0.8 mbar, time of reaction = 30 minutes and positioned 8-9 cm from the live electrode. These conditions gave rise to a surface texture which possessed a highly faceted texture and thus probably a very high surface area.

REFERENCES

1. Coburn, J.W.; **IEEE Plasma Sci. 1991**; 19(6), 1048.
2. Hess, D.W.; **J. Vac. Sci. & Technol. 1990**; A8(3), 1677.
3. Chou, C.H.; Phillips, J.; **J. Appl. Phys. 1990**; 64(5), 2415.
4. Boenig, H.V.; **Plasma Science & Technology**, Cornell Uni. Press: London, 1982.
5. Savage, C.R.; Timmons, R.B.; Lin, J.W.; **Chem. Mater. 1991**; 3(4), 575.
6. Huber, F.; Springer, J.; Mukler, M.; **J. Appl. Polym. Sci. 1997**; 63, 1517.
7. Greiner, J.H.; **J. Appl. Phys. 1974**; 45(1), 32.
8. ***Private Communication*** with Dr. Zdenek Hauptman (University of Durham).
9. Garbassi, F.; Mona, M.; Occhiello, E.; **Polymer Surfaces: From Physics to Technology**: John Wiley & Sons: Chichester, 1996.
10. Stewart, A.D.G.; Thompson, M.W.; **J. Mater. Sci. 1969**; 4, 56.
11. Sumiyama, K.; Wakoh, K.; Oishi, T.; Hohl, G.; Hihara, T.; Sakurai, M.; Yamamuro, S.; Suzuki, K.; **Mater. Trans. JIM 1993**; 34(8), 646.
12. Chaston, J.; **J. Inst. Metals 1945**; 1(74), 23.
13. Bhan, M.K.; Nag, P.K.; Miller, G.P.; Gregory J.C.; **J.Vac. Sc. & Technol. 1994**; A12(3), 699.
14. Hondras, E.D.; Moore A.J.W.; **Acta Met. 1960**; 8, 647.
15. Grill, A.; **Cold Plasma in Materials Fabrication,** IEEE Press: 1994.
16. Wehner, G.K.; **J. Vac. Sci. & Technol. 1985**; A3(4), 1821.
17. Kasukabe, S.; **J. Crys. Growth 1993**; 65, 384.
18. Okabe, T.; Nakagawa M.; **J. Crys. Growth. 1979**; 46, 504.
19. Flytzani-Stephanopoulos, M.; Scmidt, L.D.; **Prog. Surf. Sci. 1979**; 9, 83.
20. Brenner S.S.; **Acta Met. 1956**; 4, 62.
21. Sears, .G.W.; **Acta Met. 1955**; 3, 367.
22. Brenner, S.S.; **Acta Met. 1939**; 7, 677.
23. Bao, X.; Lehmpfuhl, G.; Weinberg, G.; Schlogl, R.; Ertl, G.; **J. Chem. Soc. - Faraday Trans. 1992**; 88(6), 865.
24. Lyubovsky, M.R.; Barelko, V.V.; **J. Catal. 1994**; 149, 23.

25. Chou, C.H.; Phillips, J.; **J. Vac. Sci. &Technol. 1990**; A8(6), 3 941.

26. Vaija, P.; Lahouidak, J.; Durand, J.; Cot, L.; **J. Eur. Ceram. Soc. 1993**; 11, 551.

27. Utsugi, Y.; **Jap. J. Appl. Phys. 1993**; 32(6B), 2969.

28. Bao, X.; Barth, J.V.; Lehmpfuhl, G.; Schuster, R.; Uchida, Y.; Schlogl, R.; Ertl, G.; **Surf. Sci. 1993**; 284, 14.

29. Briggs, G.W.D.; Fleischmann, M.; Lax, D.J.; Thirsk H.R.; **Trans. Faraday Soc. 1968**; 64, 3120.

30. Corish, J.; O'Briain, C.D.; **J. Mater. Sci. 1971**; 6, 252.

31. Chou, C.H.; Phillips, J.; **J. Vac. Sci. & Technol. 1991**; 9, 2727.

32. Briggs, D.; Seah, M.P.; **Auger & X-ray Photoelectron Spectroscopy** Volume 1; John Wiley & Sons: New York, 1990.

33. Goodhew, P.J.; Humphreys, F.J.; **Electron Microscopy & Analysis**; Taylor & Francis: 1988.

34. Hollohan, J.R.; Bell, A.T.; **Techniques & Applications of Plasma Chemistry**; John Wiley & Sons: New York, 1974.

35. Chapman, B.; **Glow Discharge Processes**; John Wiley & Sons: New York, 1980.

36. Shibata, M.; Nakano, N.; Makabe, T.; **J. Phys. D.: Appl. Phys. 1997**; 30, 1219.

37. Shibata, M.; Nakano, N.; Makabe, T.; **J. Appl. Phys. 1996**; 80 (11), 6142.

38. Ichikawa, Y.; Wu, R.L.C.; Kaneda, T.; **J. Appl. Phys. 1990**; 67 (1), 108.

39. Wayne, R.P.; **Principles and Applications of Photochemistry**; Oxford University Press: New York, 1988.

40. Hasson, V.; Nicholls, R.W.; **J. Phys. B At. Mol. Phys. 1971**; 4, 1778.

41. Feoktistov, V.A.; Mukhovatova, A.V.; Popov, A.M.; Rakhimova, T.V.; **J. Phys. D - Appl. Phys. 1995**; 28, 1346.

42. Collart, E.J.H.; Baggerman, J.A.G.; Visser, R.J.; **J. Appl. Phys. 1991**; 70(10), 5278.

43. Elias, L.; Ogryzlo, E.A.; Schiff, H.I.; **Can. J. Chem. 1959**; 37, 1680.

44. Hancock, G.; Toogood, M.J.; **Appl. Phys. Lett. 1992**; 60(1), 35.

45. Filseth, S.V. ; Welge K.H. **J. Chem. Phys. 1969,** 51, 839.

46. Stoffels, E.; Stoffels, W.W.; Vender, D.; Kando, M.; Kroesen, G.M.W.; deHoog, F.J.; **Phys. Rev. E 1995**; 51(3), 2425.

47. Noyes L.; **Photochemistry of Gases,** Reinhold: New York, 1941.

48. Godyak, V.A.; Piejak, R.B.; **Phys. Rev. Lett. 1990**; 65, 996.

49. Vossen, J.L.; Kern, W.; **Thin Film Processes II**; Boston Academy Press: Boston, 1991.

50. Greiner J.H.; **J. Appl. Phys. 1974**; 45(1), 32.

51. Wahl, M.; Wucher, A.; **Nuc. Inst. & Met. in Phys. Res. B 1994**; 94, 36.

52. Sebastian, K.; Frischat, G.H.; **Phys. & Chem. of Glasses 1992**; 33(5), 199.

53. Sears, W.M.; Love D.A.; **Phys. Rev. B 1993**; 47(19), 12973.

54. Atkins, P.W.; **Physical Chemistry 4th Edition**; Oxford University Press: Oxford, 1991.

CHAPTER 4

POWDER DIFFRACTION STUDIES OF PLASMA PRODUCED SILVER OXIDES

4.1. Introduction

Chapter 3 showed that by changing the conditions of an oxygen plasma, various surface textures could be produced. However, the oxides responsible for forming these structures were not established. This is what this chapter aims to achieve.

4.1.1. Structural Chemistry of Silver Oxides

Various silver oxides are known which possess individual physical and chemical characteristics [1]

The two most common oxides encountered are the silver (I) and (I,III) systems [2].

Silver (I) oxide, Ag_2O, is black in colour and has the silver species in the I oxidation state[3]. It has a typical density of 7.143 gl^{-1} and a standard heat of formation of -7.306 kcal mol^{-1} (-30.57 $kJmol^{-1}$) [4]. This oxide is stable up to temperatures of approximately 230°C, above which it decomposes into metallic silver and gaseous oxygen [5]. Its structure consists of a face centered cubic lattice of silver

ions interpenetrated by a body centered cubic order of oxygen ions [2]. The silver-silver and silver-oxygen distances are 3.336 Å and 2.043 Å respectively[2].

Silver (I,III) oxide or AgO (Ag_2O_2) appears black in colour [6] and is stable up to temperatures of approximately 100°C [4]. It has a specific density of approximately 7.44 gl^{-1} [4]. The chemical formula indicates that the oxidation state of the Ag is (II), but this is not the case. There are in fact two distinct silver sites and two silver-oxygen distances corresponding to two different oxidation states - Ag (I) and Ag (III) [7]. The lower oxidation state of the silver exists in a co-linear arrangement with two oxygen ions (Ag-O bond distance = 2.18 Å), while the smaller Ag (III) exists within a square planar arrangement of oxygen ions (Ag-O separation of 2.05 Å) [2]. Due to the greater polarising power of Ag (III), compared with Ag(I), the Ag(III)O distances will tend to be more covalent than for Ag(I)O distances. A schematic of AgO's unit cell is shown below:

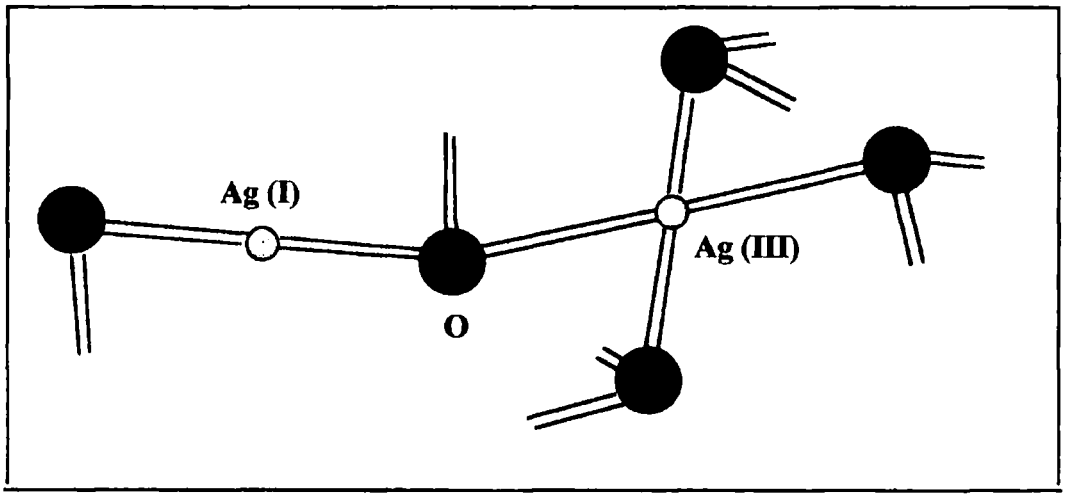

Silver atoms in two different coordination states - co-linear and tetragonal. The silver atoms are the small grey spheres while the black spheres are oxygen atoms.

Another oxide often encountered is Ag_2O_3, frequently produced when silver electrodes are electrochemically treated using KOH [8]. The silver ions present within this oxide are in the (III) oxidation state only [9]. Here the shortest Ag-Ag distance is 3.04 Å, whereas the Ag-O distances are 2.04 Å and 1.98 Å [10].

Oxides where the silver ion is in a lower oxidation state than Ag_2O have also been reported, such as Ag_3O (an anti-Bi structure) [11] and Ag_4O (has a tetragonal arrangement) [12] which have anti Bi structure and tetragonal silver arrangements respectively. Other oxides possible, but which have less information available on them are Ag_3O_4 [13], AgO_4 [14], AgO_2 [15] and AgO_3 [16].

A variety of analytical techniques have been used to obtain physical and chemical information about the above oxides. Some of these are Powder X-ray Diffraction [17], Temperature Programmed Desorption (TPD) [18], Raman Spectroscopy (RS) [19], Infra-red Spectroscopy (IR) [20], Secondary Ion Mass Spectroscopy (SIMS) [21], X-ray Photoelectron Spectroscopy (XPS) [22,23] and various Electrochemical techniques [24].

4.2. Experimental

The plasma oxidised silver foils were produced using the same experimental apparatus and conditions as those stated in Chapter 3 (the orientation results were not analysed). The oxidised samples were fixed to an aluminium or perspex sample holder using a Pritt Glue Stick. Subsequent powder X-ray diffraction was carried out using a Philips powder diffractometer which had a copper X-ray source (energy = 8048eV). The angles over which 2θ was scanned were 4 to 90°, using angle

increments of 0.02° and residence times of the counter at each increment of 2s. The data were collected using an IBM Personal Computer System and a spectrum of intensity against 2θ angles was obtained.

4.3. Results

The results are presented as follows :

(a) **XRD's of standard silver oxides,**

(b) **XRD's of the sample holder and silver foil,**

(c) **XRD's of oxides produced when the rf power is varied,**

(d) **XRD's of oxides produced when the oxygen pressure is altered,**

(e) **XRD's of oxides produced as the time of reaction is varied**

and (f) **XRD's of the oxides produced when the position of the foil with respect to the live electrode is varied.**

The error for all d-values quoted within the tables below was 0.03 Å.

4.3.1. XRD's of Silver Oxide Standards

The two silver oxide standards analysed were Ag_2O and AgO. Data from the other silver oxides (Ag_2O_3, Ag_2O_2 , Ag_3O_4) were obtained from an XRD database.

A perspex holder was used to hold the powder standards. The results were as follows:

A. **Ag_2O - (see spectrum 4.1.)**

2θ ANGLE (DEGREES)	D-SPACING (ÅNGSTROMS)	CRYSTALLOGRAPHIC PLANE
32.74	2.735	<111>
37.98	2.369	<200>
54.8	1.675	<220>
65.3	1.429	<311>
68.6	1.368	<222>

B. **AgO - (see spectrum 4.2.)**

2θ ANGLES (DEGREES)	D-SPACING (ÅNGSTROMS)	CRYSTALLOGRAPHIC PLANE
32.1	2.788	<200>
32.34	2.768	<$\bar{1}$11>
34.22	2.620	<002>
37.22	2.416	<111>
39.44	2.285	<$\bar{2}$02>
52.56	1.741	<020>
53.92	1.700	<$\bar{3}$11>
54.78	1.676	<202>
56.76	1.622	<$\bar{1}$13>
62.90	1.478	<220>
63.72	1.461	<311>
64.16	1.452	<022>
65.62	1.423	<$\bar{4}$02>
66.32	1.409	<113>
67.06	1.396	<$\bar{3}$13> / <400>

67.64	1.385	<$\bar{2}$22>
69.40	1.354	<$\bar{2}$04>
72.00	1.312	<004>
79.32	1.208	<222>
86.46	1.126	<$\bar{1}$31>
88.74	1.102	<$\bar{4}$02> / <$\bar{4}$22>

The planes in the above two standards were matched to the d-spacings from the corresponding oxides within a crystallographic database.

4.3.2. XRD's of the Aluminium Holder and Original Silver Foil

The aluminium sample holder also produced certain diffraction lines, and these were subtracted from all silver oxide diffraction patterns. The diffraction lines associated with the holder are as follows (see **spectrum 4.3.**):

2θ ANGLE (DEGREES)	D-SPACING (ÅNGSTROMS)	CRYSTALLOGRAPHIC PLANES
38.18	2.357	<111>
44.42	2.039	<200>
64.82	1.438	<220>
77.96	1.226	<311>
82.22	1.172	<222>

The original silver foil before plasma oxidation occurs gives rise to the diffraction lines (see **spectrum 4.4.**):

2θ ANGLE (DEGREES)	D-SPACING (ÅNGSTROMS)	CRYSTALLOGRAPHIC PLANES
38.1	2.362	<111>
44.26	2.046	<200>
64.42	1.446	<220>
77.40	1.233	<311>

4.3.3. Silver Foil Cleaned Using a Hydrogen Plasma

A piece of silver foil was cleaned using a hydrogen plasma and subsequently analysed by X-ray powder diffraction. The results were as follows (see **spectrum 4.5.**) :

2θ ANGLE (DEGREES)	D-SPACING (ÅNGSTROMS)	CRYSTALLOGRAPHIC PLANES
37.96	2.370	Ag <111>
44.14	2.052	Ag <200>
64.32	1.448	Ag <220>
77.26	1.235	Ag <311>
81.42	1.182	Ag <222>

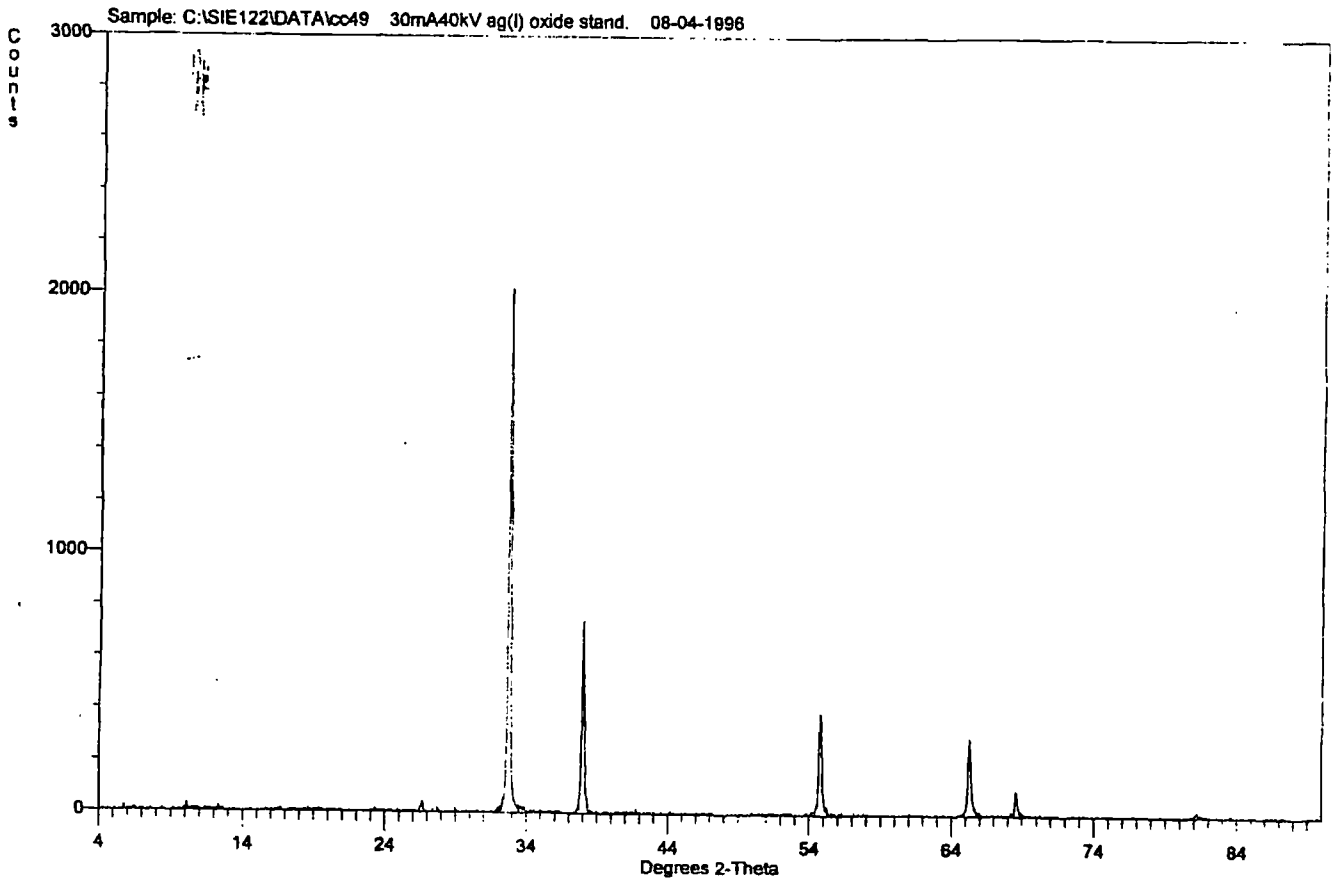

Spectrum 4.1. Powder diffraction of Ag_2O

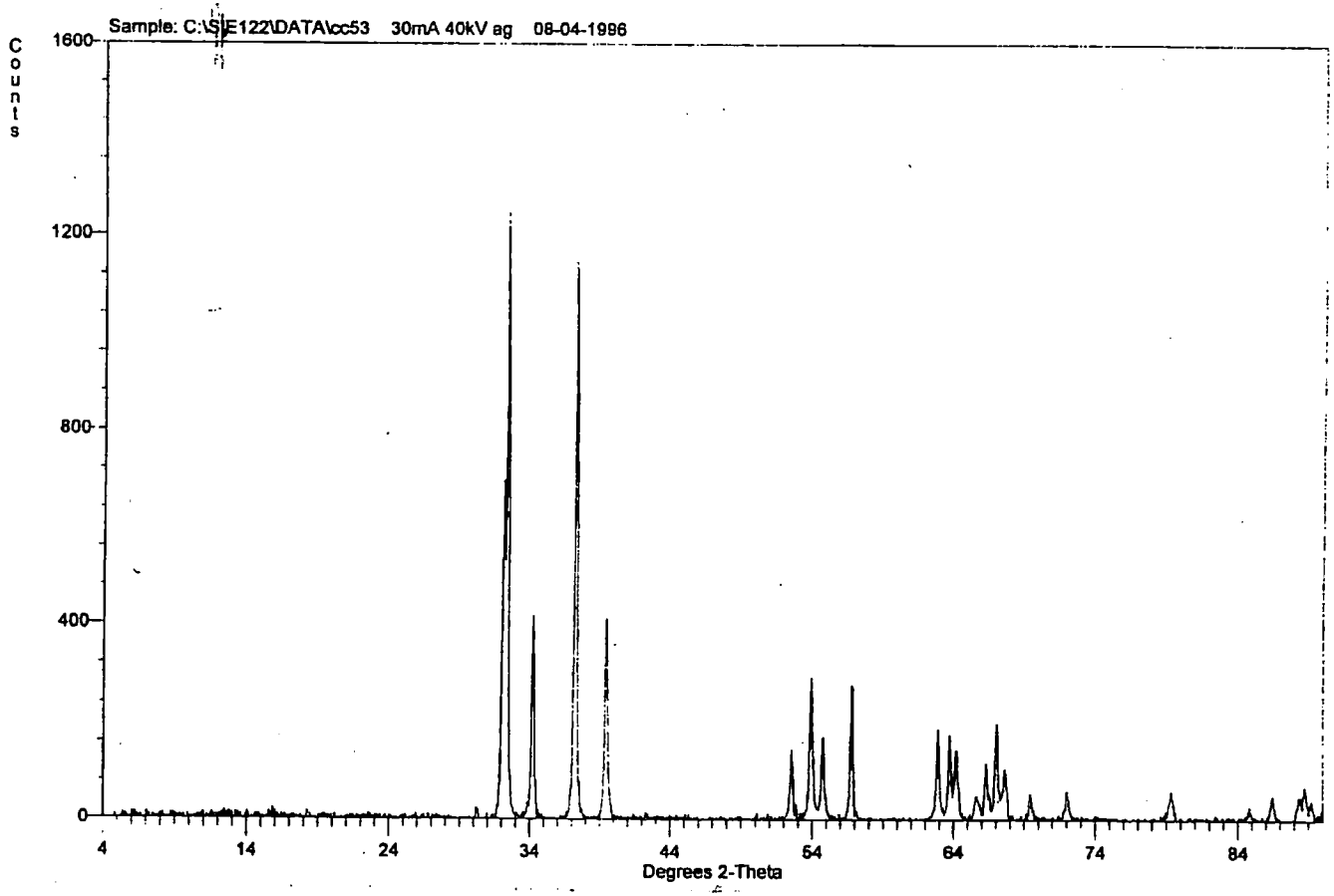

Spectrum 4.2. Powder diffraction of AgO

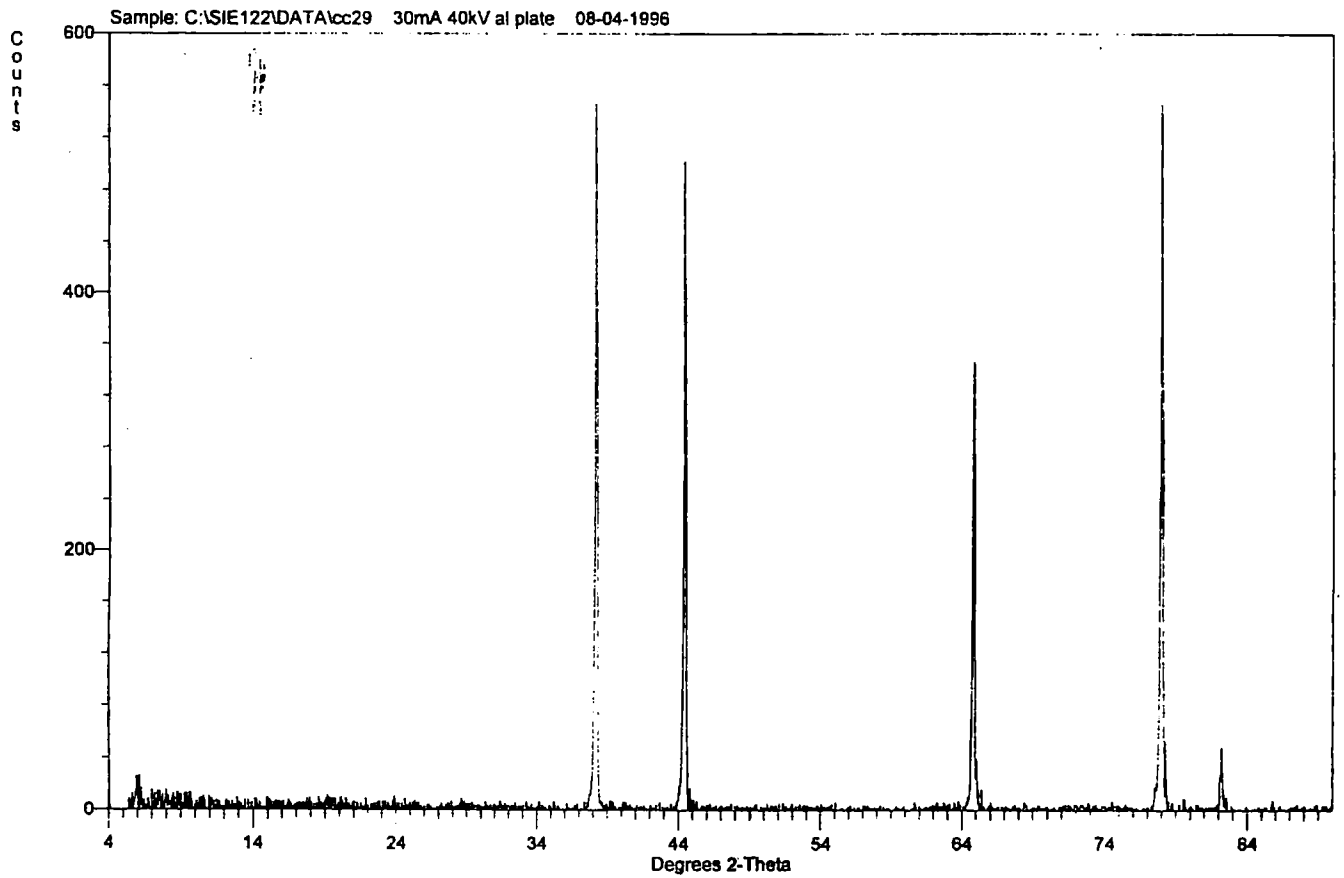

Spectrum 4.3. Powder diffraction of aluminium holder

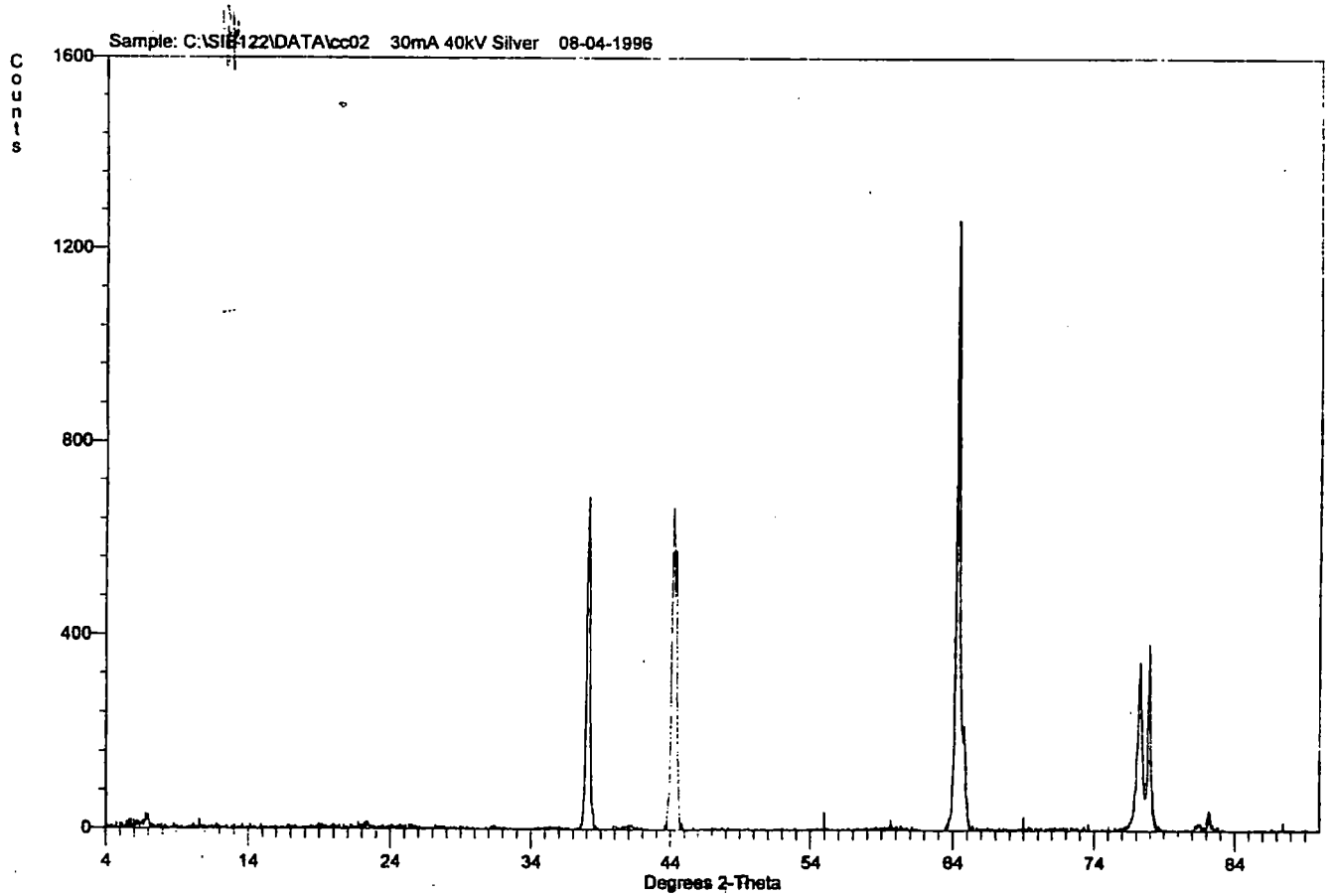

Spectrum 4.4. Powder diffraction of untreated silver foil

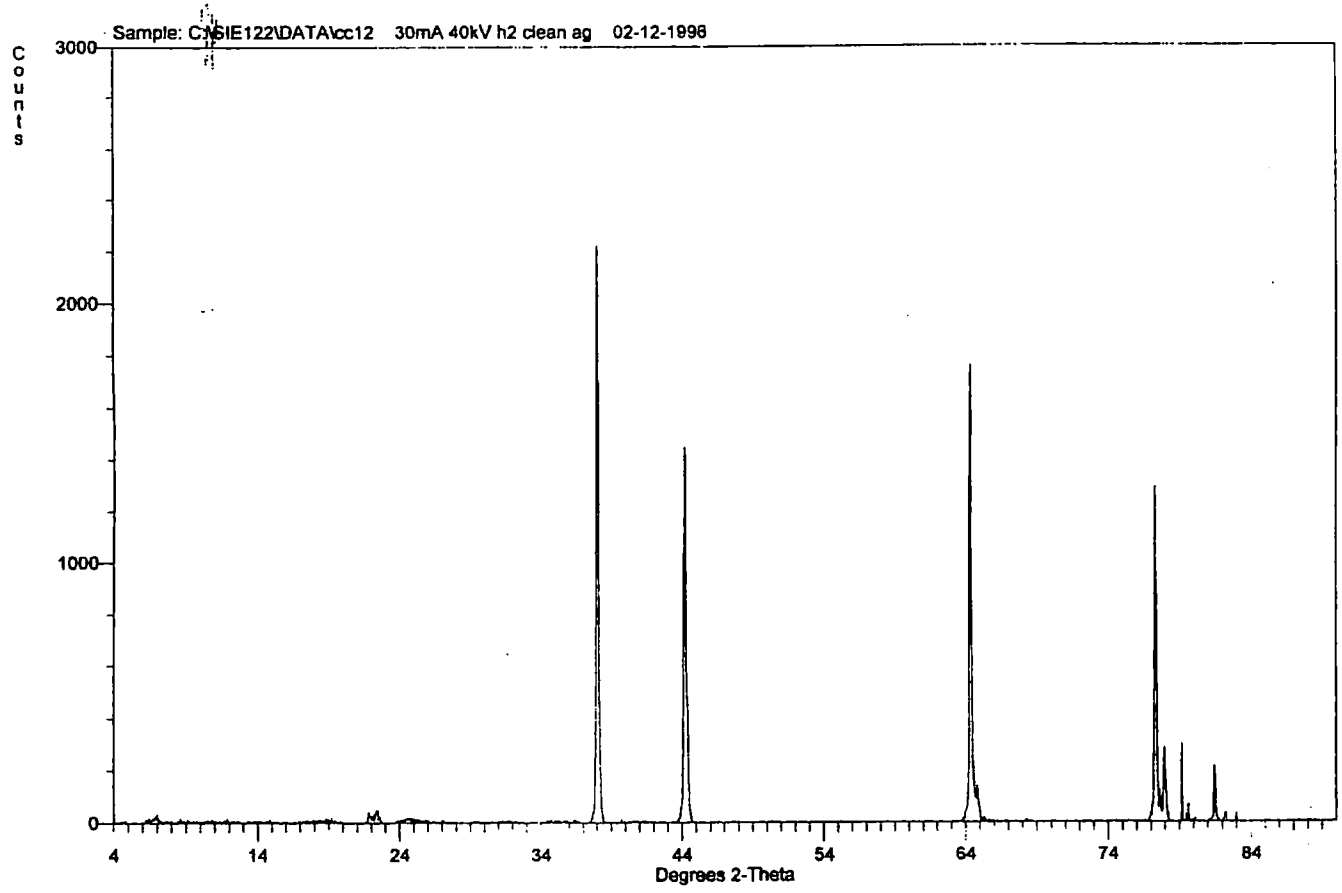

Spectrum 4.5. Powder diffraction of silver cleaned by a hydrogen plasma

4.3.4. The Effects of Plasma Power on Oxide Production

All foils studied were of similar dimensions than those used in the SEM study. The rf powers studied were 15, 20, 25, 30 and 50 W. The other parameters studied were held constant (see Chapter 3 plasma power results section).

The initial power studied was 15 W and the silver/silver oxide planes present were (see **spectrum 4.6.**):

2θ ANGLE (DEGREES)	D-SPACING (ÅNGSTROMS)	CRYSTALLOGRAPHIC PLANES
32.22	2.778	AgO <$\bar{1}$11> / <200>
32.60	2.747	Ag_2O <111>
34.14	2.628	AgO <002>
37.08	2.425	AgO <111>
38.2	2.356	Ag <111>/Al/Ag_2O <200>
39.32	2.291	AgO <$\bar{2}$02>
44.46	2.038	Ag <200>/Al
52.46	1.744	AgO <020>
53.48	1.713	AgO <$\bar{3}$11>
56.66	1.625	AgO <$\bar{1}$13>
64.1	1.453	AgO <022>
64.38	1.447	Ag <220>
77.32	1.234	Ag <311>
79.08	1.211	AgO <222>

The main oxide produced at this plasma power is AgO, however planes corresponding to the oxide Ag_2O are also present. No significant lines corresponding

to other oxides were observed. The aluminium lines have not been included in the above table except for those which overlap with silver peaks.

The powder diffraction pattern for the 20 W plasma treatment is practically the same as that for the 15 W treatment (**see spectrum 4.6.**).

Further increases in rf power gave rise to patterns where the 32.58° (Ag_2O) peak becomes more prominent than that at 32.18° (AgO <111>). Other peaks which appear to become more prominent with increasing rf power are at 54.6° (AgO <202> or Ag_2O <220>) and 55.2° (either AgO <202> or Ag_2O <220>) (**see spectrum 4.6.**).

Increasing the power to 30 and finally 50 W produces a diffraction pattern similar to that of the standard Ag_2O. The major regions where peak intensity changes occur are at 32.56° (Ag_2O <111>) and between 53-57° - where eventually the only diffraction peak present is located at 54.7°. The diffraction peaks present after the 50 W plasma treatment are tabulated below (**see spectrum 4.6.**):

2θ ANGLE (DEGREES)	**D-SPACING (ÅNGSTROMS)**	**CRYSTALLOGRAPHIC PLANES**
32.66	2.742	Ag_2O <111>
37.90	2.347	Ag <111>/Ag_2O <200>
54.70	1.678	Ag_2O <220>/AgO <200>
65.22	1.430	Ag_2O <311>

All results produced within this section were at least reproduced twice.

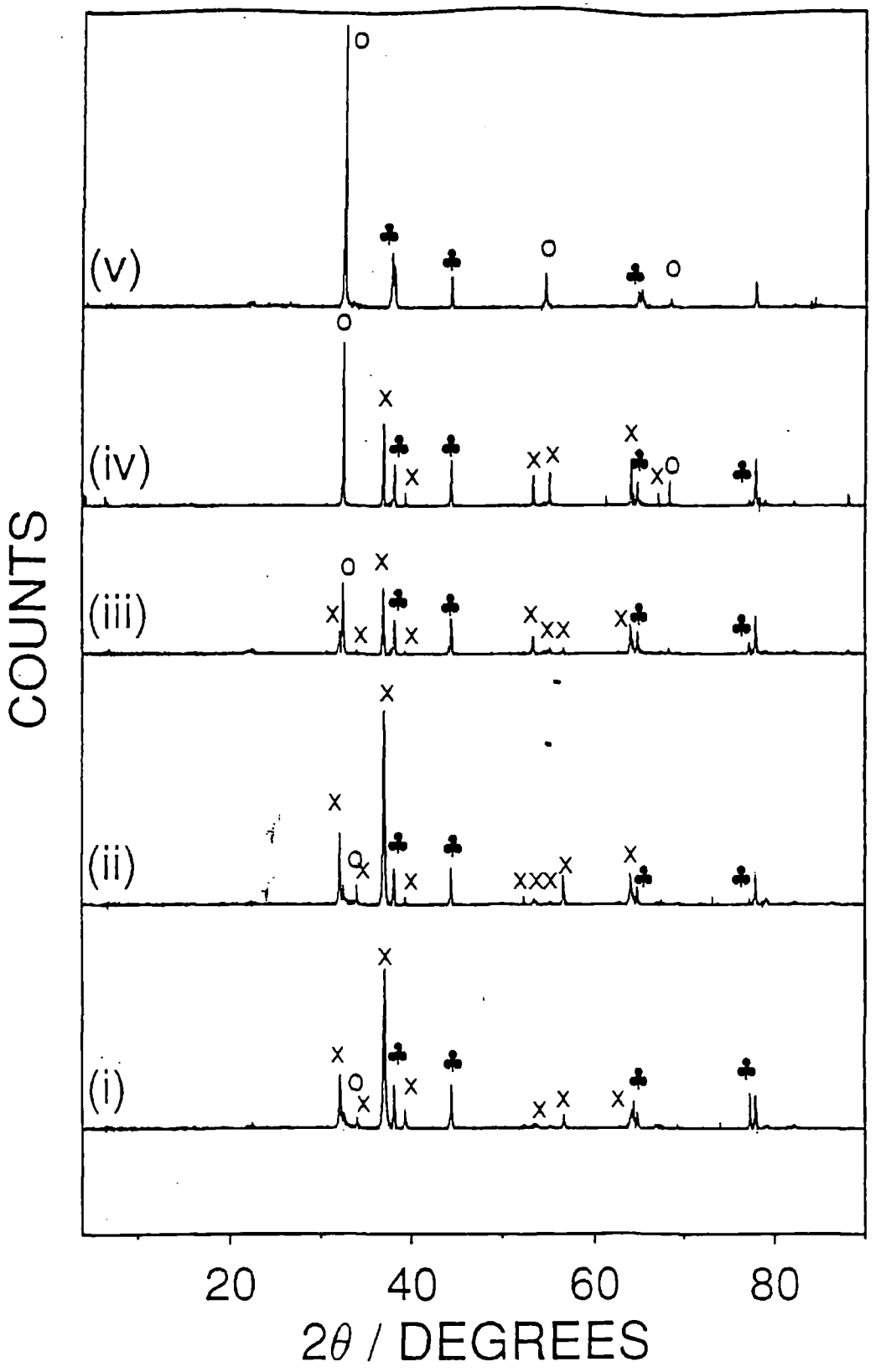

Spectrum 4.6. Diffraction Patterns for the Power Study - (i) 15 W (ii) 20 W, (iii) 25 W, (iv) 30 W, and (v) 50 W (Ag lines = ♣, AgO lines = x and Ag_2O lines = o (aluminium lines not labelled)

4.3.5. Effects of Gas Pressure on Oxide Production

The gas pressures studied were between 0.2 and 0.6 mbar. All other variables were held constant (see results section in chapter 3).

At 0.2 mbar the crystallographic planes present were (see **spectrum 4.7.**):

2θ ANGLES (DEGREES)	D-SPACING (ÅNGSTROMS)	CRYSTALLOGRAPHIC PLANES
32.52	2.753	Ag_2O <111>
37.76	2.382	Ag <111>/Ag_2O <200>/Al
54.54	1.683	Ag_2O <220>/AgO <202>
65.10	1.433	Ag_2O <311>

At 0.2 mbar the powder diffraction pattern is characteristic of Ag_2O.

Increasing the pressure to 0.4 mbar produces additional peaks at 37.02° (AgO <111>), 53.42 (AgO <$\bar{3}$11>), 55.16° (AgO <202>), 64.06° (AgO <022>) and 64.32° (Ag <220>) within the spectra (see **spectrum 4.7.**).

At 0.6 mbar treatments, the diffraction pattern obtained corresponds to AgO with Ag_2O also present. The 0.6 mbar spectra is similar to the 0.8 mbar treatment. The 0.8 mbar treatment diffraction planes are listed below (see **spectrum 4.7.**):

2θ ANGLE (DEGREES)	D-SPACING (ÅNGSTROMS)	CRYSTALLOGRAPHIC PLANES
32.12	2.787	AgO <200>
32.70	2.739	Ag_2O <111>
33.98	2.638	AgO <002>
36.98	2.431	AgO <111>

37.94	2.372	Ag <111>/Al/Ag_2O <200>
39.24	2.296	AgO <$\bar{2}$02>
44.12	2.053	Ag <200>/Al
52.34	1.748	AgO <020>
53.38	1.716	AgO <$\bar{3}$11>
56.56	1.627	AgO <$\bar{1}$13>
63.98	1.455	AgO <022>
64.26	1.449	Ag <220>/Al
67.44	1.389	AgO <$\bar{2}$22>
77.24	1.235	Ag <311>/Al

All results produced, in the diffraction study on the effects of gas pressure on the silver oxides formed, were at least reproduced twice.

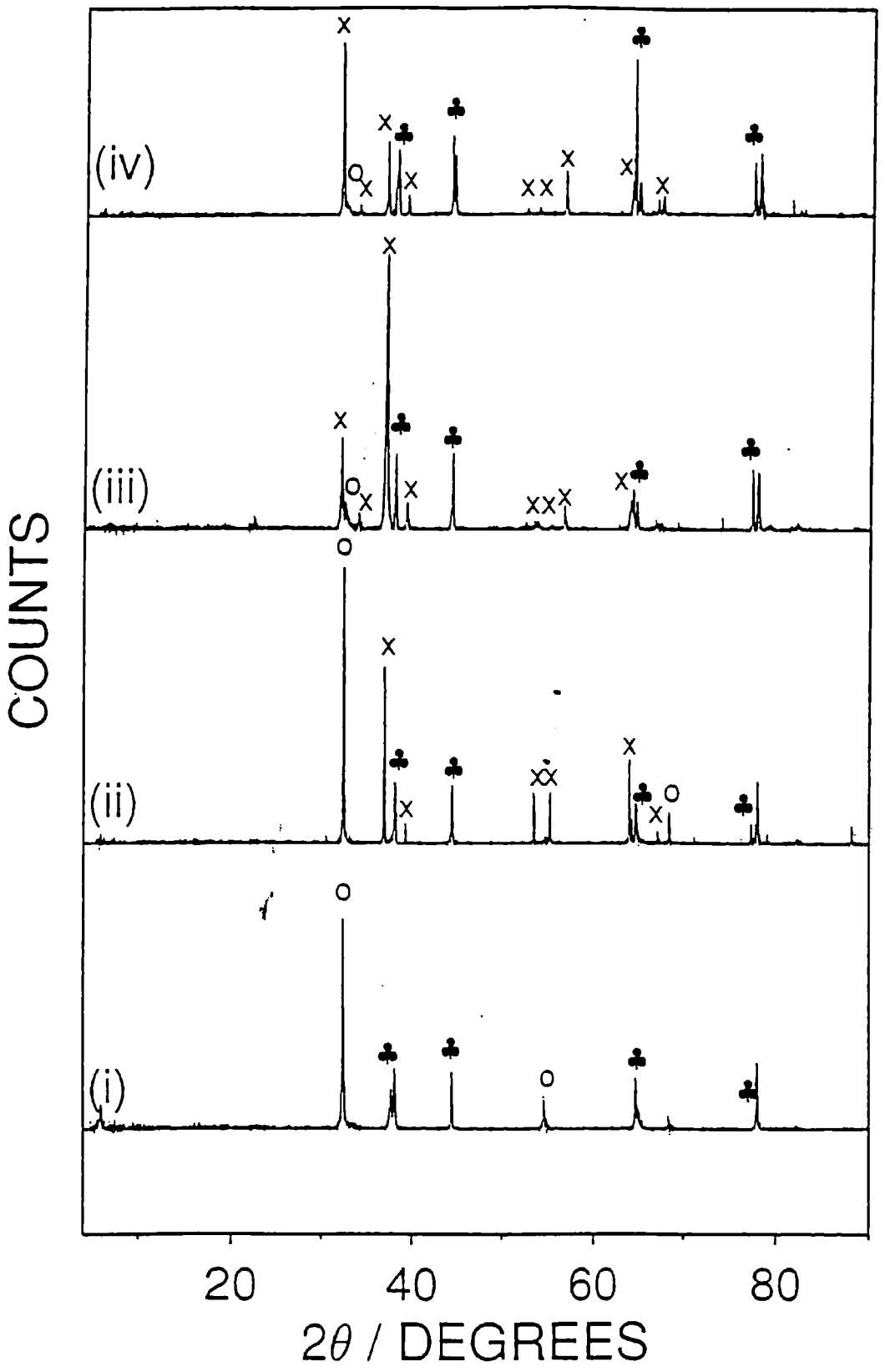

Spectrum 4.7. Pressure study diffraction patterns - (i) 0.2 mbar, (ii) 0.4 mbar, (iii) 0.6 mbar and (iv) 0.8 mbar (Ag lines = ♣, AgO lines = x and Ag_2O lines = o (aluminium lines are not labelled)).

4.3.6. Effects of the Time of the Oxidation Reaction on the Oxides Production

All the results produced within this section were at least reproduced twice. The oxidation times studied for this investiagtion were between 1 min. and 2 hrs. The variables held constant are the same as those detailed in the results section of Chapter 3 for the same time study, but where SEM was the analytical instrument of choice.

Initially 1 min. oxidation times were looked at, but this gave rise to very little diffraction detail. The only significant peak, which was indicative of AgO and Ag_2O, as well as species of the formula $Ag_{n>2}O$ was located a approximately 32-33° (see **spectrum 4.8.**). However increasing the time to 5 min. leads to further oxide diffraction planes appearing due to an increase in the extent of oxidation. These are tabulated below (see **spectrum 4.8.**):

2θ ANGLE (DEGREES)	D-SPACING (ÅNGSTROMS)	CRYSTALLOGRAPHIC PLANES
32.14	2.785	AgO <200>
32.56	2.750	Ag_2O <111>
32.98	2.716	Not Known
33.38	2.684	Not Known
34.04	2.634	AgO <002>
36.98	2.431	AgO <111>
38.02	2.367	Ag <111>/Al/Ag_2O <200>
39.18	2.299	AgO <202>
44.18	2.050	Ag <200>/Al
53.46	1. 741	AgO <$\bar{3}$11>
56.68	1.624	AgO <$\bar{1}$13>
64.32	1.448	Ag <220>/Al

77.28	1.235	Ag <311>/Al

After treating for 15 min. the diffraction pattern is similar to that observed before (see **spectrum 4.8.**).

Treatments of 30 min., 1 and 2 hrs produced very similar spectra. For the 2 hr. oxidation the data obtained is tabulated below (see **spectrum 4.8.**):

2θ ANGLE (DEGREES)	**D-SPACING (ÅNGSTROMS)**	**CRYSTALLOGRAPHIC PLANES**
32.16	2.783	AgO <200>
32.56	2.750	Ag_2O <111>
34.04	2.634	AgO <002>
37.02	2.428	AgO <111>
38.06	2.350	Ag <111>/Al/Ag_2O<200>
39.26	2.295	AgO <$\bar{2}$02>
44.14	2.052	Ag <200>/Al
52.38	1.747	AgO <020>
53.42	1.715	AgO <$\bar{3}$11>
55.14	1.666	AgO <113>/Ag_2O <220>
56.58	1.627	AgO<$\bar{1}$13>
64.04	1.454	AgO <022>
64.28	1.449	Ag <311>/Al
66.86	1.399	AgO <400>/<$\bar{3}$13>
67.46	1.388	AgO <$\bar{2}$22>/Ag<222>
77.26	1.235	Ag <311>

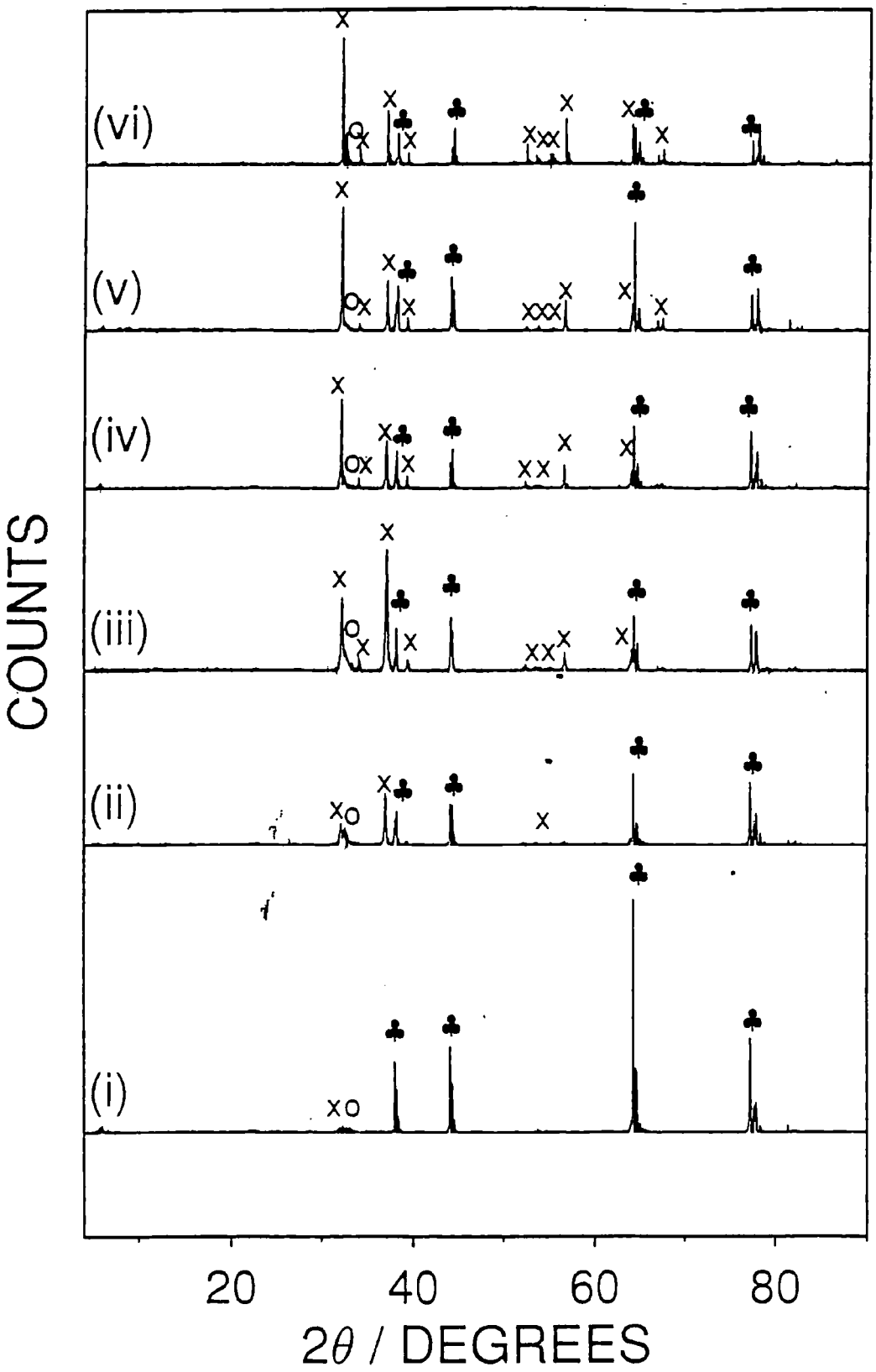

Spectrum 4.8. Time study diffraction patterns - (i) 1 min., (ii) 5 mins., (iii) 15 mins., (iv) 30 mins., (v) 1 hr. and (vi) 2 hrs. (Ag lines = ♣, AgO lines = x and Ag_2O lines = o (aluminium lines are not labelled)).

4.3.7. Effects of Position of Foil With Respect to the Live Electrode on Oxide Production

The results which follow within this section were all reproduced at least twice. The positions of the foils placed within the reactor were between zero and 17 cm. All other variables were held constant (see results section in Chapter 3 dealing with the efects of position of the foil within the reactor and the subsequent effects of the treatment on its morphology).

For the foil placed 0-1 cm from the live electrode the data obtained is as follows (see **spectrum 4.9.**):

2θ ANGLES (DEGREES)	D-SPACING (ÅNGSTROMS)	CRYSTALLOGRAPHIC PLANES
32.6	2.747	Ag_2O <111>
55.24	1.663	Ag_2O <220>
64.1	1.453	AgO <022> / Ag <220>
68.4	1.372	Ag_2O <222>/AgO <104>

Increasing the distance further to 4-5 cm gave rise to new diffracting planes at 32.18° (AgO <$\bar{1}$11> or <200>), 32.82° (Not Known), 37.02° (AgO<111>), 64.32° (Ag <220>), 67.18° (Ag <$\bar{3}$13> or <400>) and 77.28° (Ag <311>) (see **spectrum 4.9.**).

Further increases in distance to 8-17 cm, gave similar diffraction patterns, with the only new diffracting planes being located at 33.98° (AgO <002>), 44.12° (Ag <200>), 52.34° (AgO <020>), 53.38° (AgO <311>$\bar{}$) and 56.68° (AgO <113>$\bar{}$). This indicates that the oxide is probably an AgO/Ag_2O mix (see **spectrum 4.9.**).

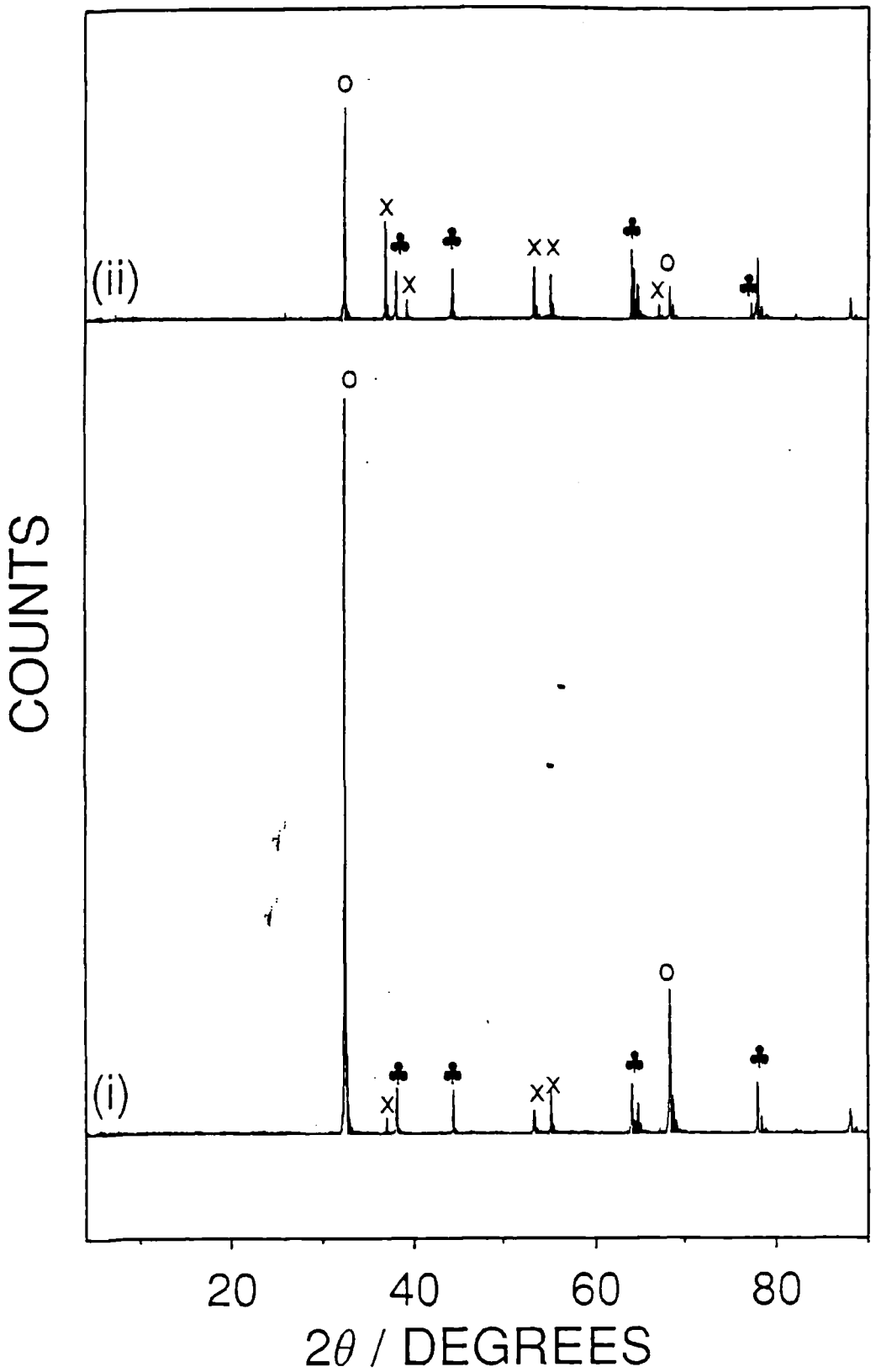

Spectrum 4.9. Position study diffraction patterns - (i) 0-1 cm, (ii) 4-5 cm (Ag lines = ♣, AgO lines = x and Ag_2O lines = o (aluminium lines are not labelled)).

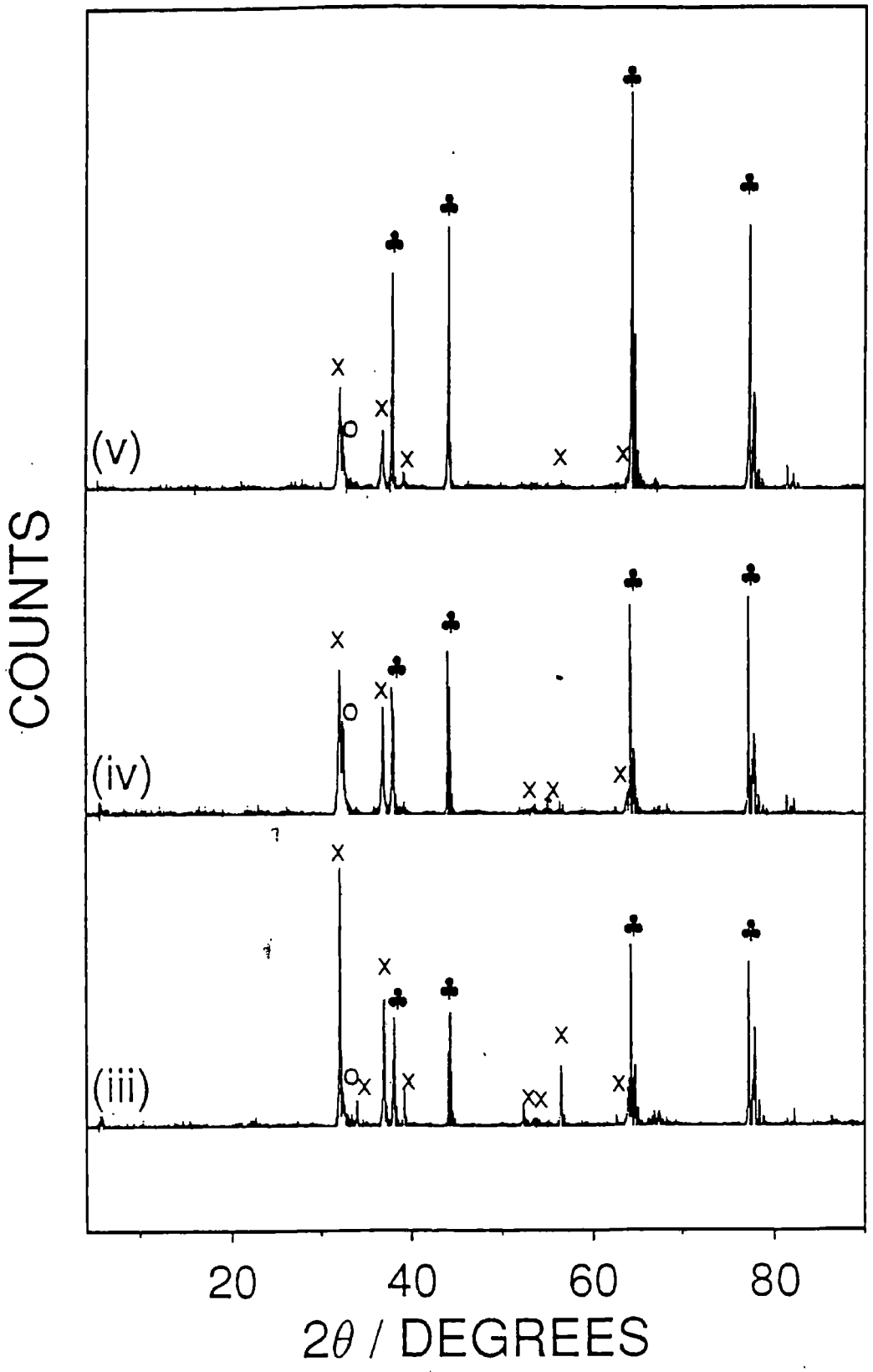

Spectrum 4.10. Diffraction patterns for the various positions studied - (iii) 8-9 cm, (iv) 12-13 cm and (v) 16-17 cm (Ag lines = ♣, AgO lines = x and Ag_2O lines = o (aluminium lines are not labelled)

4.4. Discussion

First of all, in analysing the results it should be noted that some of the planes have slightly different d values to those quoted within the literature, for thermally produced oxides of silver. This is because in plasma treatment of the oxides the surface and subsurface layers will be affected by ion bombardment, resulting in a slight dislocation or distortion of the crystallographic planes and thus affecting their unit cells.

Both AgO and Ag_2O appear to be present within the plasma oxidised layers, however the ratio of these depends on the reaction conditions chosen. In the time study, it can be seen that after only a minute's treatment, the planes present cannot be all that well defined. This is probably due to the low extent of oxidation, as indicated by the thin film growth (observed by the naked eye). It is also probable that lines for Ag_3O and Ag_4O may be present at the oxide/metal interface, due to the low oxidation extent, but identification of these planes representative of these oxides cannot be firmly identified.

Increasing the treatment time, produces various planes which are representative of a mixed metal oxide film, containing both AgO and Ag_2O [25]. These two oxides will probably have preferential locations of growth within the film, due to the existence of a concentration gradient of reactive atomic oxygen present within the sample [26]. It is postulated that at the oxide/metal interface, where the oxide front is advancing [27], the more probable oxide will be Ag_2O, due to the low concentration of oxygen atoms, compared to that of the silver atoms [26,28]. However it is also probable that Ag_3O and Ag_4O compositions are present within this region, but the diffraction

lines are masked by that of Ag and Ag_2O. The diffusion coefficients for silver metal and some of its oxides are tabulated below.

Material	Diffusion Coefficient of O_2 (cm^2s^{-1})
Ag Metal	2.7×10^{-5} (T = 810°C) [29]
Ag_2O	approx. 2×10^{-7} (T = 810°C) [30]
Ag_2O_3	Not Known
AgO	6.13×10^{-15} (T not stated) [31]

Table 4.1. Diffusion coefficients for oxygen through silver and certain oxides.

At the plasma/oxide interface, the more probable oxide is AgO, due to the higher concentration of oxygen atoms present at this boundary [32]. However at the very surface of the oxide film, another process could be competing against AgO formation. This reaction is the catalytic reduction of AgO by atomic oxygen, which leads to Ag_2O formation plus molecular oxygen (see **Figure 4.1.**) [33]. This reaction is well documented within the literature and it has been stated that the most probable oxide present upon the silver catalysts surface, during ethylene epoxidation, is Ag_2O [33]. Further increases in the oxidation reaction time leads to little change in the oxide films composition.

The results from the studies on the effects of plasma power, gas pressure and position of the foil within the reactor, have shown that Ag_2O is the more favoured oxide produced at high powers, low pressures and at positions nearer to the live electrode. The possible reasoning behind this is that more energy will be transferred to the oxide surface, thus pushing the thermodynamic equilibrium over towards Ag_2O

formation [25] (Ag_2O decomposes at T> 300°C ; AgO decomposes at T < 100°C). This theory is backed-up by the presence of AgO at lower powers, higher pressures and at greater distances from the live electrode.

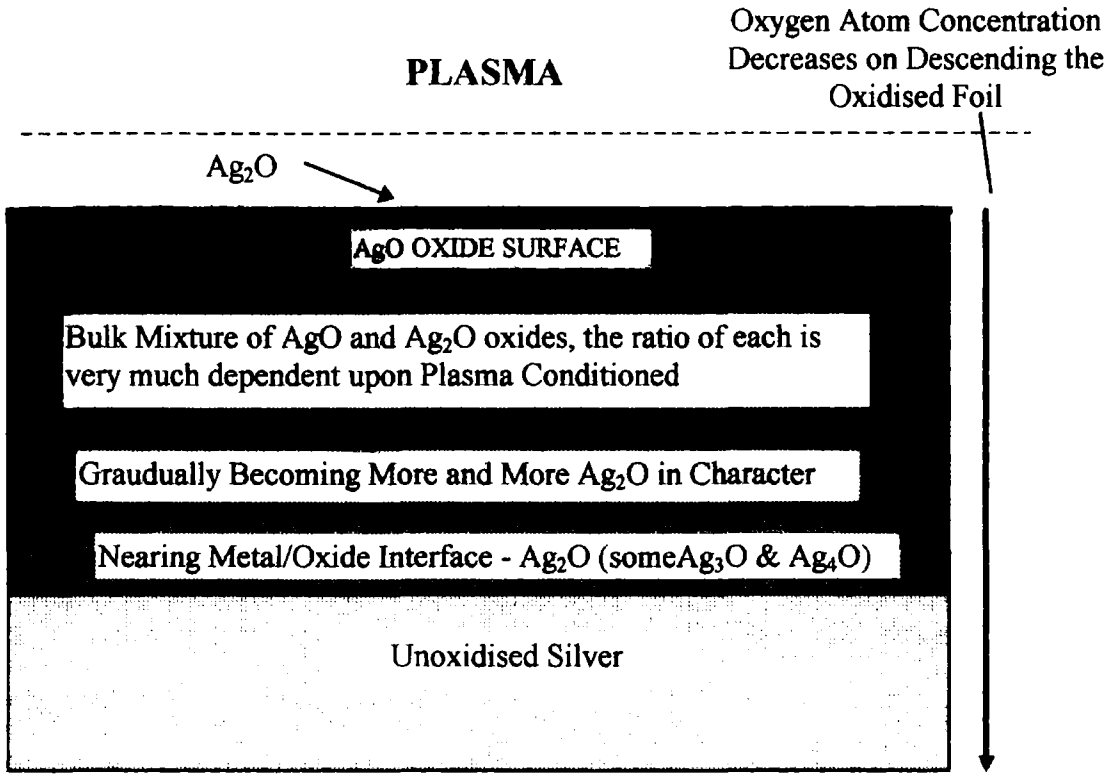

Figure. 4.1. Schematic of an idealised depth profile of a plasma oxidised silver foil.

It appears consistent to say that when microstructures are observed upon the oxide surface [25], a mixed metal oxide system is present, whereas cluster formation occurs when Ag_2O is the favoured oxide. The formation of these differing structures, with changes in oxide composition, backs up our initial proposed mechanism (stated within chapter 3), where the oxide with the greater silver diffusion coefficient appears to give rise to the formation of clusters (i.e. $Ag_2O = 0.61 \times 10^{-11}$ cm^2s^{-1} $AgO = 5.4 \times 10^{-13}$ cm^2 s^{-1} both at 85°C) [34]. Evidence also appears in the literature suggesting that

the mobile component may even be the Ag (I) species. Experimental evidence for this, is the formation of clusters when only Ag_2O is present, which consists solely of Ag (I) species. However when AgO is present the extent of diffusion decreases because AgO contains both Ag (I) and the more covalent Ag (III) species (which highly polarising), and thus the quantity of the mobile species has been reduced.

Further evidence suggesting that the mobile species is indeed Ag (I) comes from previous whisker formation studies. The materials studied then also contained the Ag(I) species, for example Ag_2S [35], AgCl [36], AgBr [37], AgI [37]. The reasoning behind why the silver (III) species may not be as mobile, could be linked to the number of bonds which have to be broken, for it to become mobile, and thus the greater activation energy that have to be overcome for diffusion to occur [38].

The above hypothesis may explain the extent of mobility within the different oxides, however as to why the microostructures appear instead of the domed cluster shapes must be related to the way in which the oxide grows. It is well known that crystallographic planes growing within an oxide will do so at different rates [39]. Now, if it is imagined that there are three planes growing at once, and that the plane growing perpendicular to the surface is growing rapidly whereas the planes at approximately 30° to this growing slowly, then the following scenario will exist (see **Figure 4.2.**). As the three planes grow, the more rapidly growing plane, will tend to eventually outgrow itself, leaving only the two slow growing planes present, thus producing a pointed surface structure [39] (see **Figure 4.2.**).

However as for the formation of the clusters, the rate of growth of the planes, which make up the mound, must be very similar and thus no planes will disappear, so producing a more rounded structure (see **Figure 4.3.**) [39].

An alternative theory to that off before, for the formation of microstructures and clusters, is that increases in ion bombardment of the surface of the oxide film at higher powers, lower gas pressures and closer to the live electrode will result in melting of the surface, and cause the microplatelets to sinter - as well as favour Ag_2O formation.

Schematic of the Growth of Crystal Planes

(A) Microplatelet Growth

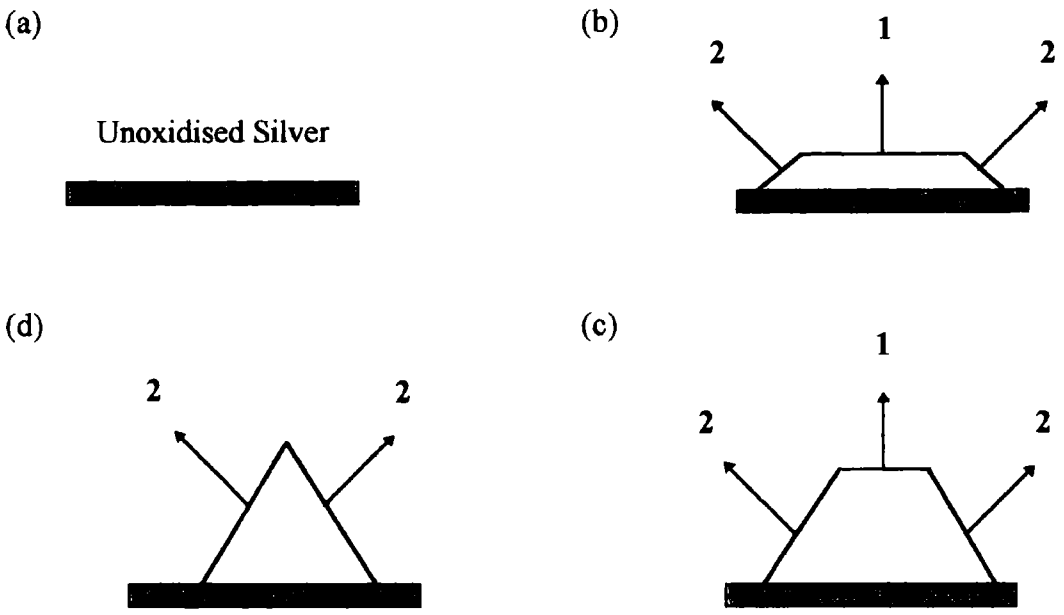

Figure. 4.2. (a) Silver before plasma oxidation (b) Microplatelet growth commences with two slow growing planes (**labeled 2**) propagating from the silver surface at about 30°, while a fast growing planes (**labeled 1**) propagates perpendicular to the surface. (c) Further growth of the planes (d) The fast growing plane out grows itself and thus is no longer present the slow growing planes now determine the shape of the microplatelet.

(B) Cluster Growth

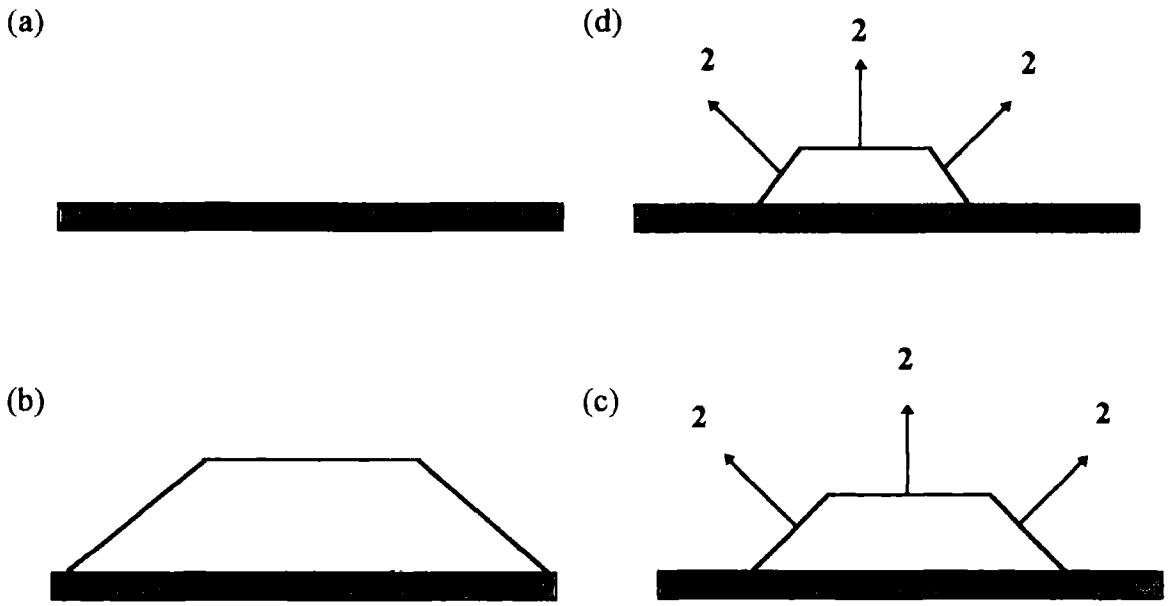

Figure. 4.3. (a) Unoxidised Silver Foil (b) Globular structure grows similarly to that of the microplatelet except that all faces are growing at the same rate **(labelled 2)** (c) All three planes continue to grow at the same rate (d) The final structure produced still has all faces present and a more globular structure is thus formed.

4.5. Conclusion

Increasing the rf power, decreasing the gas pressure, and moving the foil closer to the live electrode during the plasma oxidation process, leads to the formation of Ag_2O. Doing the opposite (to the above) such as decreasing the rf power, increasing the gas pressure and moving the foil away from the electrode preferentially leads to the formation of AgO. The reasoning behind the formation of these oxides can be related to the amount of energy being transferred to the surface by ion bombardment of the substrate. The time study shows the gradual growth of the microplatelet structures and suggests that a mobile species is responsible for the growth of these surface textures. The mobile species has been suggested to be Ag (I). The actual shapes of the surface textures is thought to be dependent on the rate of growth of the oxides crystallographic planes, with AgO giving the microplatelets and Ag_2O the clusters.

REFERENCES

1. Cotton, F.A.; Wilkinsons, G.; **Advanced Inorganic Chemistry**; 4th Edition, Interscience: 1972.
2. Greenwood, N.N; Earnshaw, A.; **Chemistry of the Elements**; Pergammon Press: 1984.
3. MacKay, K.M.; Mackay, R.A. Modern Inorganic Chemistry
4. Lide, D.R.; **Handbook of Chemistry & Physics**; 71st Edition, CRC Press: USA, 1990-91.
5. **Basic Inorganic Chemistry Book**
6. Varkey, A.J.; Fort, A.F.; **Sol. Energy Mater. Sol. Cells, 1993**; Vol. 29, 253.
7. Wells, A.F.; **Structural Inorganic Chemistry**; 3rd Edition, Clarendon Press: Oxford, 1962.
8. Casey, E.J.; Moroz, W.J.; **Can. J. Chem., 1965**; Vol.43, 1199.
9. McMillan, J.A.; **Chem. Rev., 1962**; Vol.62, 65.
10. Standke, B.; Jansen, M. **Angew. Chem. Int. Ed. Eng., 1985**; Vol. 24 (2), 118.
11. Beesk, W.; Jones, P.G.; Rumpel, H.; Schwarzmann, E.; Sheldrick, G.M.; **JCS Chem. Comm., 1981,** 664.
12. Mellor, J.W.; **A Comprehensive Treatise on Inorganic & Theoretical Chemistry**; Longmans Green & Co. Ltd: London 1928.
13. Standke, B.; Klemm, W.;**Angew. Cem. Int. Edition English, 1986,** Vol.25 (1), 77.
14. Fischer, P.; Jansen, M.; **Acta Chem. Scand., 1991**; Vol. 45(8), 816.
15. Wales, C.P.; **J. Electrochem. Soc., 1964**; Vol. 111 (2), 131.
16. Moore, W.M.; Codella, P.J.;**J. Phys. Chem., 1988**; Vol. 92, 4421.
17. Briggs, G.W.D.; Fleischmann, M.; Lax, D.J.; Thirsk, H.R.; **Trans. Faraday Soc., 1968**; Vol. 64, 3120.
18. Engelhardt, H.A.; Menzel, D.; **Surf. Sci., 1976**; Vol. 57, 591.
19. Iwasaki, N.; Sasaki, Y.; Nishina, Y.; **Surf. Sci., 1988**; Vol. 198, 524.
20. Slager, T.L.; Lindgren, B.J.; Mallman, A.J.; Greenler, R.G.; **J. Phys. Chem., 1972,** Vol. 76 (6), 940.

21. **Cookson Internal Report (1991)**
22. Weaver, J.F.; Hoflund G.B.; **Chem. Mater, 1994**; Vol. 6, 1693.
23. Weaver, J.F.; Hoflund, G.B.; **J. Phys. Chem., 1994**; Vol. 98, 8519.
24. Mayer, S.T.; Muller, R.H.; **J. Electrochem. Soc., 1988**; Vol. 135 (9), 2133.
25. Chou, C.H.; Phillips, J.; **J. Vac. Sci. & Technol., 1991**; A9 (5), 2727.
26. Dickens, P.G.; Heckingbottom, R.; Linnett, J.W.; **Trans. Farday Soc., 1968**; Vol. 64, 2235.
27. Takada, J.; Kuwahara, H.; Manabe, Y.; Kimura, M.; Yanagihara, K.; **J. Mater. Sci., 1991**; Vol. 26, 6288.
28. Barradas, R.G.; Fraser, G.H.; **Can. J. Chem., 1964**; Vol. 42, 2488.
29. Bazan, J.C.; **Electrochim. Acta, 1968**; Vol. 13(8), 1883 (Abs).
30. Osipchuk, N.Y.; **Zh. Fiz. Khim., 1971**; Vol. 45(7), 1660 (Abs).
31. Farhart, E.; Robin, K.S.; **Thin Solid Films, 1974**; Vol. 23(3), 315 (Abs).
32. Shard, A.G.; Badyal, J.P.S.; **J. Phys. Chem., 1991**; Vol. 95, 9436
33. Khasin, A.V.; **Kinet. i Katal., 1993**; Vol. 34 (1), 42.
34. Rozenblyum, N.D.; Bubyreva, N.S.; Bukhareva, V.I.; Kazakevich G.Z.; **Russ. J. Phys. Chem., 1966**; Vol. 40 (10), 1324.
35. Sinclair, J.D.; **J. Electrochem. Soc., 1982**; Vol. 129 (1), 33.
36. Brenner, S.S.; **Acta Met, 1956**; Vol. 4, 62.
37. Brenner, S.S.; **Acta Met, 1959**; Vol. 7, 677.
38. ***Private Discussion*** with Dr. Banister
39. Atkins, P.W.; **Physical Chemistry, 4th Edition**; Oxford University Press: Oxford, 1991.

CHAPTER 5

HYDROGEN PLASMA REDUCTION OF PLASMA PRODUCED SILVER OXIDE FOILS

5.1. Introduction

The reduction of oxidised silver foils, shown within Chapter 3 could be important in the fields of catalysis and adhesion, so, in-situ hydrogen plasma reduction of the plasma oxides was carried out, and the resultant morphologies and extent of reduction were studied.

5.1.1. Conductive Adhesives

Solder, a lead/tin alloy, is one of the most important adhesives used in the electronic industry [1]. However, due to new government legislation, an alternative must be sought, due to a duty tax being imposed on the use of lead [2]. So far the most promising system appears to be silver filled epoxy adhesives, due to their low resistivity and toughness [3,4]. These materials consist of a resin (usually an epoxy) which has dispersed within it, silver powder or flake [5]. Further additional components can be added to improve properties such as mechanical strength or curing ability of the resin (time taken to harden) [6].

The conductive adhesive is added to the component which is to be adhered, as a paste and is usually then thermally or photochemically cured. Here the epoxy

hardens forming a join between the component and board. It is during this process that a pathway of low resistance is formed by interconnected silver particles within the resin [3]. This occurs due to polymerisation of the resin, which forms a 3-D polymeric cross-linked network [3]. It is these growing chains which orientate the silver particles to touch end-to-end and form a conductive pathway [2,3].

The advantages of these adhesives over solder are that they cure at lower temperatures, are lead free and eliminate post interconnection cleaning [7]. However, many needs have to be addressed before these alternatives replace solder such as, obtaining good conductivity, increased wetting ability of most surfaces, greater mechanical strength and finally to be able to repair and replace defective joints [7].

5.1.2. Catalytic Conversion of Ethylene to Ethylene Oxide

Silver is an important industrial catalyst, (usually supported on α-alumina), as it is the only known metallic material able to convert ethylene to ethylene oxide efficiently by the following reaction [8,9]:

$$C_2H_4 + {}^1/_2\,O_2 \longrightarrow C_2H_4O$$

This is a multi-million pound industrial process and is invaluable to the petrochemical industry [10].

However competing against the above reaction is the complete combustion of ethylene to carbon dioxide and water [11]. This occurs as shown below :

$$C_2H_4 + {}^1/_2O_2 \longrightarrow CO_2 + H_2O$$

This second reaction is a serious problem, when using a clean silver catalyst, as the selectivity for the conversion of ethylene to ethylene oxide is only 45% [12]. However the combustion reaction can be suppressed by adding a small quantity of chlorinated hydrocarbon to the reactant feedstock [13]. Here the chlorine atoms from the additive are thought to block sites on the catalyst, which possess a high heat of adsorption [14]. It is these sites which are thought to be responsible for CO_2 formation [14]. However whether this is the actual process by which CO_2 formation is inhibited is still widely debated [14]. Addition of the chlorinated hydrocarbon increases the selectivity up to approximately 80% [9,12]. It is also possible to increase the selectivity for the epoxidation reaction by adding alkali metal promoters to the catalyst, such as cesium and potassium [10,11].

There is still some debate as to which oxygen surface species is actually involved in the reaction of ethylene to ethylene oxide [15]. It is thought by most researchers that adsorbed atomic oxygen is responsible, however it appears that subsurface oxygen species must also be involved [15,16]. Many academic and industrial researchers have used a variety of techniques to determine this process, such as IR [17,18], RS [19], LEED [20], NMR [21], TPD [22], AES [23] and finally XPS [23].

5.2. Experimental

Oxidation of the silver foils was carried out using the optimum conditions determined, and the equipment and procedure given in Chapter 3. The oxidised foils were then reduced in a hydrogen plasma. For this process the reactor was flushed for a period of 10 minutes with hydrogen gas (BOC: purity 99%). The plasma was then

ignited at various rf powers, gas pressures and the reduction process was carried out for various times.

The surface of the treated foil was then analysed using an S600 Scanning Electron Microscope as stated in Chapter 3.

XRD analysis, used to monitor the extent of reduction of the oxide, was carried out using Philips Powder Diffractometer in the same manner as that given in Chapter 4.

5.3. Results

The effects of the following processing parameters have on the surface topography and extent of reduction of the hydrogen plasma treated oxidised foil were:

(a) Input Power

(b) Gas Pressure

and (c) Reaction time

5.3.1. Input Power

The powers studied were between 15 and 50 W. All other variables were held constant (i.e. gas pressure 0.6 mbar, time of reaction = 1 hr, centre of foil = 8.5 cm from the live electrode).

INPUT POWER = 15W (scale 10μm = 1.5 cm)

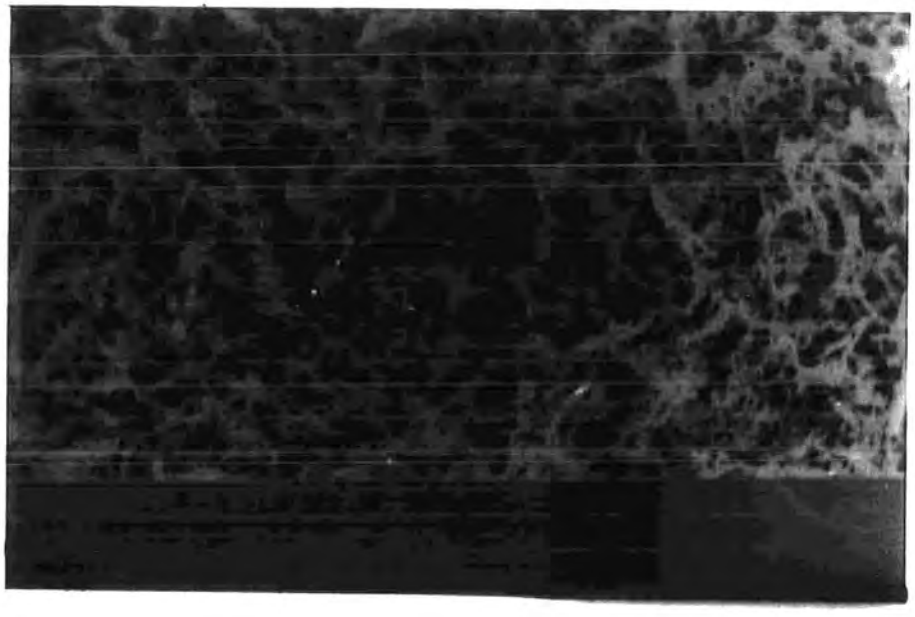

INPUT POWER = 20W (scale 10μm = 1.5 cm)

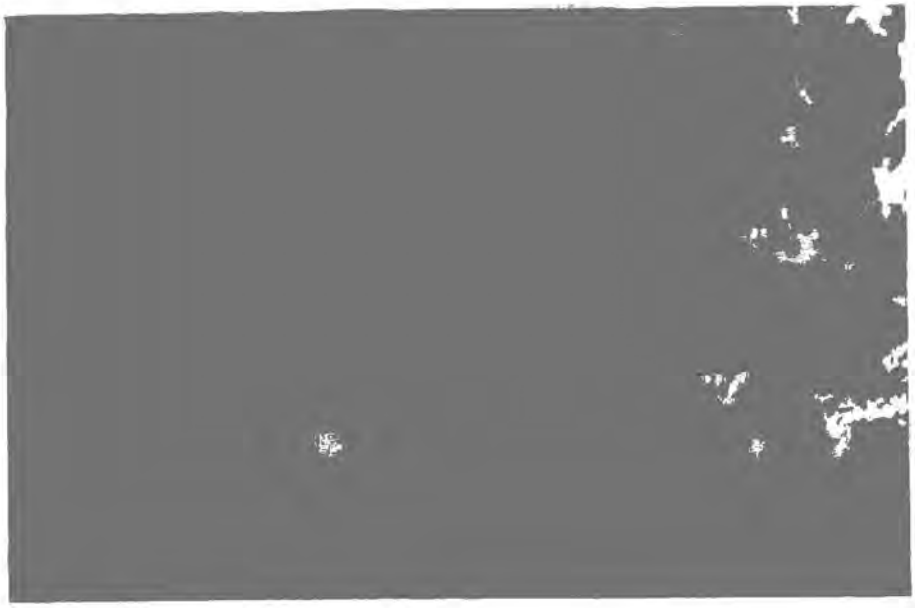

INPUT POWER = 25W (scale 10μm = 1.5 cm)

INPUT POWER = 50W (scale 10μm = 1.5 cm)

Treatment at 15 W rf power, produced a sintered net-like texture, when compared to that of the original oxidised foil (see Chapter 3).

Increasing the power further enhances this sintering process until finally at 50W, the surface appears to have melted, resulting in a clustered structure.

The 15W reduction process is the optimum rf power, as this led to the least sintered surface.

5.3.2. Gaseous Pressure

The gas pressures studied were between 0.2 and 0.8 mbar, while all other parameters were held constant i.e power 15 W, time of reaction = 1 hr and position of foil with respect to the live electrode.

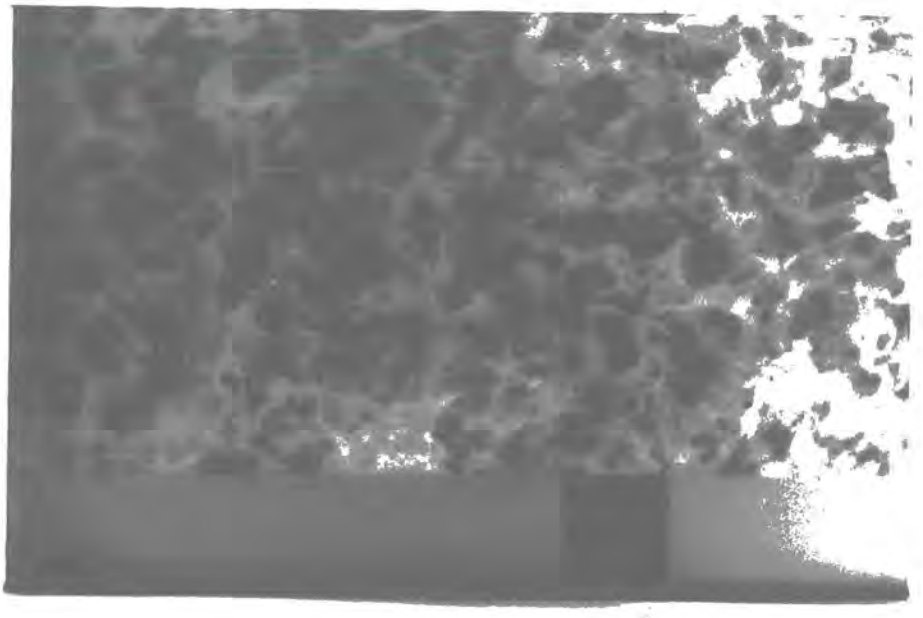

GAS PRESSURE = 0.2 mbar (scale 10μm = 1.5 cm)

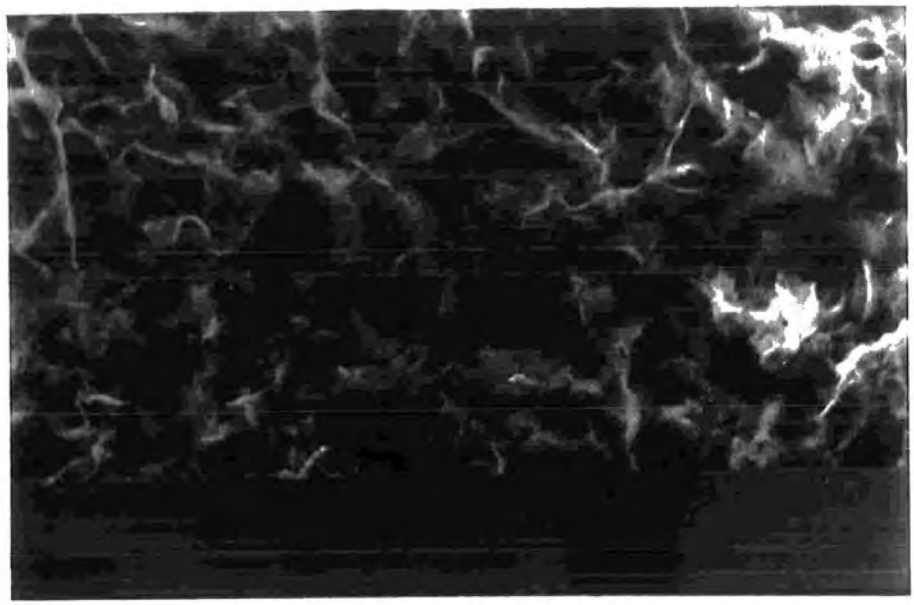

GAS PRESSURE = 0.4 mbar (scale 10μm = 1.5 cm)

GAS PRESSURE = 0.6 mbar (scale 10μm = 1.5 cm)

GAS PRESSURE = 0.8 mbar (scale 10μm 1.5 cm)

At 0.2 mbar a net-like sintered texture analogous to that of the 30W power treatment was formed.

As the pressure is increased to 0.8 mbar, the surface begins to approach a texture similar to that observed for the oxidised foil, with only a small degree of sintering occurring at 0.8 mbar.

Thus 0.8 mbar was the chosen gas pressure for the subsequent reactions.

5.3.3. Time of Reaction

The reaction times studied were between 5 mins. and 2 hrs., however two different regimes were chosen for the SEM and XRD studies. For the SEM, 5 and 30

minutes were chosen along with 1 and 2 hrs treatment,. whereas for the diffraction study the times chosen were 1, 5, 15, 30 mins. and 1,2 hrs.. The power and pressure of the system were operated at the pre-determined optimum conditions.

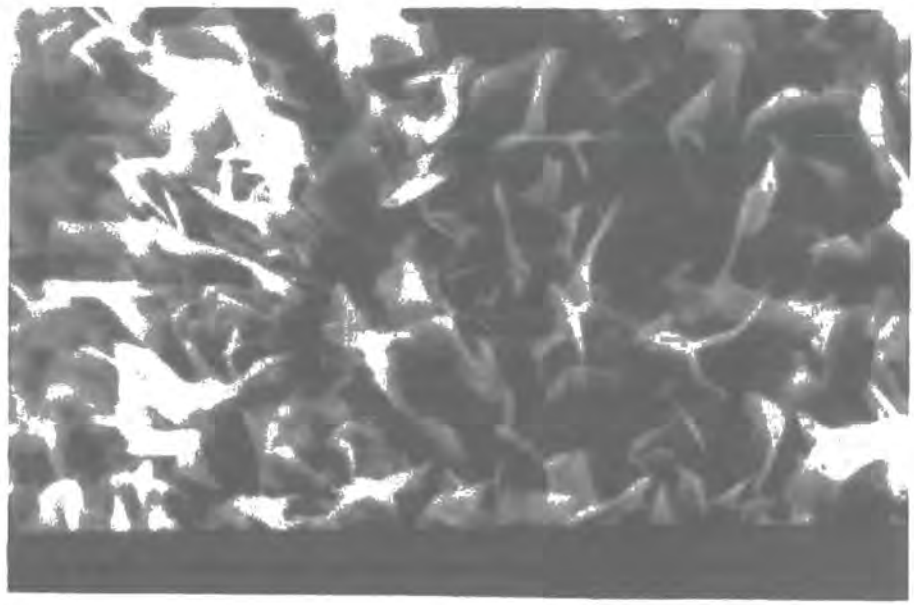

TIME OF REACTION =15 min (scale 10μm = 1.5 cm)

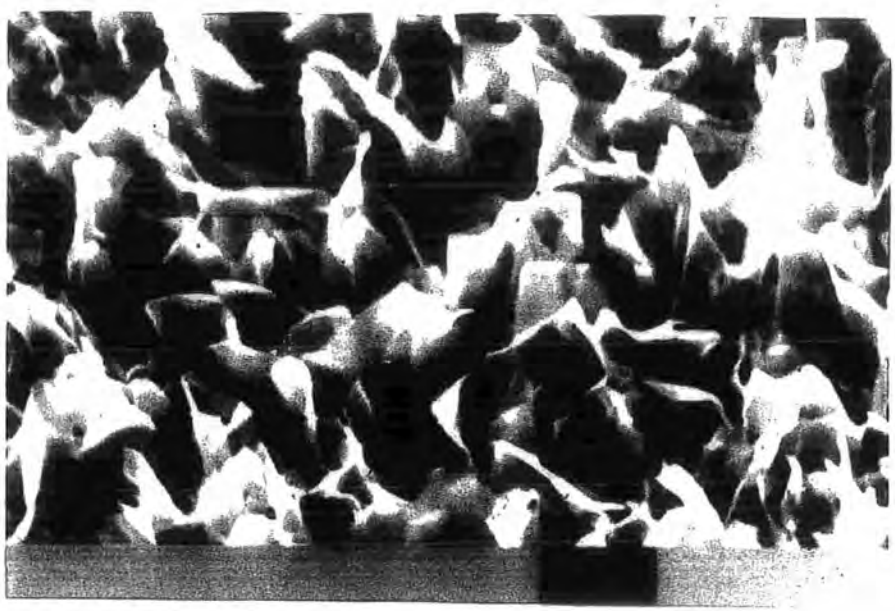

TIME OF REACTION = 30 min (scale 10μm = 1.5 cm)

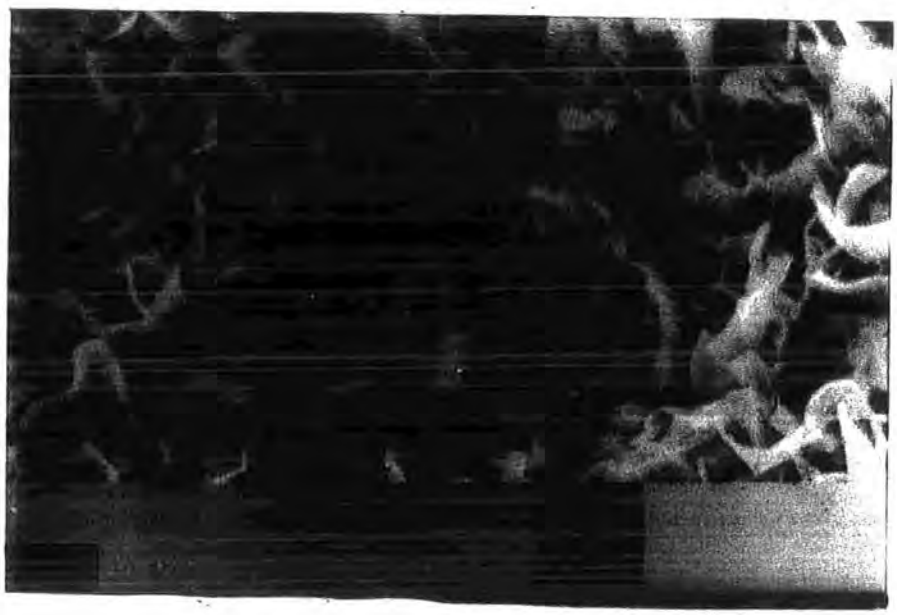

TIME OF REACTION = 1 hr (scale 10μm 1.5 cm)

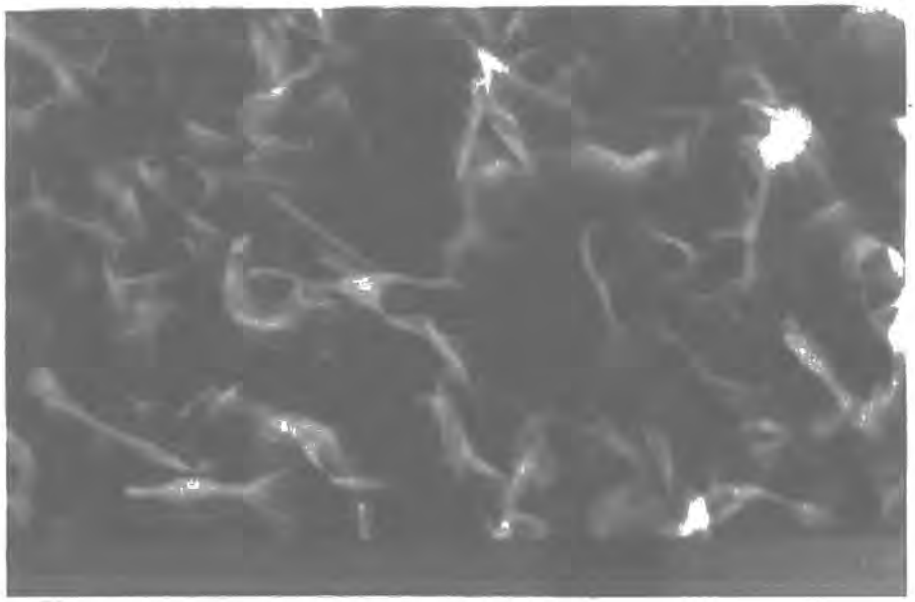

TIME OF REACTION = 2 hrs (scale 10μm = 1.5 cm)

Studying the SEM photographs, it is apparent that little change in surface texture occurs between 5 mins. and 1 hr. treatments, however increasing the time further to 2 hrs. led to a slight sintering of the surface. It should be noted that in going from 1 to 2 hrs. treatments, that a change in colour of the reduced foil occurs, from a dull grey to a whitish colour.

The XRD results overleaf show the gradual reduction of the plasma produced oxide back to silver metal.

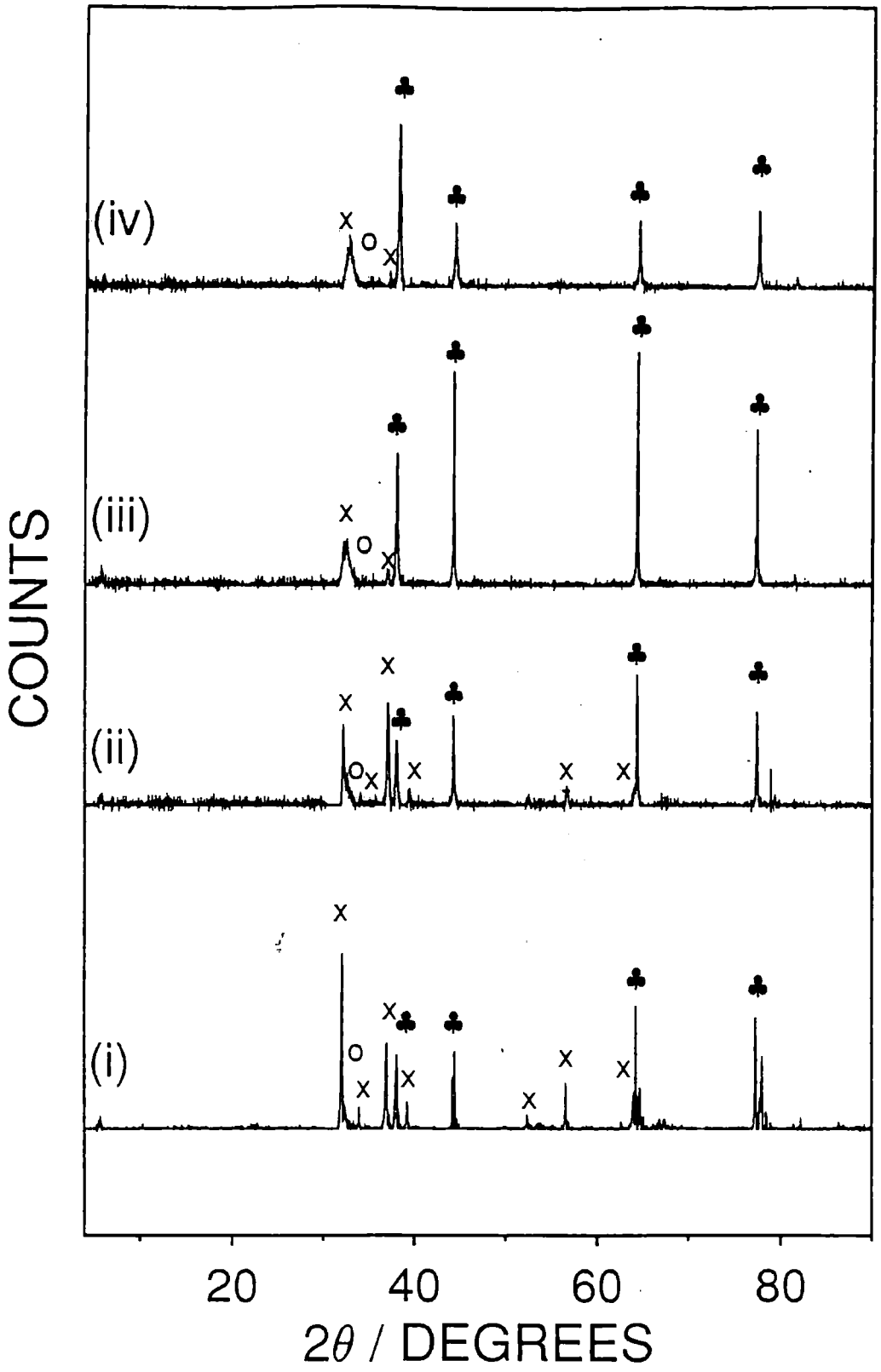

Figure 5.1. XRD time profiles for the reduction of silver oxides (i) plasma produced silver oxide (ii) 1 min (iii) 5 minutes (iv) 15 minutes (AgO lines = x, Ag_2O lines = o, Ag lines = ♣, (aluminium lines are not labelled))

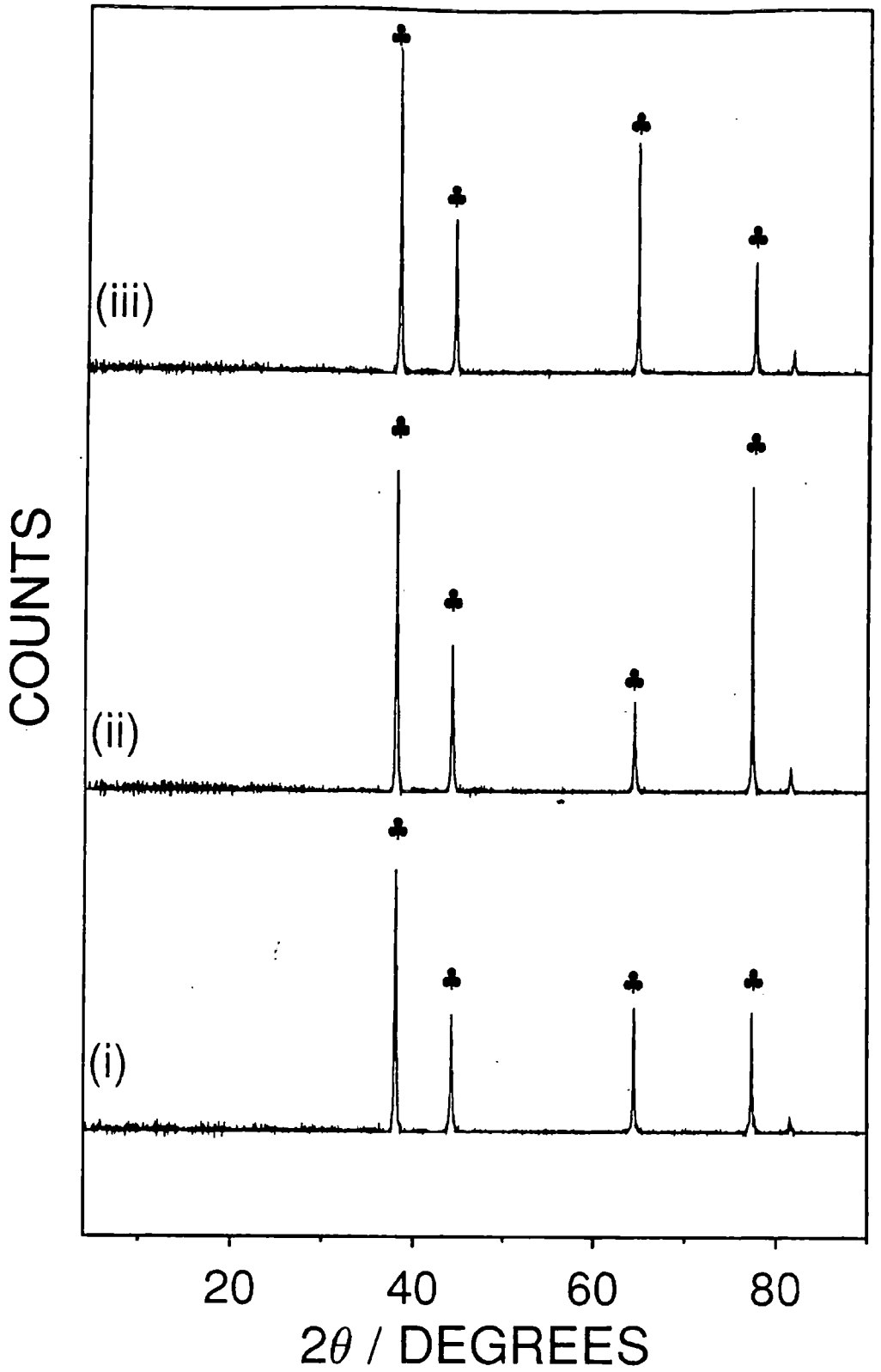

Figure 5.2. XRD profiles for the reduction of silver oxides (i) 30 mins (ii) 1 hr (iii) 2 hrs (AgO lines = x, Ag_2O lines = o, Ag lines = ♣, (aluminium lines are not labeled)).

5.4. Discussion

Hydrogen plasmas contain atoms, ions (both positive and negative) metastables, excited species and electrons, and also emit a broad continuum of electromagnetic radiation [24]. The concentration of these species and the intensity of the radiation, depend on the reaction conditions chosen [24].

Various excited states of hydrogen have been observed within glow discharges such as H_2 ($B^1\Sigma_u$) [25,26] the Lyman Band (Lyman System) and H_2 ($C^1\Pi_u$)[25,26] the Werner Bands (Werner Systems). Both these excited species on relaxing back to the ground state of hydrogen emit VUV radiation (<170 nm) [26].

Several excited atomic species have also been noted within hydrogen plasmas, such as Hβ (observed at 4861 Å) [27], Hγ (observed at 4340.5 Å) [27], Hδ (observed at 4101.7 Å) [27] and finally Hε (observed at 3970 Å) [27]. These atomic excitations give rise to the Balmer lines [27]. Another atomic emission line is the Hα Lyman line which can be observed at 121.5nm [26]. It is this line that is used to monitor the concentration of atomic hydrogen species as a function of power and pressure [26].

Atomic hydrogen is probably the most abundant reactive species within a discharge, and can be generated by either electron impact (occurs as low as 4.5 eV) or by photon induced dissociation [24]. Hydrogen is dissociated as follows:

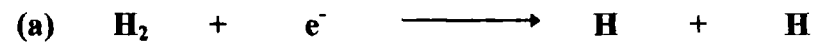

Positively charged hydrogen ions are also produced, at a density of 1.2×10^{10} cm^{-3}, within an electron initiated discharge (discharge current = 2A, voltage = 50V

and gas pressure = 0.01 mbar) [26]. These species are either produced by photon or electron initiated chemical reactions [26]. The ionisation potential for a hydrogen molecule has been reported as being 15.4 eV [29]. These species are mainly involved in the plasma/substrate interfacial chemistry [30].

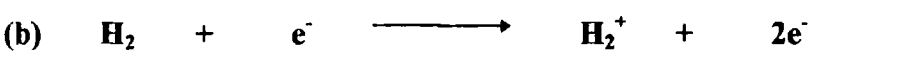

Atomic hydrogen has an ionisation potential value greater than its molecular counterpart, at approximately 18 eV [28].

Negatively charged hydrogen atomic species have also been reported to occur within low pressure discharges [31]. The atomic negative ion is usually produced by electron impact dissociation of an excited molecular species [26]. As for H_2^- no evidence for the existence of this species within a plasma could be found.

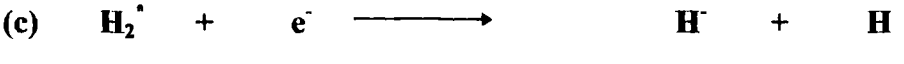

It has also been reported that H_3 species are present in hydrogen plasmas, however this is still widely debated [29].

The hydrogen plasma used within this experiment is typically lilac in colour and follows similar trends in terms of size and growth to that of the oxygen plasma, with increasing rf powers and gas pressures. However, for an hydrogen plasma of 20W the glow is more luminous and slightly larger than that for an oxygen plasma created using similar rf powers.

The SEM photographs, show that (on plasma treatment of a silver foil with an oxygen plasma) increasing the power or decreasing the gas pressure, the surface sinters considerably. In this case the microplatelet structures give way to a mangled net-like texture, which finally melts at 50W treatments. This suggests that too much energy is being transferred to the surface. This energy is probably transferred to the surface before the oxide can be fully reduced back to silver metal, and thus the surface structure melts forming a more impermeable barrier to reduction. This means that the reduction process is very sensitive to temperature. Large amounts of sputtering would not be expected, when using hydrogen plasmas, due to the low mass of the hydrogen ions [32], however considerable energy gain by the ions traversing the sheath would occur due to their high velocity [33]. This is shown from the equation below where the kinetic energy of a species (E_k) is dependent on the square of its velocity (v) and half its mass (m) [33].

$$E_k = {}^1/_2 mv^2$$

Investigating the chemistry occurring, appears to show that the surface of the oxide is fully reduced after 30 minutes reduction. However, it can be seen from the powder diffraction data that this process is gradual. This is shown by the gradual disappearance of the oxide lines. It would be expected that the reduction process would occur by the following procedure [34]:

(a) First reduction of the surface oxides will occur, forming a barrier to further reduction.

(b) Vacuum UV reduction will also help to reduce the oxide surface and will aid with the reduction of the bulk oxide.

(c) Hydrogen atoms or positive ions would then have to diffuse through the reduced silver surface layer to reach the bulk oxide, so it to can be reduced. This diffusion process will be the rate determining step.

(d) The rest of the plasma oxide would be reduced producing a new modified interface between the original silver foil and the plasma reduced silver foil.

This mechanism of reduction is shown diagramatically below.

(a)

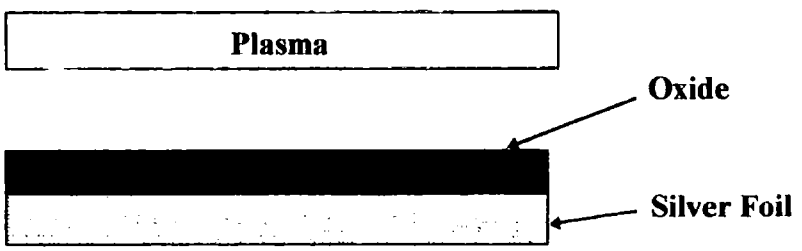

Silver oxide/silver substrate placed within the plasma system forming a sheath in front of the sample. Hydrogen ions and atoms will arrive at the silver oxide surface.

(b)

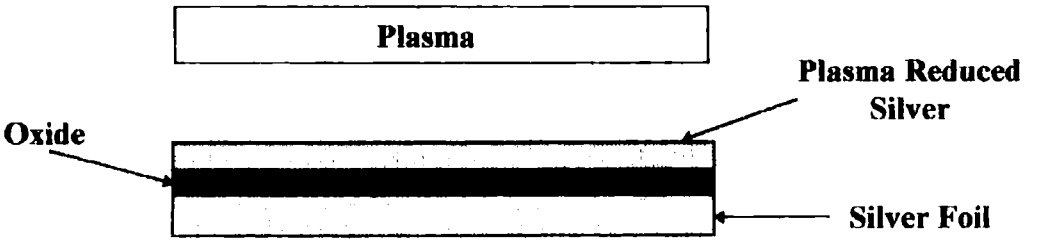

The oxide is gradually reduced from the surface inwards forming two oxide/metal interfaces. This reduction process is due to the reaction of hydrogen atoms/ions with the oxide and also due to the effects of VUV. For further reduction to occur, hydrogen atoms must diffuse through the new plasma reduced layer

.

(C)

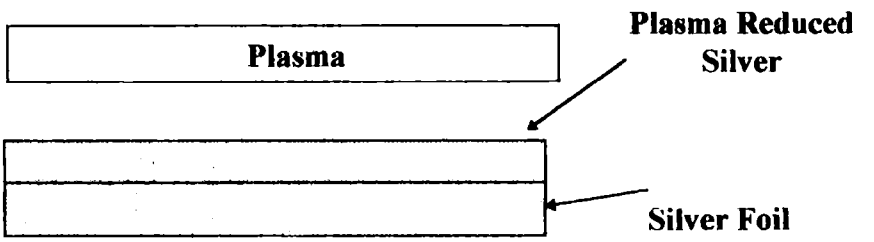

The oxide is now fully reduced back to silver metal.

5.5. Conclusion

Plasma produced silver oxides can be reduced completely back to silver metal using a low pressure hydrogen plasma. This process is gradual due to the diffusion of hydrogen atoms through the reduced layer, and also the gradual reduction of the oxide by vacuum uv.. The surface properties of the plasma oxide produced from Chapter 3 can be maintained once the conditions of rf power and gas pressure have been

optimised. The conditions chosen to produce a high surface area silver metal were 15W rf power, 0.8 mbar gas pressure and for a period of 30 mins.

REFERENCES

1. Nguyen, G.P.; Williams, J.R.; Gibson, F.W.; **Albestik Internal Report**, 1993.
2. Nriagu, J.O.; Pacyna, J.M.; **Nature, 1988**; Vol. 333, 134.
3. Lovinger, A.J. ; **J. Adhesion, 1979;** Vol.10 1.
4. ***Private Communication*** with Matthew Holloway **(Cookson Technology Centre).**
5. Lyons, A.M.; **Polym. Eng & Sci.**, 1991; Vol. 31, 445.
6. Ellis, B.; **Chemistry and Technology of Epoxy Resins**; Pergammon Press, (1986).
7. Allenby, B.R.; Ciccarelli, J.P.; Artaki, I.; Fisher, J.R.; Schoenthaler, D.; Carroll, T.A.; Melton, C.; **Executive Summary, Cooksons Report**, 1992
8. Gates, B.C.; **Catalytic Chemistry**; John Wiley & Sons: Singapore, (1992).
9. Minahan, D.M.; Hoflund, G.B.; **J. Catal., 1996**; Vol 158, 109.
10. Bond, G.C.; **Heterogeneous Catalysis: Principles and Applications 2nd Edition**; Clarendon Press: New York, (1990).
11. Thomas, J.M.; Thomas, W.J.; **Introduction to the Principles of Heterogeneous Catalysis**; Academic Press: London, (1967).
12. Jorgensen, J.A.; Hoffmann, R.; **J. Phys. Chem., 1990**; Vol. 94, 3046.
13. Campbell, C.T.; Koel, B.E.; **J. Catal., 1985**; Vol. 92, 272.
14. Karavasilis, Ch.; Bebelis, S.; Vayenas, C.G.; **J. Catal., 1996**; Vol. 160, 205.
15. Grant, R.B.; Lambert, R.M.; **J. Catal., 1985**; Vol. 92, 364.
16. Tan, S.A.; Grant,R.B.; Lambert, R.M.; **J. Catal. 1987**; Vol. 104, 156.

17. Wang, X.D.; Tysoe, W.T.; Greenler, R.G.; Truszkowska, K.; **Surf. Sci., 1991**; Vol. 257, 335.

18. Force, E.L.; Bell, A.T.; **J. Catal., 1975**; Vol. 38, 440.

19. Pettenkofer, C.; Pockrand, I.; Otto, A.; **Surf. Sci., 1983**; Vol. 135, 52.

20. Bange, K.; Madey, T.E., Sass, J.K.; Stuve, E.M.; **Surf. Sci., 1987**; Vol. 183, 334.

21. Fernandes, E.F.; Benesi, A.J.; Vannice, M.A.; **J. Phys. Chem., 1994**; Vol. 98, 8498.

22. Barteau, M.A.; Madix, R.J.; **Surf. Sci., 1980**; Vol. 97, 101.

23. Bronin, A.I.; Bukhtiyarov, V.I.; Vishnevskii, A.L.; Boreskov, G.K.; Savchenko, V.I.; **Surf. Sci., 1988**; Vol. 201, 195.

24. Hollohan, J.R.; Bell, A.T.; **Techniques & Applications of Plasma Chemistry**, Wiley & Sons: New York, 1974.

25. Perrin, J.; Delafosse, E.; **J. Phys. D: Appl. Phys., 1980**; Vol. 13, 759.

26. Graham, W.G.; **J. Phys. D: Appl. Phys., 1984**; Vol. 17, 2225.

27. Hollander, A.; Wertheimer, M.R.; **J. Vac. Sci. Technol., 1994**; Vol. A12(3), 879.

28. Kouchi, N.; Ukai, M.; Hatano, Y.; **J. Phys. B: Atomic Molecular Optical Physics**, 1997; Vol. 30, 2319.

29. Goodyear, C.C.; Von Engel, A.; **Proc. Phys. Soc., 1962**; Vol. 79, 732.

30. Hess, D.W.; **J. Vac. Sci. Technol., 1990**; Vol. A8(3), 1677.

31. Fukumasa, O.; Saeki, S.; **J. Phys. D: Appl. Phys., 1987**; Vol. 20, 1987.

32. **Chemical Periodic Table** (Hydrogen Mass)

33. Chapman, B.; **Glow Discharge Processes**; Wiley & Sons: New York, 1980.

34. Sawada, Y.; Tamaru, H.; Kogoma, M.; Kawase, M.; Hashimoto, K.; **J. Phys. D: Appl. Phys.**, 1996; Vol. 29, 2539.

CHAPTER 6

PULSED OXYGEN PLASMA TREATMENT OF SILVER FOILS

6.1. Introduction

In the previous chapters, it was observed, that when silver foils are treated with a continuous oxygen plasma, microplatelets are produced. In the next stage of this thesis a mechanism for the formation of these microplatelets will hopefully be established. The initial investigation is concerned with looking at the effects of pulsing an oxygen discharge on the morphology obtained on the oxidised foil.

6.1.1. Pulsed Plasmas

Pulsed plasma treatment of a substrate is an alternative to using continuous wave plasmas [1,2]. Pulsing the discharge involves having both a plasma on (t_{on}), and off period of known times (t_{off}) [3]. The time between the start of one pulse and the beginning of the next is termed the pulse period (t_p) [3]. This is shown schematically in **Figure 6.1.**.

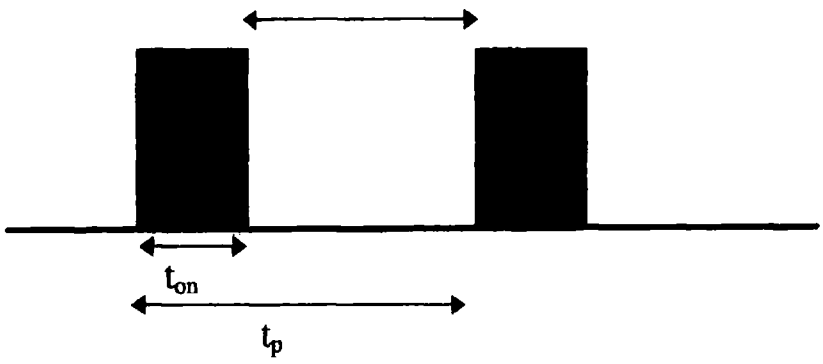

Figure. 6.1. Schematic of the pulsing mode used in plasmas.

Varying the pulse on and off periods and the peak power of the pulse allows the user considerable control over the plasma parameters, such as electron temperature and atom concentration, which in turn leads to more control over the chemistry occurring within the discharge [4]. Two important parameters which must be known when using pulsed plasmas are the duty cycle [5] (the ratio of time on, to the sum of on and off times) and the average power of a pulse [5]. Both the duty cycle and average power delivered to a system can be determined from **equation 7.1.** [4]

$$\langle P \rangle = P_o + \frac{t_{on}}{t_{on} + t_{off}}$$

$\langle P \rangle$ = Average rf power applied
P_o = Peak Power Applied
t_{on} = pulse time on
t_{off} = pulse time off

Equation 7.1. Average power absorbed by the plasma for a pulsed system.

Pulsed plasma systems have several important advantages over continuous plasmas [6]. The first of these is the greater control over the chemical functionality and properties of a product [7]. This is done by altering the on/off times and the peak power of the pulse [7]. Changing the off time may allow certain species within the plasma to relax fully (if sufficient time is allowed) before reignition of the plasma occurs [8]. Also the off time can be chosen to selectively produce certain gaseous and surface chemical functionalities, which may be incorporated into the final product. This can aid with the elucidation the species responsible for producing the materials, and why it has particular physical and chemical characteristics [9,10].

The temperature of the substrate and the extent of ion bombardment of the sample can also be controlled using pulsed plasmas, by the longer the plasma on period, the greater the ion bombardment of the substrate [11]. Thus by shortening the on time, the damage to the sample can be minimised, while the desired properties of the substrate (produced by the reactive radicals) can still be maintained. The temperature of the sample rises as the ion bombardment time increases [12].

It has been reported that the total ultra-violet (UV) emission (for a plasma operated at the same power and time) from a plasma decreases when a discharge is pulsed [14]. This conclusion was reached, due to the reduction in the extent of oxidation of polymeric samples when using a pulsed oxygen plasma [14,15]. This has been linked to lower atomic oxygen concentrations, which can be related to a decrease in UV induced photodissociation [14,15].

Pulsed discharges have also been used for analytical purposes, such as determining the chemical species present within a plasma, and also for investigating

the chemical reactions which may be occurring within it [16]. This usually involves looking at the emission spectra from an ionised gases as a function of time [16].

The main reason for investigating pulsing, within this study, is to observe the effect of decreasing the overall on-time of the plasma, (and hence ion bombardment of the sample), on the surface morphology.

Pulsed oxygen systems have rarely been used; most of the pulsing work has been either for etching [17,18] (using fluorinated species) or deposition of various polymeric coatings e.g. PTFE [19,20].

6.2. Experimental

The experimental set-up used was similar to that described in Chapter 3 section 3.2., the only difference being that a Thander TG 503 5MHz Pulse/Function generator (to generate a pulsed voltage) and a Hitachi V-252 20MHz oscilloscope were incorporated into the apparatus.

Before any plasma experiments on the substrates commenced, the minimum power at which plasma ignition could occur was determined. This was found by ramping up the rf power until a visible glow was observed. For this experiment the reaction times used were 50 ms on and 1 s off. The minimum pulsed power used to generate a discharge was 30 W. After establishing the minimum power, the maximum duty cycle was determined, which was found to be 2.5. The minimum on time of a pulse was limited to 50 μs due to the rise time (the time taken for the generator to reach the pulse peak voltage chosen) of the ENI rf generator being 40μs.

The oxidised silver foils were analysed by scanning electron microscopy (SEM), as described in Chapter 3 section 3.2., and by powder diffraction as described in Chapter 4 section 4.2., with the exception that a perspex sample holder was used instead of aluminium for XRD experiments.

6.3. Results

The three parameters investigated were a constant on-time, a constant off-time and finally a constant duty cycle.

6.3.1. Constant On Time

The on-times studied were 50ms with 125ms, 50ms and 500μs as off-times, and also 100μs on-times with 50μs and 10μs off-times. The electron micrographs of the surface topographies obtained are shown.

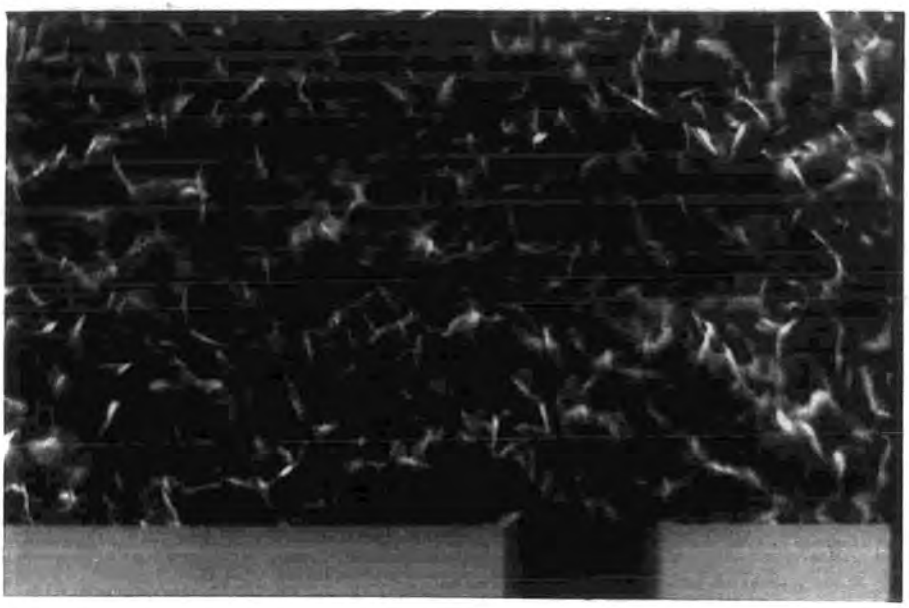

50ms on / 125ms off (scale 10μm = 1.5cm)

50 ms on / 50 ms off (scale 10μm = 1.5cm)

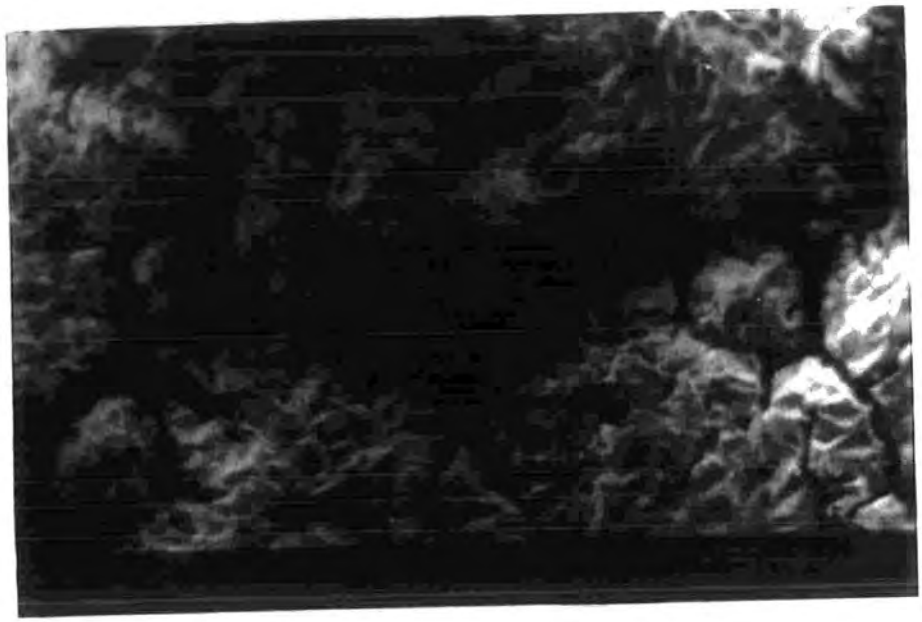

50ms on / 1ms off (scale 10μm = 1.5cm)

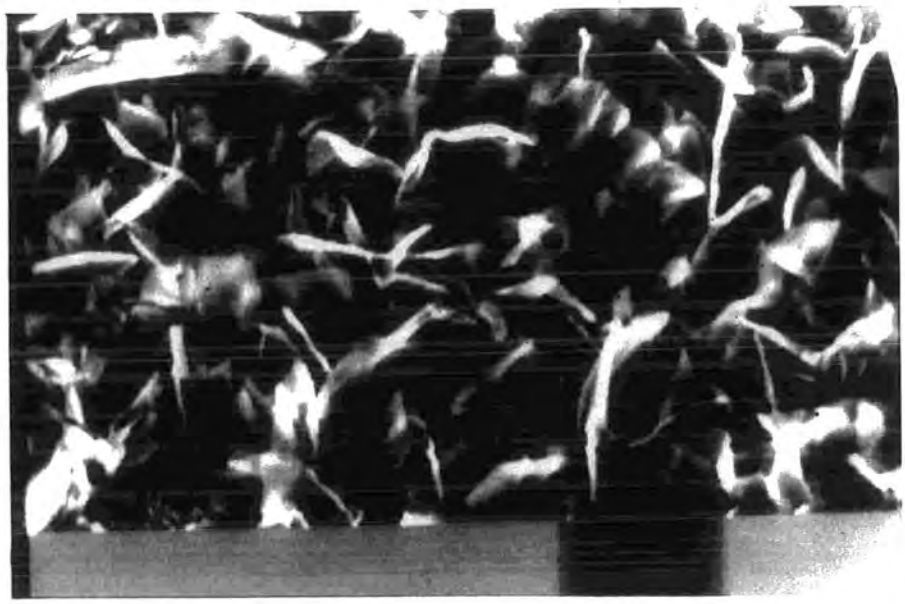

100μs on / 50μs off (scale 10μm = 1.5cm)

100μs on / 10μs off (scale 10μm = 1.5cm)

The SEM micrographs show for 50ms on times, that as the off-time decreases, the surface texture passes from small microplatelets (100ms off time), to larger microplatelets (50ms off time) and finally to a clustered appearance at shorter off-times (500μs).

For on-times of 100μs, the results show a similar trend: as the off-time decreases the surface begins to sinter.

X-ray diffraction spectra are shown for the 50ms and 100μs on-time treatments in **Figures 6.2. and 6.3.** respectively. The off-times were the same as those chosen for the SEM studies. These can be seen on pages 143 and 144.

In the 50 ms XRD patterns, for off times of 100ms and 50ms, the major silver oxide present appears to be AgO. However decreasing the time further to 500μs

favours Ag_2O formation. For shorter on times of 100μs, AgO is the major oxide observed with some Ag_2O present. However it should be noted that species such as Ag_4O may be present, however this may be composed of a series of rows consisting of planes of silver atoms with oxygen atoms dispersed within them and may also be deduced as Ag_2O. Thus the reasoning behind there being no specific lines for Ag_4O.

All SEM results and XRD results were produced at least twice.

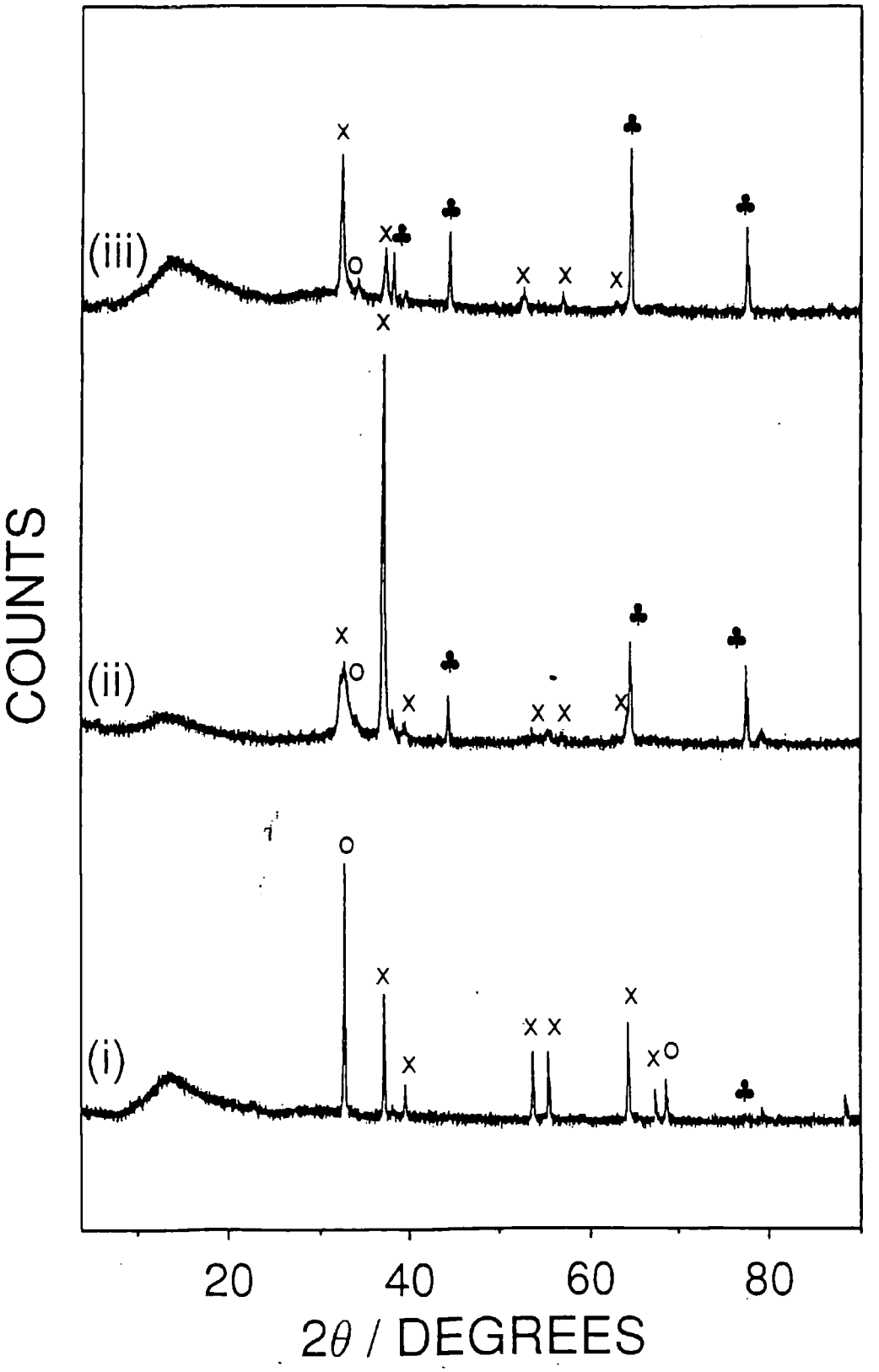

Figure. 6.2. XRD Profiles for 50ms on time ((i) 1ms, (ii) 50ms, (iii) 125ms off-times). (Ag =♣, AgO = x and Ag_2O = o)

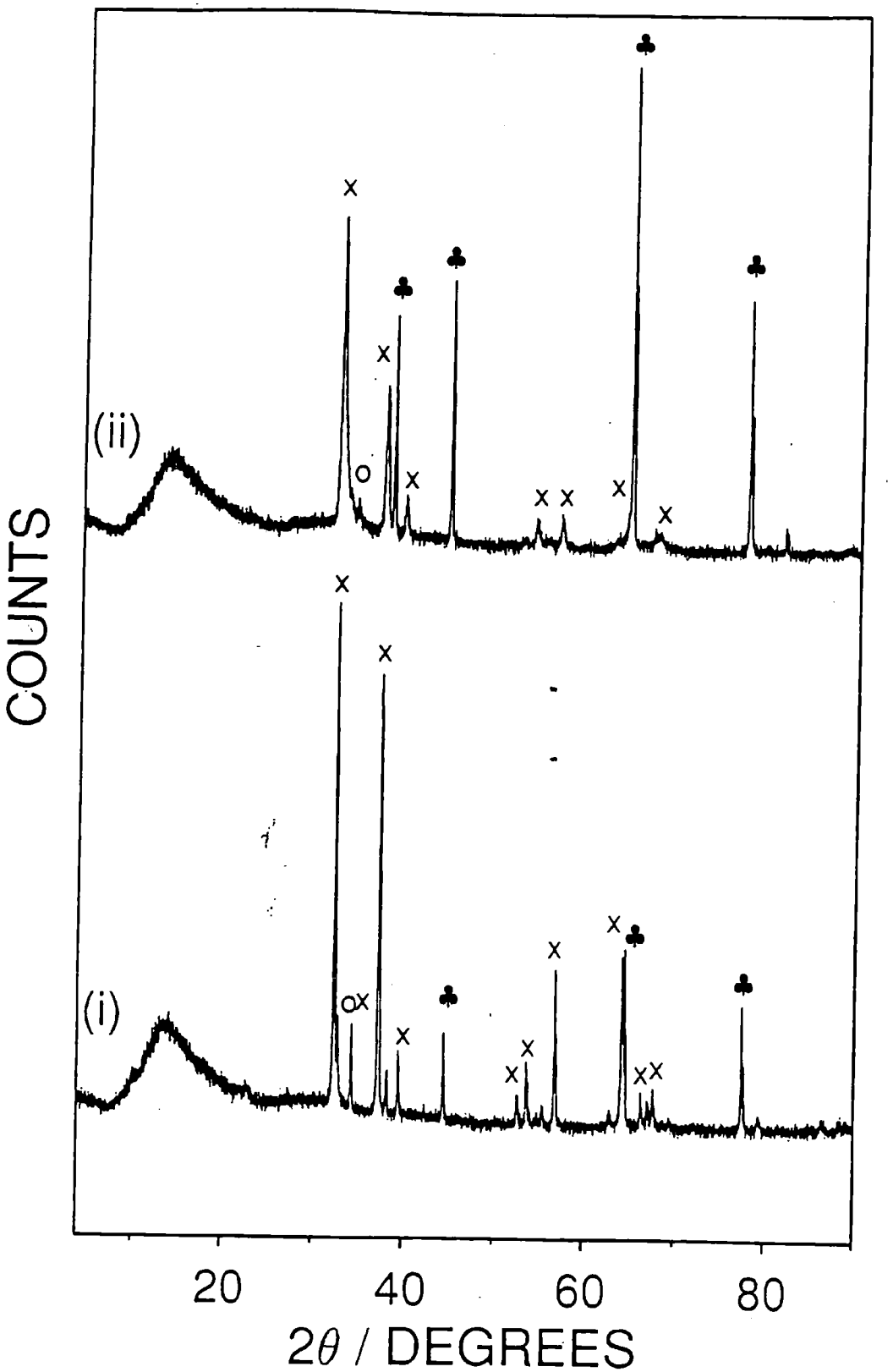

Figure. 6.3. XRD profile for 100μs on-time ((i) 10μs and (ii) 50μs off times). (Ag metal = ♣, AgO = x and Ag_2O = o)

6.3.2. Constant Off-Time

The off-times studied were 1ms (50ms, 1ms and 400μs on) and 50μs (400μs and 100μs on). The electron micrographs of the surface textures obtained are shown on below and on the following pages. XRD profiles are also shown for the same off-times as those for the SEM studies.

50ms on / 1ms off (scale 10μm = 1.5cm)

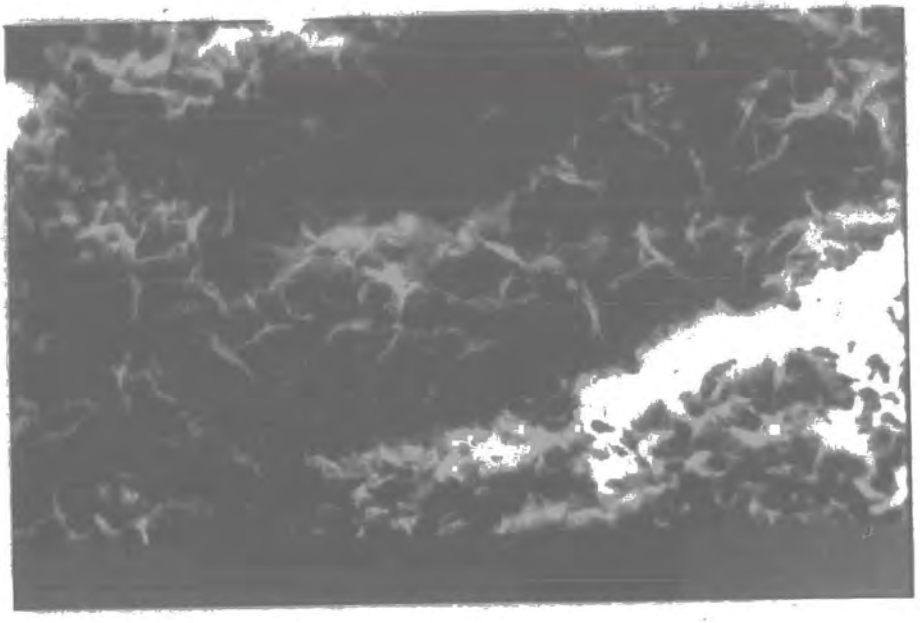

400μs on / 1ms off (scale 10μm = 1.5cm)

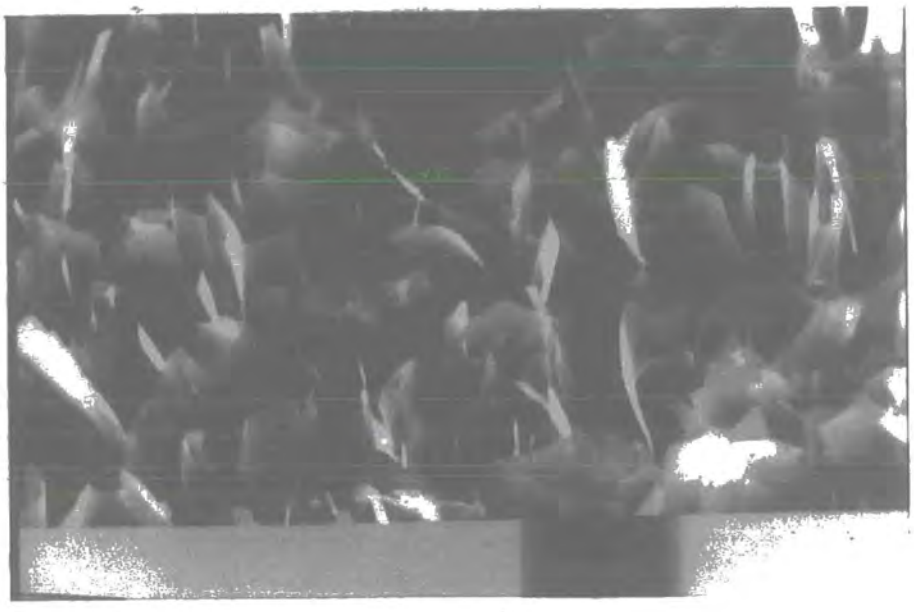

1ms on / 1ms off (scale 10μm = 1.5cm)

400μs on / 50μs off (scale 10μm = 1.5cm)

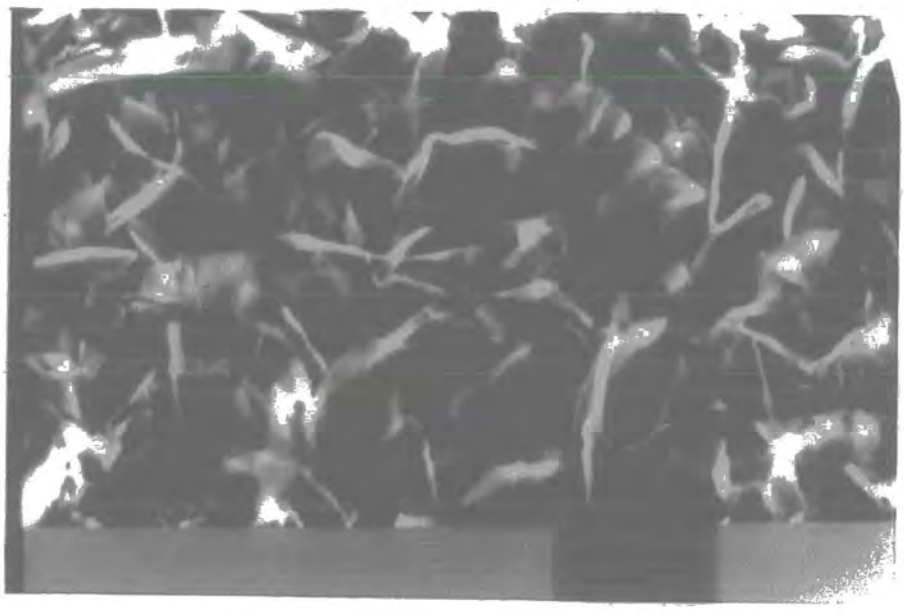

100μs on / 50μs off (scale 10μm = 1.5cm)

For constant off-times of 1ms, the surface texture appears to be affected by the plasma on-time (t_{on}). It can be seen from the photographs that the shorter the on-time, then the smaller the microoplatelets for 400 μs off-times. As the on-time is increased to 1ms the microplatelets appear larger, whereas increasing the time on further (for 50ms off-times) produces a clustered surface.

As for shorter off-times the surface textures appears to be similar, except that for an on-time of 400μs, slightly more sintering has occurred.

XRD profiles of the 1ms and 50μs off-times are shown in **Figure 6.4. and 6.5.** respectively (see page 157-158). The same off-times as those chosen for the SEM study were used.

The XRD profile for 1ms off-times, shows that for shorter on-times (400μs and 1ms off-times) the predominant oxide is AgO, whereas at longer on-times (with off-times of 50ms) the oxide present is primarily a mixed oxide of Ag_2O and AgO.

For shorter off-times the oxide present appears to be predominantly AgO.

All SEM results and XRD results were reproduced at least twice.

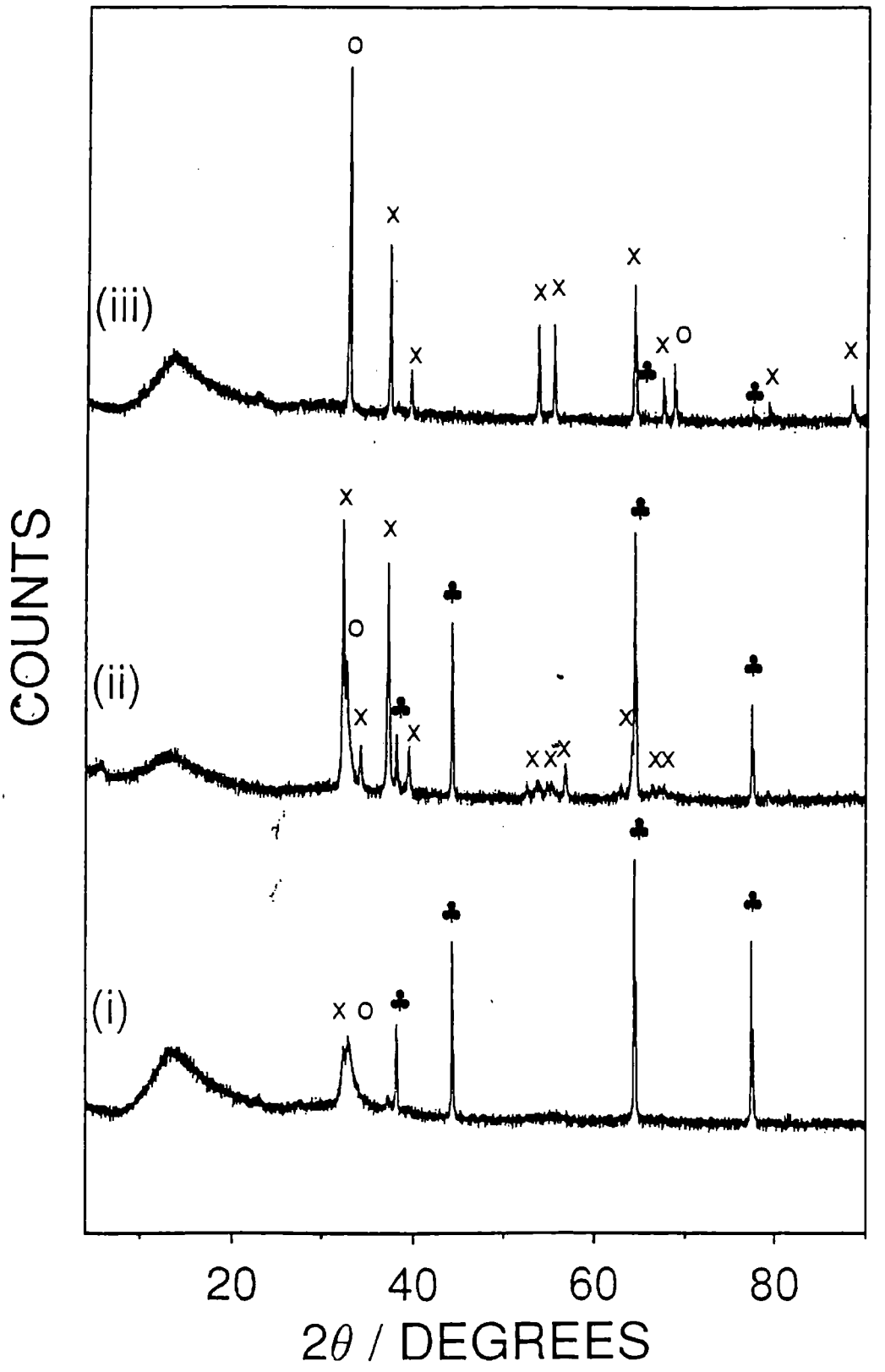

Figure. 6.4. XRD profile of 1ms constant off-time ((i) 400μs, (ii) 1ms and (iii) 50ms on-times). Labels are as follows: Ag metal = ♣, AgO = x and Ag_2O = o)

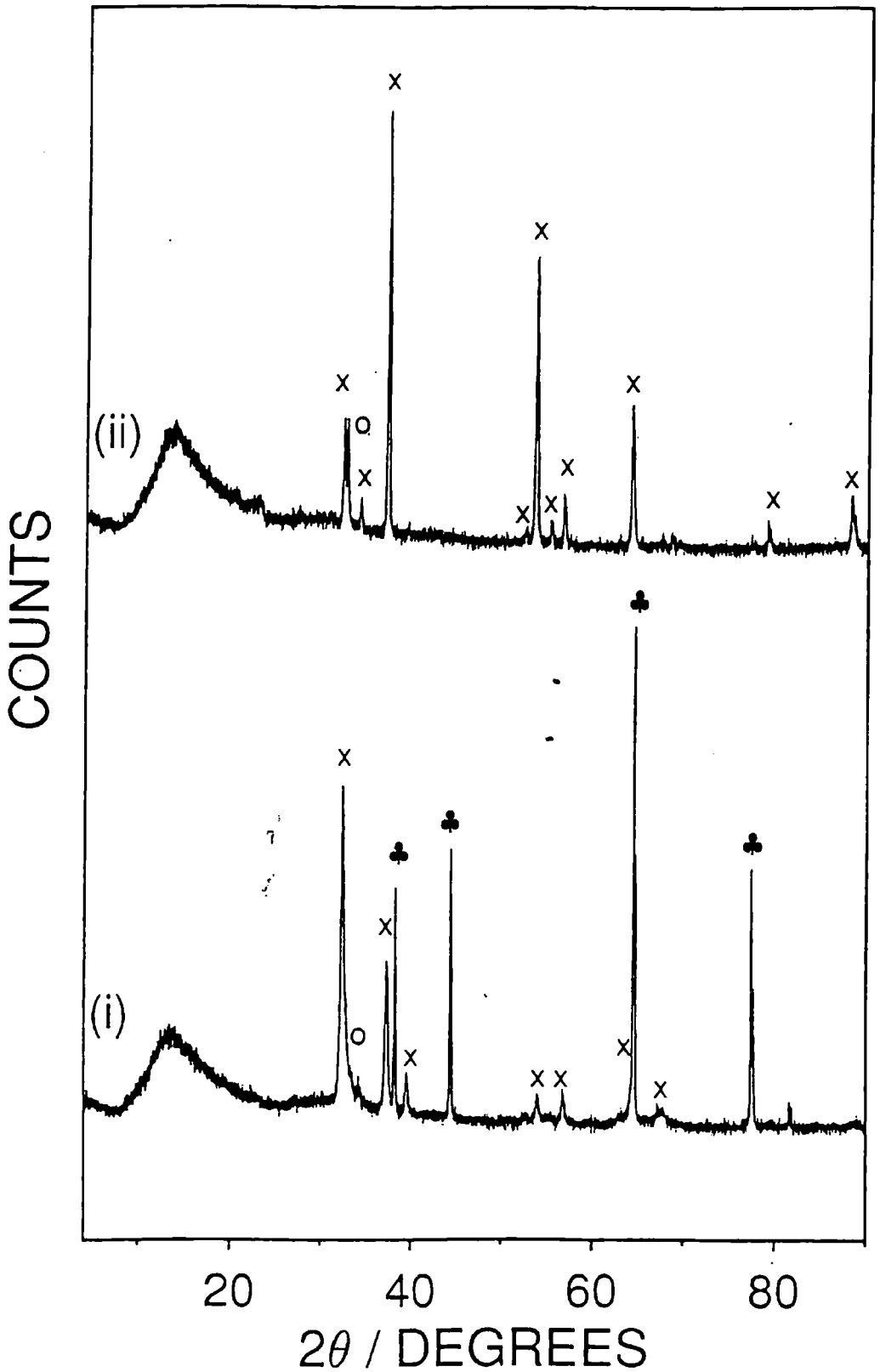

Figure. 6.5. XRD profile of 50μs off-time ((i) 400μs and (ii) 100μs on-times).

Labels are as follows: Ag metal = ♣, AgO = x and Ag_2O = o.

6.3.3. Constant Duty Cycle

The duty cycle ratio chosen to use was 2.5. This value was the largest duty cycle at which a plasma could be maintained. The three on/off times studied were 50ms on / 125 ms off, 400μs on / 1ms off and finally 100μs on / 250μs off.

50ms on / 125 ms off (scale 10μm = 1.5cm)

The photographs show that the surface textures obtained for all three conditions are very similar i.e. all appear to show the microplatelets starting to grow. The only apparent difference between the three textures obtained was the size which may be possibly due to the solid state configuration of the foils.

The XRD profile can be seen within **Figure 6.6.**. The same duty cycle was used as that for the SEM study i.e.2.5.

The XRD patterns for the three systems (showing AgO and Ag_2O) are very similar.

All XRD results and SEM results were reproduced at least twice.

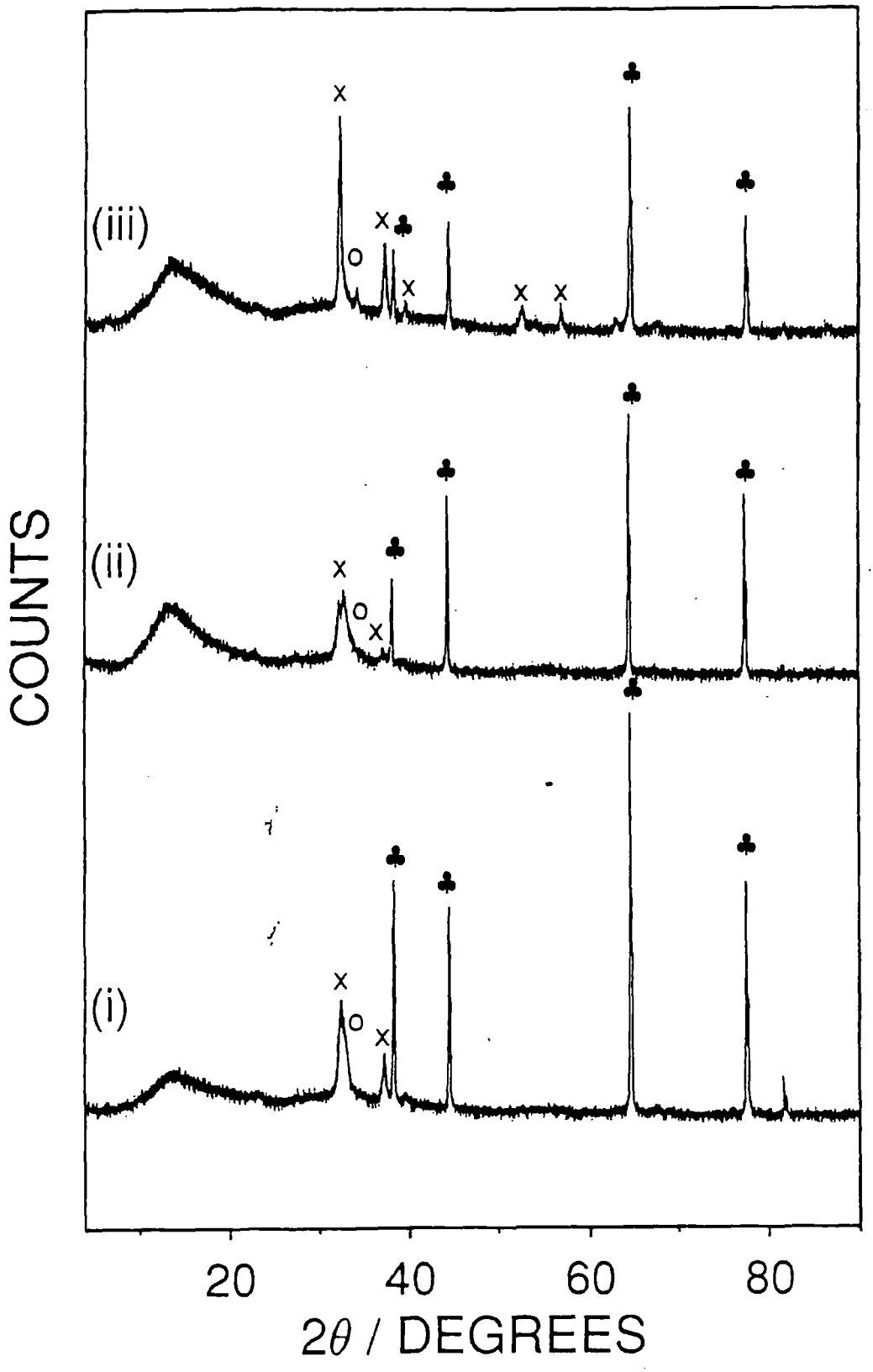

Fig. 6.6. XRD profile of constant duty cycle ((i) 100μs on/250μs off (ii) 400μs on/1ms off and (iii) 50ms on/125ms off. Labels used were as follows: Ag metal = ♣, AgO = x and Ag_2O = o.

6.4. Discussion

Pulsing has shown that both on and off times of the plasma affect the surface texture. However changing the on and off times, but maintaining the same duty cycle (i.e. average power) does not affect the surface topography considerably.

The on time of the plasma whether it be small or large, affects the surface texture of the oxidised foil. Increasing the on time leads to a series of subsequent changes in the surface texture of the foil which are as follows: **(1)** steady microplatelet growth up to a maximum obtainable size, **(2)** sintering of the microplatelets and finally **(3)** clustering of the surface (see **Figure 6.7.**). This suggests that the types of surface texture produced are on-time dependent.

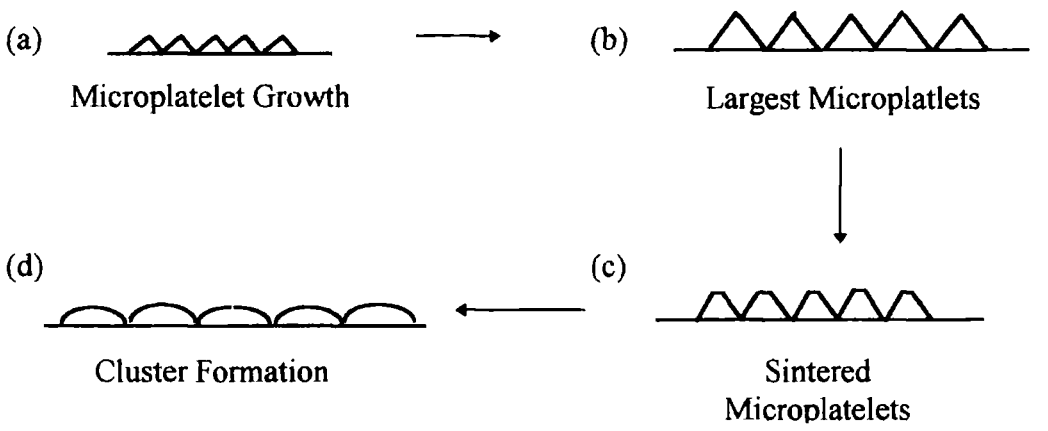

Figure. 6.7. Idealised simplified scheme of the structural changes that occur with increasing plasma on-times.

As for t_{off}, it too appears to play an important role in structural formation. Not surprisingly, decreasing the off time reduces cooling and so causes the surface structures to become more clustered or sintered.

If a closer look is taken at the effect of the on and off times of the plasma, it appears that the on time may be the more important. Evidence suggests that at short on times microplatelet growth occurs. As the on time is increased and subsequently the off time is decreased the microplatelets grow to an optimum size (have the greatest apparent surface area - observed using the naked eye). Further on-time increases cause the surface to sinter and finally clusters are formed as the on-time approaches that of a 30 minutes continuous plasma. There appears to be an optimum t_{on}:t_{off} ratio, to obtain the maximum size of microplatelets. This occurs when the t_{on}:t_{off} is approximately 1:1 or with a duty cycle of 0.5. Evidence supporting the above postulation is given within **table 6.1.**

The tabulated data suggests that the average power and t_{on} : t_{off} ratio are very important. These are the most important parameters, since it is only when the plasma is on that microplatelets will be formed. This indicates that the sheath potential and ion bombardment of the sample are very important for microplatelet growth. However as well as ion bombardment of the sample, due to ions traversing the sheath, photon irradiation of the sample may also be important [21]. Short lived atomic species are probably important in the chemistry occurring at the foils surface and in the formation of the oxide; however their involvement in structure formation will probably be very little unless it is ion-assisted [21].

Long lived species such as metastable atomic oxygen can be discounted from being the major components responsible for structural formation. The reasoning for

this is due to the longer lifetimes of these atomic species (^1D = 100s, ^1S = 0.74s at 0.1-7 torr), and thus if metastables were responsible, then the same structures would be produced for the experiments with the same on times but with differing off times [22]. This is not the case as can be seen from the SEM photographs.

Time On (t_{on})	Time Off (t_{off})	Total On Time (min)	Average Power (W)	Structures
50 ms	125 ms	10	8.3	S.M.
50 ms	50 ms	15	12.5	L.M.
50 ms	500 µs	29	24.7	C
100 µs	50 µs	20	16.7	L.M./S
100 µs	10 µs	27	22.8	S
400 µs	1 ms	8.5	7.1	S.M.
1 ms	1 ms	15	12.5	L.M.
50 ms	1 ms	29	24.5	C
400 µs	50 µs	27	22.2	S.
100 µs	50 µs	20	16.7	L.M./S
400 µs	1 ms	8.5	7.1	S.M.
100 µs	250 µs	8.5	7.1	S.M.
50 ms	125 ms	8.5	7.1	S.M.

S.M. = small microplatelets **L.M. = large microplatelets**
C = clusters **S= sintered**

Table 6.1. Tabulated data of pulsing parameters

As for the other species within the plasma, atomic oxygen will predominantly be involved in the production of the oxide film by reacting with the silver foil [23,24]. It is not known from these experiments what role negatively charged species will play in the formation of the structures [25].

The data obtained in this chapter supports the theories proposed in chapter 3, because for an ionic diffusion or ion-assisted neutral diffusion process to occur, the sheath region must be present [26,27] . This region will only be present when the plasma is on and will decay rapidly when the plasma has been extinguished [13]. This means that the mechanism proposed, the plasma on period will appear to be the most important, which is indeed observed. This prediction is very similar to that indicated by the time profile, within the oxidation study in Chapter 3, where the structure size changes with increasing reaction time.

6.5. Conclusion

Plasma on and off times affect the surface structures obtained and also the silver oxides produced. However varying the on and off times, but maintaining a constant duty cycle, does not alter the surface topography. The ratio of on to off times is important in determining what surface texture is obtained. This suggests that the most important factor is the average power delivered to the surface, which again promotes the mechanism suggested in previous chapters, where a diffusion process may be responsible for formation of the surface textures. Oxygen pulsed plasmas can also determine the extent of oxidation of the foil, where the shorter the on time the less oxidised silver foil.

REFERENCES

1. Hynes, A.M.; Shenton, M.J.; Badyal, J.P.S.; **Macromolecules, 1996**; Vol. 29, 4220.
2. Ryan, M.E.; Hynes, A.M.; Badyal, J.P.S.; **Chem. Mater. 1996**; Vol. 8, 37.
3. Nakajima, K.; Bell, A.T.; Shen, M.J.; **Polym. Sci., Polym. Chem. Ed., 1979**; Vol. 23, 2627.
4. Yasuda, H.; Hsu, T.J.; **Polym. Sci., Polym. Chem. Ed., 1977**; Vol. 15, 81.
5. Anandan, C.; Mukherjee, C.; Seth, T.; Dixit, P.N.; Bhattacharyya, R.; **Appl. Phys. Lett., 1995**; Vol. 66(1), 85.
6. Labelle, C.B.; Limb, S.J.; Gleason, K.K.; **J. Appl. Phys., 1997**; Vol. 82(4), 1784.
7. Booth, J.P.; Cunge, G.; Sadeghi, N.; **J. Appl. Phys., 1997**; Vol. 82(2), 552.
8. Llewellyn, I.; Rimmer, N.; **Thin Sol. Films, 1990**; Vol. 191, 135.
9. Savage, C.R.; Timmons, R.B.; Lin, J.W.; **Chem. Mater. 1991**; Vol. 3, 575.
10. Clark, D.T.; Shuttleworth, D..J.; **Polym. Sci., Polym. Chem. Ed., 1980**; Vol. 18, 27.
11. Boswell, R.W.; Porteus, R.K.; **J. Appl. Phys., 1987**; Vol. 62, 3123.
12. Boswell, R.W.; Henry, D.; **Appl. Phys. Lett., 1985**; Vol. 47(10), 1095.
13. Scarsbrook, G.; Llewellyn, I.P.; Ojha, S.M.; Heinecke, R.A.; **Vacuum, 1988**; 627.
14. Shard, A.G.; Badyal, J.P.S.; **Polym. Comm., 1991**; Vol. 32, 152.
15. Filseth, S.V.; Welge, K.H.; **J. Chem. Phys., 1969**; Vol. 51, 839.
16. Hansen, S.G.; Luckman, G.; **Appl. Phys. Lett., 1990**; Vol. 56(8), 719.

17. Samukawa, S.; Furuoya, S.; **Appl. Phys. Lett., 1993**; 2044.

18. Samukawa, S.; **Appl. Phys. Lett., 1994**; Vol. 64, 3398.

19. Rinsch, C.L.; Chen, X.L.; Panchalingam, V.; Eberhart, R.C.; Wang, J.H.; Timmons, R.B.; **Langmuir, 1996**; Vol. 12(12), 374.

20. Sanner, M.A.; Park, J.Y.; **Rev. Sci. Instrum., 1997**; Vol. 68(3), 1575.

21. Hess, D.W.; **J. Vac. Sci. & Tech., 1990**; Vol. A8 (3), 1677.

22. Wu, D.; Outlaw, R.A.; Ash, R.L.; **J. Appl. Phys., 1993**; Vol. 74(3), 4990.

23. Koroleva, E.A.; Khvorostovskaya, L.E.; **Soviet J. Spectroscopy, 1971**; Vol. 8, 627.

24. Peters, P.N.; Linton, R.C.; Miller, E.R.; **Geophys. Res. Lett., 1983**; Vol. 10(7), 569.

25. Moore, W.M.; Codella, P.J.; **J. Phys. Chem., 1988**; Vol. 92, 4421.

26. Chou, C.H.; Phillips, J.; **J. Vac. Sci. Technol. 1991**; Vol. A9(5), 2727.

27. Yasanaga, H.; Wu Nan, J.; **Sprin. Ser. Mater. Sci., 1992**; Vol. 17, 263.

CHAPTER 7

PLASMA OXIDATION OF AN EARTHED SILVER FOIL

7.1. Introduction

The previous chapter presented the different structures that could be obtained, after pulsed oxygen plasma treatment of silver foils. It was hoped that a possible mechanism as to why these features form could be identified. However, pulsing alone was unable to determine such a mechanism, and thus it was thought that earthing the silver foil (which will be described in this chapter) could help achieve this. This involved earthing the silver foil, during plasma treatment, to observe what effect this might have on the surface and bulk charges that can collect upon the foil. It was hoped that by combining the data from this chapter with that of the previous one, a specific mechanism could be established.

7.1.1. Why Earth the Sample?

As has been stated within previous chapters, placing a sample within a plasma environment leads to the accumulation of charge upon the sample[1,2]. The charge capacity of the sample will depend on the nature of the material being processed and the plasma conditions [1,2,3]. This charge is known as the floating potential of a sample[3]. The floating potential of a material is important, because it is the difference

between this potential and the voltage of the bulk plasma which is responsible for sheath formation i.e. the potential drop above the material [3,4]. The voltage of this sheath determines the extent of ion bombardment of a substrate [4]. It was thus thought that earthing the substrate would remove the floating potential, and thus result in less or no ion bombardment of the material. This would result in different structures being obtained to that of the unearthed sample.

It has been proposed throughout this thesis, that some form of diffusion process is responsible for microplatelet or cluster formation. It was hoped that by removing the charge from the substrate the extent of diffusion might be reduced or eliminated, and hence little disruption to the surface would occur. However, it is also possible that the surface texture obtained may be the same as that of the non-earthed sample, suggesting the diffusion process is not affected, and thus a new mechanism would have to be proposed.

Several studies have shown that the ion energy/sheath potential has been affected by biasing, or pulsing of a plasma, or by earthing of the substrate [5,6]. The oxidation of lead films has been extensively studied, especially where the lead film has been placed upon the cathode to try and increase the ion bombardment [5,6]. Other metal substrates which have also been studied, where the energy of the impacting ions is practically zero and no significant structural formation was observed [7,8]. Pulsing has also been used to try and remove or limit the effects of ion bombardment on a substrate by changing the sheath voltage e.g. etching of a silicon wafer by SF_6 [9]. Additionally permeability studies have shown that ions affect the permeability process, by increasing the diffusion through a membrane[10]. As to what effect

removing the bias from a material has on a diffusion process such as the one proposed has not been reported in the recent literature.

7.2. Experimental

The experimental set-up was similar to that used for all previous experiments, except for a slight modification to the plasma reactor. This modification involved welding a quarter inch diameter glass tube to the base of the reactor, located between 8-9 cm from the live electrode. The earthing probe could then be inserted into this tube, and sealed within it using a swagelok (1/4 to 1/8 reducing union). The probe was made of stainless steel and was connected to the earthing framework within lab 98 (see **Figure 7.1.**). The glass tile, on which the silver foil was placed, had a hole (1 cm diameter) cut through it, just below where the foil would be situated, so that contact could be made between the base of the foil and the earthing probe (see **Figure 7.1.**).

The foil's dimensions differed, from that used in previous experiments, in that the main part of the foil had a side length of 2 cm, with two small arms radiating from it. These arms were bent around the tile, so that in applying pressure between the earthing probe and foil, a decent contact could be obtained (**see Figure 7.1**).

The experiments performed were:

(a) standard oxygen plasma treatment of silver foils,

(b) treatment of the foil samples within the plasma, with the inserted probe not touching the foil,

and (c) with the earthing probe touching the silver foil.

The resultant morphologies were then observed using Scanning Electron Microscopy (see section 3.2. in Chapter 3).

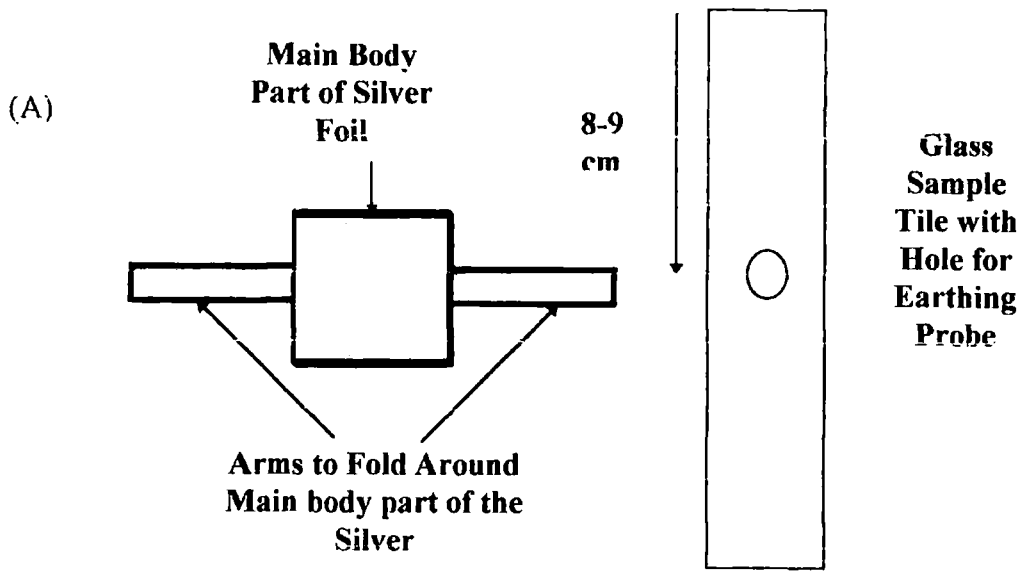

Figure. 7.1. Schematic of the silver sample treated and the supporting glass tile.

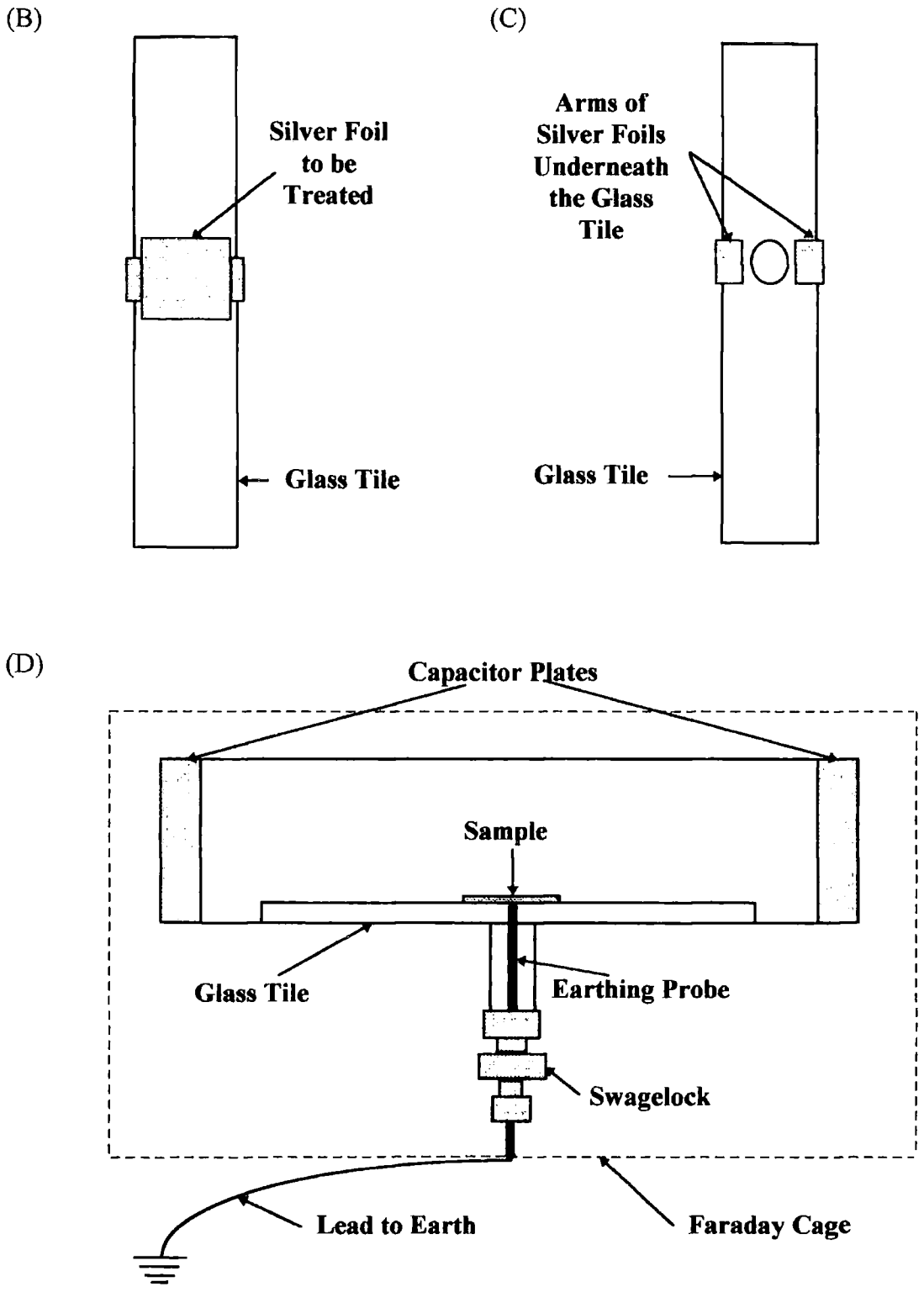

Figure. 7.1. cont. (b) Aerial view of the foil on the tile (c) Underneath view of sample on the tile (d) Diagram of the reactor assembly used for earthing studies (for the rest of the reactor see Chapter 3).

The surface had little significant surface structure when compared to the non-earthed sample. The film formed appeared very thin (observed by the naked eye) when scratched. Also the film was a faint blue colour, again suggesting that the film was thin (the silver colour was shining through the thin black oxide layer).

This experiment was repeated and simialr results were obtained.

7.4. Discussion

7.4.1. Non-earthed Sample

The photographs exhibited previously, show that earthing the sample changes the surface texture changes considerably.

Placing the silver foil within the plasma results in charge build-up on the foil. However because silver is a good conductor, it would normally be expected that this charge would conduct away from the sample [11]. As has been previously stated, the foil is situated upon a glass tile, which is non-conductive, and will thus forbid the flow of charge away from the foil [12]. This means that initially the silver foil will act in a similar way to a capacitor plate i.e. stores charge (see **Figure 7.3.**) [13].

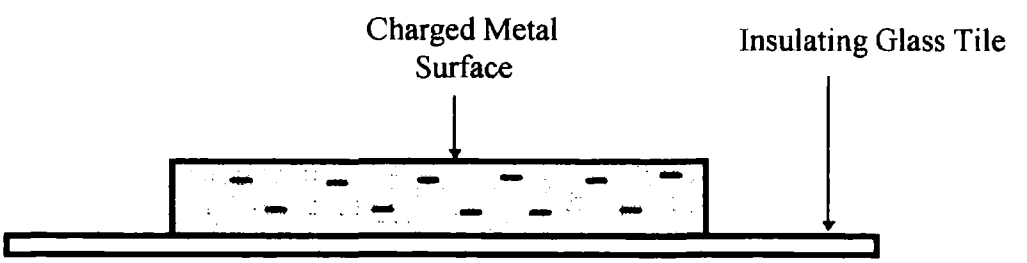

Figure. 7.3. Initial charge build-up on the silver metal surface.

However as this foil is attacked by oxygen, an oxide layer will form producing a metal/oxide interface (see **Figure 7.4.**).

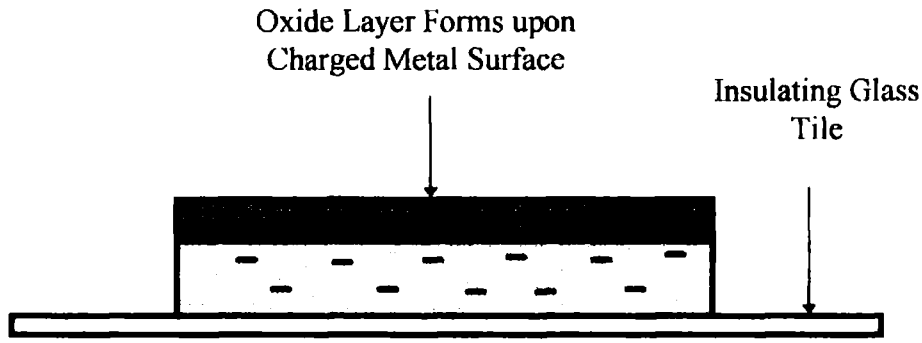

Figure. 7.4. Oxide layer formation

The oxide formed would normally possess semiconductor characteristics (Ag_2O [14] and AgO [15] are both n-type semiconductors), and thus would normally allow the electrons to flow through it and across the interface. However, the oxide layer will posses insulating properties, rather than semiconducting, due to the negative bias on the silver, which will inhibit the flow of electrons through the oxide layer (see **Figure 7.5.**).

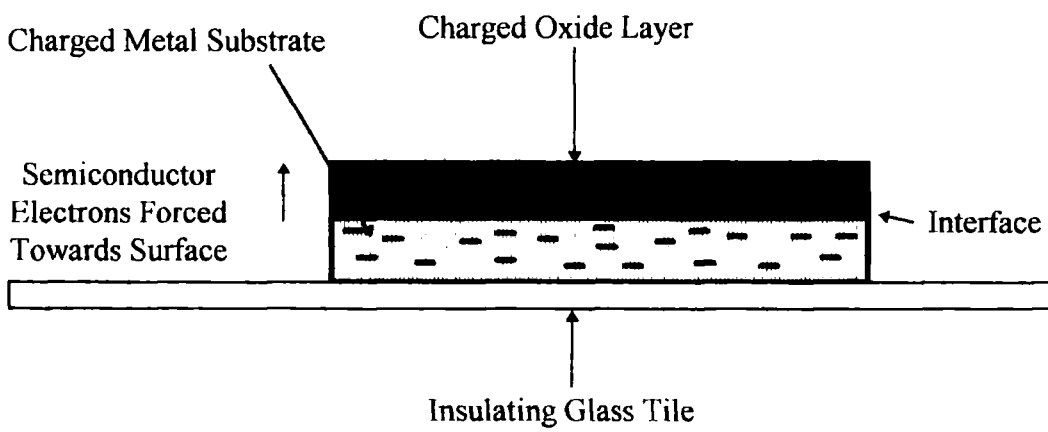

Figure. 7.5. Charge accumulation on the silver oxide

Consequently the repelled electrons will tend to reside at the furthest point from the interface, which will be the surface of the oxide[16]. This process where electrons are repelled to the furthest point from a like charge, results in charge being located within the uppermost atomic layers of the sample. This is called surface charging. This phenomena is termed surface charging. This will create a negative bias gradient tending towards the oxides surface (see **Figure 7.6.**).

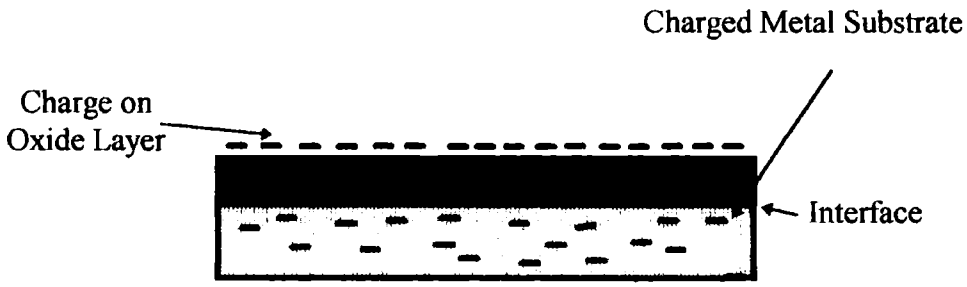

Figure. 7.6. Surface charge accumulation on the silver oxide layer

This resistance to the flow of charge across a metal/semiconductor interface may also be represented by a simple band theory model [17]. In the case which has been stated above the metal will accumulate charge, which could lead to the promotion in energy of any vacant bands within the metal to above that of the semiconducters filled conduction bands[17]. Now because the metal's accepting bands are of a higher energy than the donating bands of the oxide, the energetics of the system drastically reduces the flow of electrons across the interface (see **Figure 7.7.**)[17].

Earthing the foil with a stainless steel probe will allow electrons to flow from the metal to earth, and thus the negative bias upon the silver foil is removed or if

proper contact is not made a certain percentage of the charge may leave the sample (see **Figure 7.8.**)[18].

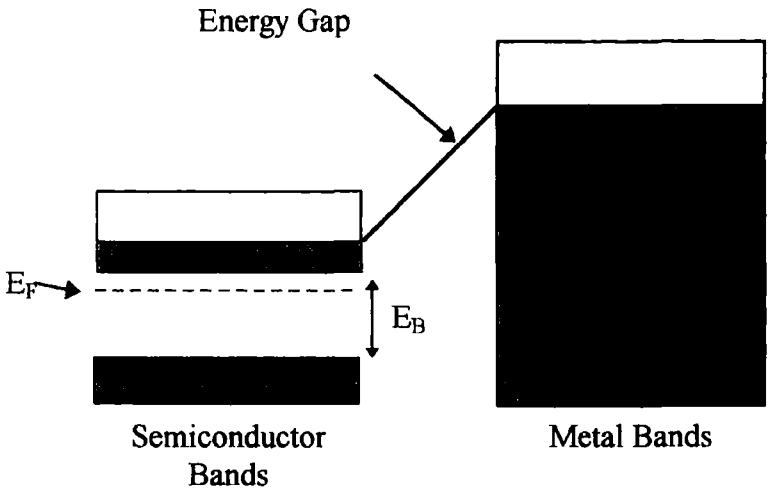

Figure. 7.7. Situation after build up on the metal and semiconductor - no charge flow occurs across interface.

7.4.2. Earthed Sample

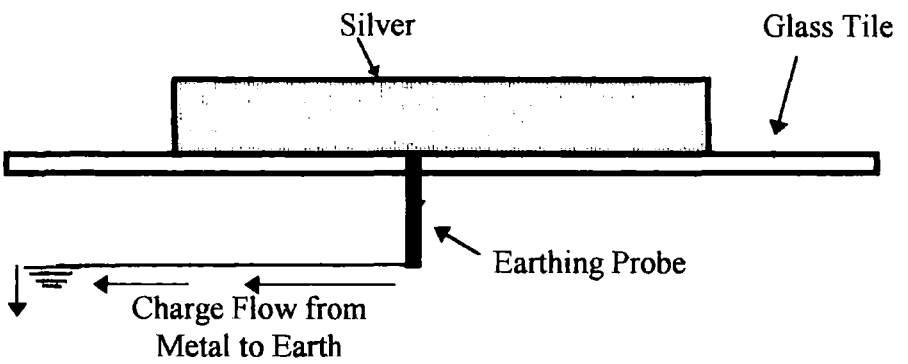

Figure. 7.8. Earthed silver sample before oxide forms.

Oxide formation occurs on the silver, and this time any electrons which collect upon it or within it will flow through the semiconductor, across the metal/oxide interface and finally to earth. This means that the negative charge which

accumulated upon the non-earthed sample will be removed when earthing the sample, due to the formation of a resistance free pathway for the flow of charge to earth. (see **Figure 7.9.**).

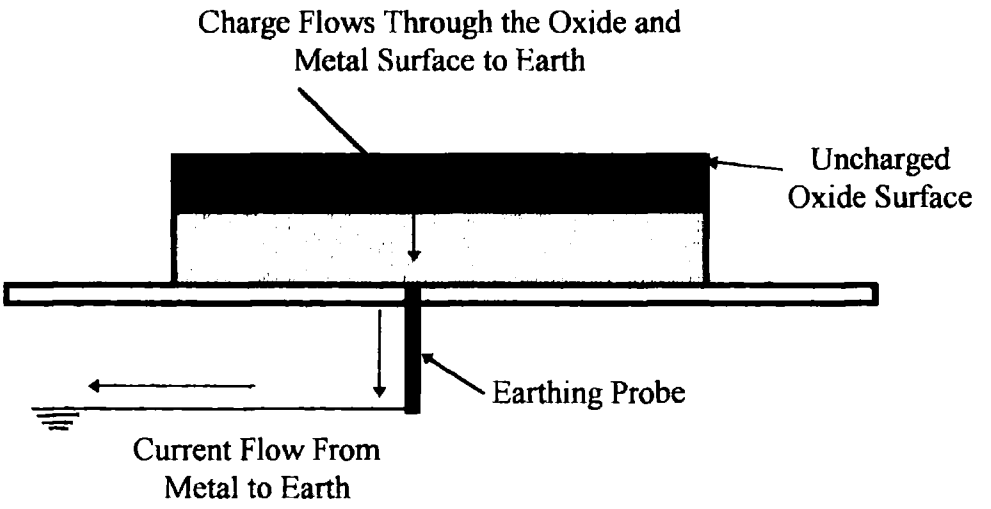

Figure. 7.9. Current flows through oxide layer and metal to earth

The sudden change in properties of the semiconductor can again be explained by general band theory. Earthing the silver results in electron flow from the foil, meaning that no charge will collect upon it. The vacant conduction bands of the metal will be at a lower energy than the donating bands of the semiconductor. This means that electrons will move from the filled conduction bands of the oxide, to the empty bands of the metal, resulting in electron flow across the metal/oxide interface. This phenomena is similar to that observed for p-n junctions in semiconductors (see **Figure 7.10.**) [17,18].

Microplatelet formation can possibly be linked to the band theory rationalisation given previously. In the first case proposed, where electron flow from the semiconductor to the metal is drastically reduced, it would be expected that any

electrons which reach the oxide may reside at the furthest point from the interface i.e. charge being located at the surface of the foil - surface charging. This would thus set up a negative potential towards the surface of the oxide which would be able to attract any positive silver ions present within the oxide layer [20].

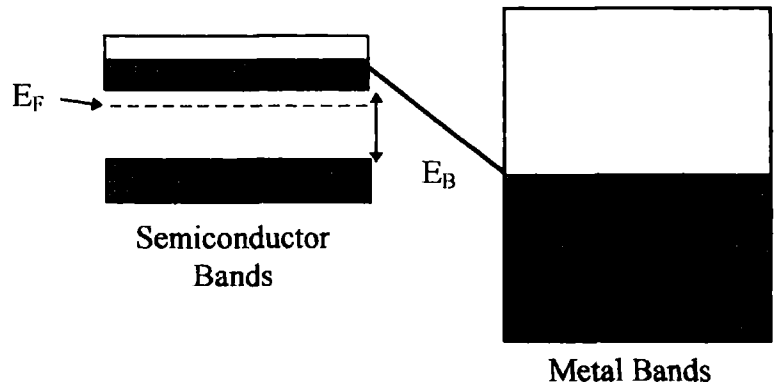

Figure 7.10. Band energy diagram for earthed sample.

These ions would migrate towards the surface, by a path determined by the solid state chemistry of the oxide [21]. This solid state structure would be affected by ion bombardment which could lead to the formation of defects such as dislocations, point defects and vacancies [21]. These defects may enhance the diffusion process. If the migration process is allowed then a roughened surface is likely.

In the second case, where the negative surface potential has been removed, then it would be expected that if the migrating species were positive, then a different surface topography would be obtained, which is what is observed. There is a strong case for ion migration over neutral migration, because if the structures formed were due to diffusion of zero valent silver, then a similar surface topography to the unearthed sample would be expected [20] (removing the negative bias upon the oxides

surface would have little effect on the diffusion of a neutral species). However ion-assisted neutral migration can still not be discounted, because removing the negative bias will reduce ion bombardment of the substrate and thus would affect the diffusion process [22].

The alternative mechanism to that suggested throughout this thesis, is sole ion bombardment of the sample [22]. However the experiments carried out cannot distinguish between ion bombardment and a diffusion processes, as both depend on the presence of a negative surface bias.

The flux of electrons and negatively charged species to the samples surface also increases if the floating potential is removed [23]. However whether these species can create similar surfaces to those observed would require further experiments.

As for the oxide layer formed, it appears (from observing with the naked eye) that the oxide layer formed upon the earthed sample is thinner than that found on the standard sample. The earthed foils layer was blue in colour which hinted also at the thinness of the layer (with the silver metal shining through) [23]. This layer is similar to that observed when the tarnishing of metals occurs. As for the standard oxide, the layer appeared far thicker and was black in colour. However as was previously stated the adherance of the oxide to the metal was poor. Positive ion bombardment appears to affect the extent of oxidation of the silver, and thus earthing the sample reduces the films thickness.

As for observing any changes in the glow around he sample as the foil when the foil was earthed was not extensively looked at. It was thought that for to observe any changes to the dark region around the sample (is approximately 1mm in thickness) with the naked eye was not good scientific practise. As for using optical

emission techniques for to look at this change, or investigate the potential around this region using a Langmuir probe, these were unable to be used due to neither of these being available within the research lab.

It would be possible to look at the current flow through the earthing probe whilst the sample is earthed to prove that earthing does really remove charge from the foil. However due to the lack of time this was unable to be done, but has been included in the further work section.

7.5. Conclusion

Non-earthed silver foils when treated within an oxygen plasma produces a microplatelet surface texture, whereas earthed substrates do not. This indicates that charge accumulation upon the surface of the growing oxide is very important in terms of growing microplatelets. This appears to be the case because when the sample is not earthed it is postulated that a high resistance to transfer of electrons from the oxide surface to the metal exists and thus accumulation of charge occurs at the oxides surface. This aids any positive ion diffusion process which may be occurring within the oxide. However when the substrate is earthed electrons are able to flow from the oxide to the metal and thus any positive ion diffusion process will not be aided. A simple band theory model has been postulated which indicates that the difference in band energy between the oxide and metal is very important in determining whether electrons can flow across the metal/oxide interface or not and thus whether microplatelet growth will occur.

REFERENCES

1. Grill, A; **Cold Plasma in Materials Fabrication**; IEEE Press: 1994.
2. Chapman, B.; **Glow Discharge Processes**; Wiley: New York, 1980.
3. Howatson, P.M.; **Introduction to Gas Discharges**; Pergammon Press: 1967.
4. Hess, D.W.; **J. Vac Sci & Technol. 1990**; Vol. A8 (3), 1677.
5. Fromhold, A.T.; Baker, M.; **J. Appl Phys, 1980**; Vol. 51 (12), 6377.
6. Greiner, J.H.; **J. Appl Phys, 1974**; Vol. 45 (1), 32.
7. Chou, C.H.; Phillips, J.; **J. Appl Phys, 1990**; Vol.68 (5), 2415.
8. Chou, C.H.; Phillips, J.; **J. Vac. Sci. & Technol. 1991**; Vol. 9,
9. Boswell, R.W.; Porteous, R.K.; **J. Appl Phys, 1987**; Vol. 62 (8), 3123.
10. Outlaw, R.A.; **J. Appl Phys, 1990**; Vol. 68 (3), 1002.
11. Greenwood, N.N.; Earnshaw, A.; **Chemistry of Elements;** Pergammon Press: 1984.
12. Lide, D.R.; **Handbook of Chemistry & Physics, 71st Edition**; CRC Press: USA, 1990-91.
13. Isaacs, A.; Pitt, V.; **Physics**; Hamlyn Press: London, 1982.
14. Rozenblyum, N.D.; Bubyreva, N.S.; Bukhareva, V.I.; Kazakevich, G.Z.; **Russ. J. Phys. Chem., 1966**; Vol. 40(10) 1324.
15. Yakovleva, A.A.; Borisova, T.I.; Vesellovsku, V.I.; **Russ. J. Phys. Chem., 1962;** Vol. 36(7), 763.
16. Frankl,D.R.; **Electrical Properties of Semiconductors Surfaces**; Pergammon Press, London, 1967.

17. Cox, P.A.; **Electronic Structure & Chemistry of Solids**;. Oxford University Press: Oxford, 1991.

18. Vossen, J.L.; Kern, W.; **Thin Film Processes II**; Boston Acadamy Press: Boston, 1991.

19. Kittel, C.; **Introduction to Solid State** Physics; Wiley & Sons: New York, 1986.

20. Sears, W.M.; Love, D.A.; **Phys. Rev. B, 1993**; Vol. 47, 12972.

21. Kofstad, P.; **Oxid. of Metals, 1995**; Vol. 44(1/2), 3.

22. Veprek, S.; Venugopalan, M.; **Elementary Processes at Solid Surfaces Immersed in Low Pressure Plasmas, Plasma Chemistyr III**; Verlag: Berlin, 1980.

23. Hartney, M.A.; Greene, W.M.; Soane, D.S.; Hess, D.W.; **J. Vac. Sci. & Technol., 1988**; Vol. B 6(6), 1892.

CONCLUSION

This thesis has examined and discussed the relevant data obtained when modifying the surfaces of silver foils by exposure to a low pressure, non-equilibrium oxygen plasma.

Modification of the surface was found to be dependent upon several processing parameters. The desired surface to be obtained was an enhanced surface area silver oxide layer and in fact this was achieved. This texture was achieved at a pressure of 0.8 mbar, power of 15W where energy transfer to the surface is low. Increasing the time from 1 min. to 2 hrs. led to a gradual growth of the microplatelets, with the optimum growth of the microplatelets occurring between 30 min. and 1 hr. The microplatelets were also found only to be produced at distances of approximately 8cm from the live capacitor electrode. Increasing the power, decreasing the pressure or moving the foil closer to the live plate led to sintering of the surface oxide with eventually a clustered arrangement being produced. The data obtained suggested that the process for microplatelet formation was probably diffusion of a neutral or ionic species towards the surface and that ion bombardment could be important.

Powder diffraction patterns showed that the production of surface nanoplatelets coincided with the presence of a mixed metal oxide (predominantly AgO). However when a clustered texture was obtained the predominant oxide was Ag_2O. The reasoning behind the link between oxide and texture obtained was linked to the different silver diffusion coefficient through these oxides. When clusters are formed Ag_2O is the major oxide which has the larger diffusion coefficient. As for AgO, which has a lower diffusion coefficient, microplatelets are formed upon the surface. Specifically the silver

species present within AgO, and in particular the immobile Ag^{III} species, could be the reasoning for this selective diffusion process.

The microplatelet oxide surface were reduced back to metallic silver if the correct conditions were chosen (15W, 0.8 mbar). At higher powers or lower pressures, a similar trend to that observed for the oxygen plasma treatment existed where the nanoplatelet structures sintered at high powers and low pressures. This was linked to the amount of energy transferred to the surface via either photons or ions. Increasing the time of the reduction process causes the gradual reduction of AgO back to silver metal.

Further evidence for a diffusion controlled process was found through pulsing and earthing experiments. The pulsing experiments showed that the average power of the plasma and thus average time on were the most important parameters. This suggests that a short-lived process is responsible for microplatelet and cluster formation. More precisely the sheath appears to be the major factor controlling the diffusion process.

The earthing studies and pulsing experiments indicated the mechanism for microplatelet formation. It was shown that nanoplatelet formation could be inhibited, by removal of the floating potential from the substrate. This indicates that the most probable process, as first predicted, is an ion diffusion mechanism.

So in summary this thesis has shown that silver foil surfaces can be modified by oxygen plasmas. The microplatelet structures produced can be reduced back to metallic silver without any apparent loss in structural integrity by a hydrogen plasma. The formation of the microplatelets is probably due to an photon/ion assisted ionic diffusion process.

RECOMMENDATIONS

In result of the conclusions reached within this thesis, about the diffusion of a charged silver species through an oxide layer to form various surface textures, the following work would be recommended for any furture studies.

(A) **Biasing Experiments** - here the foil can be biased positively or negatively by applying an elelctric potential to the substrate. This may increase the ion bombardment of the substrate by positive and negative species. This may give an indication as to which species are responsible for the surface structures. Also current measurements would also be useful to try and back up the proposed mechanism stated in Chapter 7.

(B) **Surface Area Measurements** - surface area determination of the high aspect ratio silver oxide and reduced silver should be performed.

(C) **Labelling Studies** - labelling stuies of oxygen or silver species would help to elucidate the mechanism by which these surface textures are formed. This would probably be used to determine whether the diffusion process proposed within this thesis actually occurs.

(D) **Catalytic Studies** - studies involving the newly modified silver as a catalyst for ethylene epoxidation should be investigated, as the increased surface area may advantageously effect theselectivity or rate of the formation of ethylene oxide.

(E) **Other Plasmas** - using plasmas such as H_2S and H_2O may effect the surface texture by having the oxidation/reduction processes occurring simultaneoulsy. Also reacting the foil in plasmas containing chlorine, bromine and iodine may also change the surface morphology obtained by different silver salts being formed which may have more mobile species present within it.

(F) **Manufacturing of Raney Nickel and other Metal Catalysts** - by taking alloys of various metals it may be possible to produce Raney Nickel catalysts, by reacting the alloy within a certain reactive plasma. This would etch preferentially one component of the alloy and thus leave a porous substrate behind, which may be catalytically useful.

APPENDIX I

FURTHER TECHNIQUES FOR ANALYSIS OF SILVER OXIDES

Apart from Powder X-ray crystallography, other techniques may be used to determine the oxides present at the surface and within the bulk of the plasma produced oxide layer.

The first of these is Raman Spectroscopy, which can be used to study the vibration of molecules whether they are a solid, liquid or gas, is typically a bulk analysis technique [1,2,3]. Raman Spectroscopy has significantly advanced over the past twenty years and has become a very powerful technique [1,3]. Raman Spectrosopy exists due to the interaction between electromagnetic radiation and a molecule which results in scattering of the incident photons - an effect known as Raman scattering. Raman Scattering arises due to the polarisability of a molecule - one of the conditions for a molecule to be Raman active [1,2,4]. These scattered photons are either of a lower or higher energy than the incident photons [1,2,4]. Thus there are two sets of lines which are produced within a Raman spectra and these are called the Stokes (lower in energy than the exciting photons) and anti-Stokes lines (those which are of a higher energy than the exciting photons energy) [1,2,4].

Raman Spectroscopy, in particular Surface Enhanced Raman Spectrosocpy technique (which can be used to looked at adsorbed species upon a substrate), could

be used to study the silver/silver oxide system in question [1,3]. The Raman active bands for AgO are located at 230, 410, 430 and 920 (a 2-phonon line) cm^{-1} [5,6] As for Ag_2O the relative peaks which are characteristic of this oxide are located at 410 cm^{-1}. and 535 cm^{-1}, however these peaks are relatively weak [5]. Surface Enhanced Raman Spectroscopy could suffer from possess some complications, in terms of using it to study the silver oxide system, in that due to the presence of adsorbed hydroxyl groups, adsorbed oxygen and subsurface oxygen species, the spectra could become quite complex. The peaks for these species are located at 860 cm^{-1} (OH vibration), 330 and 460 cm^{-1} (adsorbed O atoms) and also 630 cm^{-1} (subsurface oxygen) [5].

Raman Spectroscopy/Surface Enhanced Raman Spectroscopy does have, from the above results, the potential to study the silver/silver oxide system especially in using the technique as an in-situ device for studying the oxides present at certain stages of oxide growth i.e. a Raman spectra could be taken an regular intervals between 5 and 30 minutes to observe which oxides are actually present or disappearing. However some potential problems with the technique could be:

(a) Some of the peaks, especially the 410 cm^{-1} peak, can be masked by the peaks located at 330 or 460 cm^{-1}, thus prohibiting the identificationof the Ag_2O peak [5].

(b) Determination of other silver oxides present may be difficult, due to the peaks of these new oxides overlapping with the peaks for Ag_2O and AgO.

(c) The energy of laser used is very important as photochemical oxidation and reduction of the system could occur (similar to that which may occur using XRD).

Another technique which has potential to study the silver/silver oxide system is X-ray Spectroscopy (XPS) [7,8,9]. XPS is a very surface sensitive technique and can probe monolayer coverage of 10^{-3} on a surface area of $0.2cm^{-2}$ [9]. It will typically probe electrons from the top three atomic layers of a sample (typically 10Å), but this again depends on which form of the XPS technique is used , because if angle resolved XPS is used then the technique becomes even more surface sensitive [7,8]. XPS, as has already been stated, measures the kinetic energy of an ejected photoelectron, and relates this to the binding energy of the electron from a certain atom [7,8,9]. The energy of the photoelectron can be affected by the chemical environment in which the element is situated and also from which orbital the electron originated from [7,8,9]. XPS apparently appears like the ideal technique for identifying the silver oxides present within this thesis. However a problem does exist in using this technique and that is that the $Ag3d_{5/2}$ binding energy shifts for the various oxides are too small [10,11]. This can be seen from the following table of $Ag3d_{5/2}$ peaks [10,11]:

Chemical Species	**Binding Energy (eV)**
Ag metal	368.0
AgO	367.3
Ag_2O	367.7

As can be seen from the above table the binding energies for the $Ag3d_{5/2}$ peaks are so close together for just the two oxides stated above. This means that resolving which oxide is which can be very difficult. The alternatives to looking at these peaks

is to look at the oxygen binding energies for the various oxides but this can become even more confusing due to the presence of subsurface and adsorbed oxygen species [10,11]. The binding energies for the relevant oxides and the other possible oxygen species present are tabulated overleaf [10]:

CHEMICAL SPECIES	BINDING ENERGY (eV)
AgO	528.5
Ag_2O	528.8
Subsurface O	531.0
Chemisorbed O	528.2
$Ag_2CO_3/AgHCO_3$	530.2

Two other types of peaks can be observed on an X-ray photoelectron spectra which could have larger binding energy shifts i.e. valence bands and Auger peaks [7], however these also can be observed using other techniques [7], which will be described in more detail later. It thus appears that XPS can not solely be used to identify the silver oxides produced using a plasma.

Another technique which has potential for identifying the oxides present is Differential Scanning Calorimetery (DSC) [4]. DSC is the most widely used thermal analysis technique in chemistry today [4]. The technique works by subjecting the sample of choice, and a reference sample, to a precisely programmed temperature change regime [4]. When a thermal transition occurs heat is either added to the sample or reference to maintain both the sample and reference sample at the same temperature [4]. The energy transferred to the sample or the reference balances the energy either given out or taken in by the sample during a transition phase [4]. Thus

the energy put into the reference or sample gives a direct energy measurement for the transition which has occurred [4]. Thus both exothermic and endothermic processes can be measured [4]. This heat flow to the sample or reference is given by the following equation [4]:

$$\Delta H = Q_R - Q_S$$

ΔH Change in enthalpy

Q_R Heat flow to or form reference

Q_S Heat flow to or from sample

DSC is able to analyse samples from temperatures of -170°C up to 750°C in either an inert or reactive atmosphere. Sample sizes for the process range from 0.1 to 100 mg [4].

As for using DSC for studying silver oxides, it may be useful but still could suffer from some drawbacks. This technique would be useful in studying a silver oxide system which contained only AgO and Ag_2O, due to the large differences in temperatures needed to reduce the oxides back to zero valent silver (AgO can be reduced to metallic silver at 100°C [12], while for Ag_2O it occurs at 230°C [12]). Some of the problems which may exist are:

(a) If a slight deviation in structure occurs from AgO and Ag_2O, then the peaks associated with these species, in a DSC spectra will become broad due to the slight differences in reduction temperatures of these slightly modified silver oxides being present. Thus any minor modifications to the structure of the oxides may be able to be shown has occurred by DSC but as to what deviations have occurred will not.

(b) DSC is only able to identify the oxides present if the reduction temperature is known. If not then other techniques would have to be used to try and aid with the elucidation of the samples composition. This could especially be a problem in plasma oxide formation as it is well known in the plasma literature that some chemical compounds produced within a plasma environment are unable to be produced under typical thermal conditions.

(c) The sample size needed for a DSC experiment would also be a problem if the plasma oxide has been produced upon a silver foil, due to the thinness of the layer produced (typically a few 100 micrometers). This would mean that to achieve a sample size of 0.1mg, probably about twenty or more plasma runs on the one sample would have to be carried out. This problem however could be solved if powder samples could be treated, however the facilities needed to produce these samples were not available undergoing this PhD study.

Extended X-ray Absorption Fine Structure (EXAFS) could also be used to elucidate the silver oxides present. EXAFS is widely used throughout science for studying the local structure of a large class of materials [9]. It can be used to study both amorphous and crystalline materials [9]. EXAFS explores the modulations in the X-ray absorption edge from approximately 40eV above the X-ray absorption edge to 1000eV or more [9]. Analysis of this edge yields quantitative information regarding the structure of the first few coordination spheres adjacent to the central absorbing atom [9]. EXAFS can thus be used to determine the coordination number, coordination distance, disorder and also the identity of the nearest neighbours [9]. EXAFS

sensitivity makes it an ideal technique for studying small differences in silver oxide structures [9].

A study has been carried out on the silver oxide systems using EXAFS and in particular they studied slightly different forms of i.e. chemically prepared AgO and electrochemically prepared AgO [13] The data for the two systems obtained from EXAFS is shown overleaf: EXAFS has shown qualitatively that the two types of AgO are the same, but are not quantitatively [13]. In AgO there are two types of Ag-O bond distances, one where the O is bonded to both the Ag^{+} and Ag^{3+} species, while the other is just involved in the square planar coordination of the Ag^{3+} [14]. The bond length for the O-Ag^{3+} bond is 2.179A, from neutron diffraction data, and that for the O coordinated to both Ag^{+} and Ag^{3+} using neutron diffraction, are located at distances of averages 2.034, while in the EXAFS spectra these peaks are located between 1.07-1.87 Å(radial distances) for the [13]. The other oxygen atoms which are located at distances of 2.645, 2.771 and 2.894 (see neutron diffraction data) are located between 1.87 and 2.57 Å in the EXAFS spectrum [13]. As for the silver -silver distances which according to neutron diffraction data are located at 3.252, 3.358,3.404 and 3.478, while for EXAFS these peaks are located between 2.57 and 3.50 Å [13].

As for data for Ag_2O using EXAFS no relevant literature could be found but it does not seem unreasonable that EXAFS could be used to distinguish between Ag_2O and AgO, even if it has to be combined with information from XRD or Neutron diffraction t distinguish between a whole host of silver oxides. As has been stated within previous studies the formation of Ag_4O_3 as a intermediate in the formation of AgO from Ag_2O has also been suggested using EXAFS [13]. The only possible drawback is whether a new oxide has been produced or whether the silver oxides

already known have just been distorted by the resulting bombardment of the sample by ions from the plasma.

As for neutron diffraction, the data obtained using this technique is shown below. Neutron diffraction seems quite capable of distinguishing between Ag_2O and AgO and possibly other oxides [13].

	AgO						Ag_2O		
	Ag^+			Ag^{3+}			Ag^+		
i	N	Z	R	N	Z	R	N	Z	R
1	2	O(1)	2.179	2	O(1)	2.013	2	O	2.044
2	2	O(2)	2.645	2	O(2)	2.054	12	Ag^+	3.338
3	2	O(1)	2.894	2	O(1)	2.771	/	/	/
4	4	Ag^+	3.252	4	Ag^{3+}	3.252	/	/	/
5	2	Ag^{3+}	3.358	2	Ag^+	3.358	/	/	/
6	4	Ag^{3+}	3.404	4	Ag^+	3.404	/	/	/
7	2	Ag^+	3.478	2	Ag^{3+}	3.478	/	/	/

Auger Spectroscopy is another technique that could be used to look at various silver oxides present. Auger spectroscopy works by bombarding the sample with high energy electrons in keV range [9]. It is a very surface sensitive technique and typically analyses electrons in the range 10-500 eV, as this provides the best surface structure information [9]. The typical surface sample depth from which the electrons will come

from are 4-10 Å [9]. These electrons cause the ejection of a photoelectron from a core level, which then leaves behind an ionised atom in an highly unfavourable energetic state [9]. To compensate for this an electron from a higher energy orbital will fall into the vacant hole which has been created, resulting in the release of energy - equivalent to the energy separation between the two orbitals involved in the transition [9]. This energy is taken up by an electron in the same core level, which is subsequently ejected [9]. It is this second ejected electron which is known as the Auger electron [9]. A typical example is if a K-shell electron is ejected, an electron from the L-shell will fall into the vacant hole in the K-shell, with the subsequent release in energy [9]. This energy is then taken up by an adjacent electron in the L-shell which is also ejected. This ejected L-shell electron is the Auger electron [9].

As for using Auger to study the silver/silver oxide systems, it again appears to suffer from the same problems as XPS in that the binding energy shifts are relatively small. The binding energy of the three species of interest are Ag metal (357.7eV or 352.2eV), Ag_2O (356.4eV or 351.0eV) and AgO (356.7eV or 352.2eV) (the Auger peak mostly studied is the MNN) [10,15]. It appears that Auger might be slightly better for use in differentiating between Ag_2O and silver metal or AgO but there appears to be some problem in distinguishing between AgO and Ag metal [10,15]. It also appears to suggest that using Auger to identify other silver oxides may not be all that easy due to these relatively small shifts in binding energies. However Auger would tell the investigator that another oxide is present, but not the actual identity of the oxide.

Even though using Auger Spectroscopy may not be of any great use in identifying typical oxides it may be useful in providing information on the depth profile proposed in Chapter 4. In this process ions are accelerated to energies of

approximately 0.5-50keV [7,9]. These ions are then focused to a sputtering spot diameter of 1-5mm [7,9]. The focused ion beam is then raster scanned over the samples surface (typical area of up to $10mm^2$ (the information depth i.e. resolution is typically 0.5-3.0nm)) [7,9]. The sample after being sputtered can then be analysed and this is where Auger has its advantages over XPS in that the area analysed is very small compared to the sputtered region [7,9]. This will thus guarantee that the signal obtained only originates from the sputtered region and not from the surrounding areas.

Another spectroscopy technique could be used is Ultraviolet Photoelectron Spectroscopy (UPS) [9]. This technique is similar to XPS in its fundamentals, except that the exciting source here is a ultraviolet lamp which is of lower energy (use He(I) resonance line = 21.2eV and He(II) resonance line = 40.8 eV) [9] than the x-rays used in XPS (1254eV) [7]. The use of a lower energy exciting source is intentional, as in this technique it is the valence band structure of the atoms which is being probed [9]. The typical energy of electrons ejected from the surface which UPS will monitor are in the range of 5-30 eV [7,9]. UPS can typically probe surfaces with 10^3 monolayers on a substrate [9].

For the silver/silver oxide system data has been found on UPS studies of silver, AgO and Ag_2O,, but no further data on other oxide systems was found. Ag metal has a BE of 4.8 eV (FWHM = 3.3 eV), AgO has a very similar BE of 4.7 eV (FWHM = 2.7 eV) and Ag_2O has a binding energy of 5.1 eV (FWHM = 2.3 eV) [10,11]. Again there appears to be little chance of distinguishing between AgO and Ag metal due to their binding energies being very similar. This suggests that for oxides of silver with a higher oxidation state than that of AgO, the separation distance in binding energy will be very small and will move even closer to the metals. As for oxides of

lower oxidation state than AgO these peaks would move towards the peak for Ag_2O which again could complicate the spectra.

Another problem with this technique and XPS for sorting BE of peaks which are located so close is that the broadness of the peaks is quite considerable for the identification of lines which range in binding energies from 4.7 eV to 5.1 eV and 367-369 eV [7,10,11].

Two other techniques which may be important in determining what silver oxides are present, but of which little data could be found, are Solid State Nuclear Magnetic Resonance and Secondary Ion Mass Spectrometery.

Solid State NMR which involves looking at the nuclear spin of the atoms present would be very useful for studying the silver/silver oxide systems within this thesis. Silver has two nuclei which are NMR active and these are Ag^{107} and Ag^{109} [16,17]. Both these nuclei have spins of 1/2 which satisfies the selection rule for NMR. However both nuclei differ in terms of abundance, magnetic moment strength and receptivity with respect to carbon and hydrogen. Ag^{107} is approximately 51.82% abundant with a magnetic moment of -0.1966 and a receptivity compared with that of the proton of 3.48×10^{-5} and a receptivity compared with that of carbon of 0.197 [16,17]. As for Ag^{109} which has a natural abundance of 48.18%, with a magnetic moment of -0.2260 and a receptivity to a proton and carbon of 4.92×10^{-5} and 0.279 respectively [16,17]. If the receptivity values are looked at it can be seen that for to obtain the spectra for silver oxides, looking at these nuclei will take some time to accumulate the data compared with a material which contains protons or carbon. This technique would probably give concrete evidence as to what oxides are actually present, but likely problems with it will be cost in running a sample and again

obtaining enough sample to be able to run a solid state spectra. Some studies have been undertaken in looking at the silver catalyst which has been used for the epoxidation of ethylene [18]. However in this study the nuclei studied was C^{13}. The oxygen nuclei could also be looked at if the plasma reaction was carried out using O^{17}, but again this would be a relatively expensive method.

As for Secondary Ion Mass Spectrometery which involves smashing ions into a sample and analysing the ionic fragments emitted from the surface [9]. SIMS has a detection limit of 10^{-5} monolayers and thus this technique is very surface sensitive [9]. In SIMS the incident ions are able to penetrate a certain distance into the sub-surface of the substrate. In doing this the primary ion must dissipate its energy to the atoms in the surrounding area, a small amount of this energy is imparted to the surface atoms, with a momentum direction pointing outwards from it [9]. This results in the emission of secondary particles which may be atoms or molecules and may be in the charged or uncharged state [9]. The ions typically used are inert gaseous ions such as Ne^+, Ar^+ with energies of approximately 3keV [9]. The beam current of the incident ions is typically 10^{-11} to 10^{-8} Å and thus the technique is very surface sensitive [9]. Also the depth at which the surface can be eroded can be controlled considerably to typically $1Åh^{-1}$ [9]. This technique is a good qualitative tool but is not that good quantitatively. Also the techniques sensitivity is dependent on the sputtering yield of the sample, which is dependent on the samples composition [9].

SIMS could be useful in studying the silver/silver oxide system in question, however the data obtained from this technique would probably have to be combined with data from other techniques listed previously. The ultimate problem with SIMS would be that some clusters generated by the technique may actually be made form a

combination of smaller clusters or species i.e. dimers. SIMS would be able to identify molecular ion peaks for the oxides AgO and Ag_2O and probably for oxides of formulas typically Ag_2O_3, Ag_4O and other intermediate oxides. SIMS does have its advantages in that if in-situ SIMS could be carried out on the plasma oxidation treatment of the silver then a study of the oxides produced with extent of oxidation i.e. reaction time, may be of invaluable use (that is the oxide present as the oxidation of the profile may be able to be determined. This could also verify the XRD data already obtained. SIMS would also be useful in proving whether the depth profile postulated in chapter 4 is indeed correct.

Thus concluding, it appears that no individual technique is able to be used to identify the all the different oxides that may be present during plasma oxidation of a silver foil. This means that a range of techniques would be the best choice for trying to identify the silver oxides present as in this way the advantages of one technique may counteract the disadvantages of another. Thus using a range of techniques would be able to confirm whether as predicted from this thesis that the major oxides present are AgO and Ag_2O, or whether some other oxides are also present. However it must be stressed that care should be taken in saying yes a new oxide is indeed formed, or whether what has actually been observed is just AgO or Ag_2O with lattice defects present, due to the effects of the plasma.

This appendix has been included within this thesis as a potential way to try and elucidate what silver oxides are actually present in a more in-depth study. An initial study has been carried out using XRD, but due to the lack of time and also the aim of this thesis being to produce high surface area silver, only an quick look and see

at what oxides were present was carried out. For a more in-depth study as to which oxides are needed at least a further 2 years study would be needed.

REFERENCES

1. Ebsworth, E.A.V.; Ranklin, D.W.H.; Cradock, S.; **Structural Methods in Inorganic Chemistry**, 2nd Edition; Blackwell Scientific Pub., Oxford 1991.
2. Colthup, N.B.; Daly, L.H.; Wiberley, S.E.; **Introduction to Infrared and Raman Spectroscopy;** Academic Press: New York, 1964.
3. **Netscape site:** http://staff.vscht.cz/-matejkap/SERS.html#Experiment
4. Atkins, P.W.; **Physical Chemistry, 4th Edition;** Oxford University Press: Oxford, 1990.
5. Pettenkofer,C.; Pockrand, I.; Otto, A.; **Surf. Sci. 1983,** 135, 52-64.
6. Pettinger, B.; Bao, X.; Wilcock, I.; Muhler, M.; Schlogl, R.; Gerhard Ertl; **Angew. Chem. Int. Ed. Engl. 1994**, 33(1), 85.
7. Briggs, D.; Seah, M.P.; Auger and X-ray Photoelectron Spectroscopy Volume 1; John Wiley & Sons: New York, 1990.
8. O'Connor, D.J.; Sexton, B.A.; Smart, R.St.C.; **Surface Analysis Methods in Materials Science;** Springer Verlag: 1992.
9. Thomas, J.M.; Thomas, W.J.; **Principles and Practice of Heterogeneous Catalysis;** VCH: Weinheim,1996.
10. Weaver, J.F.; Hoflund, G.B.; **J. Phys. Chem. 1994,** 98(34), 8519.
11. Weaver, J.F.; Hoflund, G.B.; **Chem. Mater. 1994,** 6, 1693.
12. Lide, D.R.; **Handbook of Chemistry & Physics, 71st Edition;** CRC Press: USA, 1990-91.
13. Mansour, A.N.; **J. Phys. Chem. 1990,** 94, 1006.
14. McMillan, J.A.; **Chem, Rev. 1962,** 62, 65.

15. Kaushik, V.K.; **J. Elec. Spec. & Rel. Phen.,** 1991, 56, 273.

16. Harris, R.K.; **Nuclear Magnetic Resonance;** John Wiley & Sons: New York, 1986.

17. Popov, A.I.; Hallenga, K.; **Modern NMR Techniques & Their Applications in Chemistry;** Marcel Dekker Inc.: New York, 1990.

18. Fernandes, E.F.; Benesi, A.J.; Vannice, M.A.; **J. Phys. Chem., 1994,** Vol. 98, 8498.

APPENDIX II

03-0921 Wavelength= 1.54056

Ag

Silver

d Å	Int	h	k	l
2.36000	100	1	1	1
2.03000	80	2	0	0
1.44000	80	2	2	0
1.23000	80	3	1	1
1.18000	60	2	2	2
.936000	80	3	3	1
.913000	80	4	2	0

Rad.: CuKa1 λ: 1.5405 Filter: d-sp:

Cut off: Int.: I/Icor.:

Ref: Jung. Z. Kristallogr., Kristallgeom., Kristallphys., Kristallchem., 64. 422 (1926)

Sys.: Cubic S.G.: Fm3m (225)

a: 4.074	b:	c:	A:	C:
α:	β:	γ:	Z: 4	mp: 960.5

Ref: Ibid.

Dx: 10.596 Dm: 10.500 SS/FOM: F_7=5(.202, 7)

Color: White

Specimen cut from a sheet of silver metal. Boiling point 2152°. PSC: cF4. Deleted by NBS card. Mwt: 107.87. Volume[CD]: 67.62.

Ag2O

Silver Oxide

Rad.: CuKa1 λ: 1.5405 Filter: Mono. d-sp: Calculated

Cut off: 15.0 Int.: Calculated I/Icor.: 14.69

Ref: Grier. D., McCarthy. G., North Dakota State University. Fargo. North Dakota. USA. ICDD Grant-in-Aid. (1991)

Sys.: Cubic S.G.: Pn3m (224)

a: 4.726 b: c: A: C:

α: β: γ: Z: 2 mp:

Ref: Ibid.

Dx: 7.291 Dm: SS/FOM: F_{14}=399(.0018, 20)

Peak height intensity. Calculation of diffractometer peak intensities done with MICRO-POWD v. 2.2 (D. Smith and K. Smith) using default instrument broadening function (NBS Table). diffracted beam monochromator polarization correction. and atomic scattering factors corrected for anomalous dispersion. Cell parameters from 12-793. Atomic positions from Wyckoff: Ag in 4b. O in 2a. Isotropic thermal parameters estimated as B=1.0 for each atom. Intensity threshold for <1=0.1%. Ag2 O type. PSC: cP6. Mwt: 231.74. Volume[CD]: 105.56.

d Å	Int	h	k	l
3.34200	2	1	1	0
2.72900	100	1	1	1
2.36300	40	2	0	0
1.92940	<1	2	1	1
1.67090	30	2	2	0
1.49450	<1	3	1	0
1.42490	28	3	1	1
1.36430	7	2	2	2
1.26310	<1	3	2	1
1.18150	4	4	0	0
1.08420	10	3	3	1
1.05680	8	4	2	0
.964700	8	4	2	2
.909500	8	5	1	1

22-0472 Wavelength= 1.54056 C

Ag2O2

Silver Oxide

Rad.: λ: Filter: d-sp: Calculated

Cut off: Int.: Calculated I/Icor.:

Ref: Vogt, General Electric Co., Schenectady, New York, USA. Private Communication

Sys.: Monoclinic S.G.: $P2_1/c$ (14)

a: 5.852 b: 3.478 c: 5.495 A: 1.6826 C: 1.5799

α: β: 107.5 γ: Z: 2 mp:

Ref: Ibid.

Dx: 7.713 Dm: SS/FOM: F_{30}=18(.0169,100)

Peak height intensity. Ag O type. PSC: mP8. Mwt: 247.73. Volume[CD]: 106.66.

d Å	Int	h	k	l	d Å	Int	h	k	l
2.95200	2	1	1	0	1.10100	3	$\bar{5}$	1	2
2.79100	47	2	0	0	1.09600	3	1	3	1
2.76700	100	$\bar{1}$	1	1	1.08800	3	4	2	0
2.62100	38	0	0	2	1.06800	3	$\bar{2}$	2	4
2.41300	89	1	1	1	1.06360	3	3	1	3
2.28300	38	$\bar{2}$	0	2	1.05140	3	$\bar{5}$	1	3
1.73900	11	0	2	0	1.04660	3	0	2	4
1.69900	23	$\bar{3}$	1	1	1.04100	2	$\bar{1}$	1	5
1.67600	12	2	0	2	1.01370	2	$\bar{3}$	1	5
1.62100	19	$\bar{1}$	1	3	.996200	2	$\bar{3}$	3	1
1.47600	12	2	2	0	.988100	2	$\bar{5}$	1	1
1.45900	10	3	1	1	.979600	2	$\bar{1}$	3	3
1.44900	11	0	2	2	.973700	1	$\bar{6}$	0	2
1.42200	5	$\bar{4}$	0	2					
1.40900	9	1	1	3					
1.39400	9	$\bar{3}$	1	3					
1.38300	8	$\bar{2}$	2	2					
1.35300	4	$\bar{2}$	0	4					
1.31000	4	0	0	4					
1.20700	5	2	2	2					
1.14200	2	$\bar{4}$	0	4					
1.12400	4	$\bar{1}$	3	1					
1.10500	3	$\bar{5}$	1	1					

40-0909 Wavelength= 1.54056

Ag2O3

Silver Oxide

Rad.: CuKa1 λ: 1.5405 Filter: d-sp: Guinier

Cut off: Int.: I/Icor.:

Ref: Standke, B., Jansen, M., Z. Anorg. Allg. Chem., 535, 39 (1986)

Sys.: Orthorhombic S.G.: Fdd2 (43)

a: 12.869(1) b: 10.490(1) c: 3.6638(5) A: 1.2268 C: 0.3493

α: β: γ: Z: 8 mp:

Ref: Ibid.

Dx: 7.084 Dm: SS/FOM: F_{26}=47(.0146, 38)

Prepared by anodic oxidation of aqueous solution of either Ag B F4, Ag Cl O4 or Ag P F6 with Ag content between 0.1 and 0.4 molecules. C.D. Cell: a=10.490, b=12.869, c=3.664, a/b=0.8151, c/b=0.2847, S.G.=Fdd2(43). Quartz used as an internal stand. PSC: oF40. Mwt: 263.73. Volume[CD]: 494.60.

d Å	Int	h	k	l	d Å	Int	h	k	l
4.06806	5	2	2	0	1.32093	10	9	1	1
3.34197	100	1	1	1	1.31098	5	0	8	0
3.21889	10	4	0	0	1.29393	5	7	5	1
2.74147	90	4	2	0					
2.69410	30	3	1	1					
2.62333	30	0	4	0					
2.48158	60	1	3	1					
2.17833	50	3	3	1					
2.06530	30	5	1	1					
2.03268	10	4	4	0					
1.98580	5	6	2	0					
1.80421	20	5	3	1					
1.80421	20	1	5	1					
1.76115	20	2	0	2					
1.67572	25	3	5	1					
1.67020	20	2	2	2					
1.62340	15	7	1	1					
1.60857	10	8	0	0					
1.53666	30	8	2	0					
1.53666	30	4	6	0					
1.48621	25	7	3	1					
1.48621	25	5	5	1					
1.46263	30	2	4	2					
1.37921	10	1	7	1					
1.37123	5	8	4	0					
1.34633	30	6	2	2					

40-1054 Wavelength= 1.54056

Ag3O4

Silver Oxide

Rad.: CuKa1 λ: 1.5406 Filter: d-sp: Guinier

Cut off: Int.: I/Icor.:

Ref: Standke, B., Jansen, M., J. Solid State Chem., 67, 278 (1987)

Sys.: Monoclinic S.G.: $P2_1/c$ (14)

a: 3.5787(3) b: 9.2079(5) c: 5.6771(3) A: 0.3887 C: 0.6165

α: β: 106.135(5) γ: Z: 2 mp:

Ref: Ibid.

Dx: 7.163 Dm: SS/FOM: F_{30}=78(.0096, 40)

Prepared by anodic oxidation of aqueous solution of AgF and Ag Ce O4. Decomposes at 63 C into AgO and O2. C.D. Cell: a=5.677, b=9.208, c=3.579, β=106.14, a/b=0.6165, c/b=0.3887, S.G.=P21/a(14). Quartz used as an internal stand. PSC: mP14. Mwt: 387.60. Volume[CD]: 179.70.

d Å	Int	h	k	l	d Å	Int	h	k	l
4.68860	2	0	1	1	1.75530	20	2	1	$\bar{1}$
4.60080	10	0	2	0	1.75260	10	1	2	2
3.51800	10	0	2	1	1.74480	10	0	5	1
3.43660	5	1	0	0	1.72364	1	1	4	$\bar{1}$
3.21850	60	1	1	0	1.70151	10	1	2	$\bar{3}$
3.15570	25	1	1	$\bar{1}$	1.69062	10	0	2	3
2.75430	10	1	2	0	1.67973	4	2	0	$\bar{2}$
2.72750	40	0	0	2	1.62321	15	1	5	0
2.71540	40	1	2	$\bar{1}$	1.61406	4	1	5	$\bar{1}$
2.67550	100	0	3	1	1.61261	2	1	3	2
2.61450	5	0	1	2	1.61003	5	2	2	0
2.50390	60	1	1	1	1.57839	5	2	2	$\bar{2}$
2.50390	60	1	0	$\bar{2}$	1.57239	20	1	3	$\bar{3}$
2.41530	30	1	1	$\bar{2}$	1.56378	20	0	3	3
2.34690	5	0	2	2	1.53498	10	0	6	0
2.30410	5	0	4	0	1.52595	5	0	5	2
2.29000	10	1	3	0	1.50300	15	1	5	1
2.26450	50	1	3	$\bar{1}$	1.50300	15	2	1	1
2.26450	50	1	2	1	1.48301	10	1	5	$\bar{2}$
2.19790	20	1	2	$\bar{2}$	1.46329	15	1	4	2
2.12010	5	0	4	1	1.45104	10	2	1	$\bar{3}$
2.03850	2	0	3	2	1.44561	5	2	2	1
1.93900	5	1	3	$\bar{2}$	1.43156	10	1	1	3
1.91280	10	1	4	0	1.40889	10	1	0	$\bar{4}$
1.89900	5	1	4	$\bar{1}$	1.39625	10	1	6	$\bar{1}$
1.85630	5	1	1	2	1.37730	20	2	4	0

d Å	Int	h	k	l
1.36349	5	0	0	4
1.35702	15	2	4	$\bar{2}$
1.33744	10	0	6	2
1.32189	5	1	6	1
1.32189	5	1	5	2
1.30814	5	1	6	$\bar{2}$
1.30814	5	0	2	4
1.29820	2	1	5	$\bar{3}$
1.29359	2	0	5	3
1.28740	5	2	1	2
1.20678	2	2	2	$\bar{4}$

43-1038 Wavelength= 1.54056

AgO

Silver Oxide

Rad: CuKa1 λ: 1.5405 Filter: Mono d-sp: Calculated

Cut off: 15.0 Int.: Calculated I/Icor: 8.00

Ref: Grier, D., McCarthy, G., North Dakota State University, Fargo, North Dakota, USA, ICDD Grant-in-Aid, (1991)

Sys: Monoclinic S.G: $P2_1/c$ (14)

a: 5.8592 b: 3.4842 c: 5.4995 A: 1.6816 C: 1.5784

α: β: 107.506 γ: Z: 4 mp:

Ref: Ibid.

Dx: 7.684 Dm: SS/FOM: F_{30}=216(.0038, 37)

Peak height intensity. Calculation of diffractometer peak intensities done with MICRO-POWD v. 2.2 (D. Smith and K. Smith) using default instrument broadening function (NBS Table), diffracted beam monochromator polarization correction, and atomic scattering factors corrected for anomalous dispersion. Cell parameters from Jansen, M., Fischer, F., J. Less-Common Met., 137 123-131 (1988). Atomic positions from same source: Ag(1) in 2c, Ag(2) in 2a, O in 4e with x=0.2959, y=0.3452, z=0.2221. Anisotropic thermal parameters also from Jansen: Ag(1): U(1,1)=0.0096, U(2,2)=0.0076, U(3,3)=0.0099, U(1,2)=0.0001, U(1,3)=0.0043, U(2,3)=-0.0003; Ag(2): U(1,1)=0.0127, U(2,2)=0.0204, U(3,3)=0.0209, U(1,2)=-0.0055, U(1,3)=0.0039, U(2,3)=-0.0003; O: U(1,1)=0.0133, U(2,2)=0.0124, U(3,3)=0.0124, U(1,2)=0.0002, U(1,3)=0.0044, U(2,3)=0.0011. Intensity threshold for <1=0.1%. Ag O type. PSC: mP8. Mwt: 123.87. Volume[CD]: 107.07.

d Å	Int	h	k	l	d Å	Int	h	k	l
5.58800	1	1	0	0	1.37160	<1	$\bar{1}$	0	4
2.95700	2	1	1	0	1.36720	<1	2	2	1
2.90200	<1	0	1	1	1.35390	4	$\bar{2}$	0	4
2.79400	50	2	0	0	1.34960	2	$\bar{4}$	1	1
2.77100	100	$\bar{1}$	1	1	1.31760	<1	$\bar{4}$	1	2
2.70800	1	$\bar{1}$	0	2	1.31120	4	0	0	4
2.62200	35	0	0	2	1.27230	<1	3	2	0
2.41600	86	1	1	1	1.26200	<1	$\bar{3}$	1	4
2.28600	36	$\bar{2}$	0	2	1.23400	<1	0	2	3
2.20400	<1	$\bar{2}$	1	1	1.20810	5	2	2	2
2.18000	<1	2	1	0	1.18210	<1	3	2	1
2.13800	1	1	0	2	1.14700	<1	$\bar{3}$	2	3
2.13800	1	$\bar{1}$	1	2	1.14290	2	$\bar{4}$	0	4
2.09500	<1	0	1	2	1.12560	5	$\bar{1}$	3	1
1.91120	<1	$\bar{2}$	1	2	1.10650	4	$\bar{5}$	1	1
1.86310	<1	2	1	1	1.10250	5	4	0	2
1.86310	<1	3	0	0	1.10250	5	$\bar{4}$	2	2
1.82310	<1	1	1	2	1.09750	3	1	3	1
1.79460	<1	$\bar{3}$	0	2	1.08980	4	4	2	0
1.74210	10	0	2	0	1.08590	2	$\bar{4}$	1	4
1.70160	23	$\bar{3}$	1	1	1.07530	<1	$\bar{2}$	3	1
1.67690	12	2	0	2	1.06930	4	2	0	4
1.65330	<1	0	2	1	1.06930	4	$\bar{2}$	2	4
1.64260	<1	3	1	0	1.06450	4	3	1	3
1.62790	<1	$\bar{1}$	2	1	1.05270	3	$\bar{5}$	1	3
1.62220	19	$\bar{1}$	1	3	1.04950	2	2	2	3
1.55320	<1	$\bar{2}$	1	3	1.04760	3	0	2	4
1.48590	<1	$\bar{2}$	2	1	1.04220	3	$\bar{1}$	1	5
1.47830	13	2	2	0	1.02430	<1	$\bar{3}$	2	4
1.46510	<1	$\bar{1}$	2	2	1.01450	3	$\bar{3}$	1	5
1.46090	11	3	1	1	1.01450	3	5	0	4
1.45110	12	0	2	2	1.00440	<1	0	1	5
1.42330	5	$\bar{4}$	0	2	.997800	2	$\bar{3}$	3	1
1.40980	9	1	1	3	.989200	3	5	1	1
1.39650	13	4	0	0	.987600	2	1	2	4
1.39650	13	$\bar{3}$	1	3	.981100	2	$\bar{1}$	3	3
1.38550	9	$\bar{2}$	2	2	.975000	1	$\bar{6}$	0	2

d Å	Int	h	k	l
.969500	<1	$\bar{5}$	2	1
.967400	<1	0	3	3
.956500	<1	$\bar{4}$	1	5
.955800	2	$\bar{4}$	2	4
.942400	3	1	1	5
.941700	3	3	3	1
.931900	3	4	2	2
.931300	2	6	0	0
.927600	3	1	3	3
.925300	2	$\bar{1}$	2	5
.925300	2	4	1	3
.923700	2	$\bar{3}$	3	3
.916500	1	$\bar{2}$	0	6
.915500	<1	$\bar{6}$	1	3
.911500	2	$\bar{2}$	2	4
.902600	<1	$\bar{3}$	0	6
.897300	1	$\bar{6}$	0	4

12-0766 Wavelength= 1.54056

Ag2C03

Silver Carbonate

Rad.: CuKa1 λ: 1.5405 Filter: Ni Beta.M d-sp:

Cut off: Int.: Diffract. I/Icor.:

Ref: Natl. Bur. Stand. (U.S.) Monogr. 25. 1. 44 (1962)

Sys.: Monoclinic S.G.: $P2_1$ (4)

a: 4.863 b: 9.555 c: 3.235 A: 0.5089 C: 0.3386

α: β: 92.64 γ: Z: 2 mp:

Ref: Ibid.

Dx: 6.099 Dm: SS/FOM: F_{30}=6(.130. 42)

Color: Greenish yellow
Pattern at 25 C. Sample was prepared at NBS from solutions of silver nitrate and potassium carbonate. Spectroscopic analysis showed 0.001-0.101% Al and Si; and 0.0001- 0.001% Ca, Cu, Fe and Mg. PSC: mP12. Deleted by 26-339. Plus 10 lines to 1.3023. Mwt: 275.75. Volume[CD]: 150.16.

d Å	Int	h	k	l	d Å	Int	h	k	l
4.85000	16	1	0	0	1.63900	10	0	5	1
4.78000	35	0	2	0	1.62600	6	2	3	1
4.32000	30	1	1	0	1.61600	2	0	0	2
3.41000	2	$\bar{1}$	2	0	1.59100	10	0	1	2
3.25000	4	0	0	1	1.58700	4	0	6	0
3.08000	8	0	1	1	1.53800	2	$\bar{1}$	1	2
2.74000	60	$\bar{1}$	0	1	1.53000	4	0	2	2
2.66000	100	1	3	0	1.52600	4	$\bar{2}$	4	1
2.56000	6	1	1	1	1.51100	2	1	0	2
2.42000	20	2	0	0	1.50700	4	$\bar{2}$	5	0
2.39000	12	0	4	0	1.46800	<1	$\bar{3}$	0	1
2.38000	14	$\bar{1}$	2	1	1.45000	2	3	3	0
2.35000	8	2	1	0	1.44100	2	0	3	2
2.32000	14	1	2	1					
2.27000	40	0	3	1					
2.16000	12	2	2	0					
2.04000	10	1	3	1					
1.97600	2	$\bar{2}$	0	1					
1.93400	6	$\bar{2}$	1	1					
1.92900	10	$\bar{2}$	3	0					
1.91200	4	0	4	1					
1.87500	6	2	1	1					
1.80100	4	$\bar{1}$	4	1					
1.77700	14	$\bar{1}$	5	0					
1.70000	4	$\bar{2}$	4	0					
1.67800	10	$\bar{2}$	3	1					

APPENDIX III

COLLOQUIA, SEMINARS, PRESENTATIONS AND LECTURE COURSES.

UNIVERSITY OF DURHAM

BOARD OF STUDIES IN CHEMISTRY

COLLOQUIA AND SEMINARS FROM INVITED SPEAKERS

1993

October 4	Prof. F.J. Feher, University of California at Irvine Bridging the Gap between Surfaces and Solution with Sessilquioxanes
October 20	Dr. P. Quayle, University of Manchester Aspects of Aqueous ROMP Chemistry
October 23	Prof. R. A dams, University of S. Carolina The Chemistry of Metal Carbonyl Cluster Complexes Containing Platinum and Iron, Ruthenium and Osmium and the Development of a Cluster Based Alkyne Hydrogenating Catalyst
November 10	Prof. M.N.R. Ashfold, University of Bristol

	High Resolution Photofragment Translational Spectroscopy: A New Way to Watch Photodissociation
November 17	Dr. A. Parker, Rutherford Appleton Laboratory Applications of Time Resolved Resonance Raman Spectroscopy to Chemical and Biochemical Problems

1994

January 26	Prof. J. Evans, University of Southampton Shining Light on Catalysis
February 23	Prof. P.M. Maitlis, University of Sheffield Why Rhodium in Homogenous Catalysis
March 9	Prof. F. Wilkinson, Loughborough University Nanosecond and Picosecond Laser Flash Photolysis
October 19	Prof. N. Bartlet, University of California Some Aspects of Ag(II) and Ag(III) Chemistry
October 26	Dr. G. Rumble, Imperial College Real or Imaginary 3rd Order Non-Linear Optical Materials
December 7	Prof. D. Briggs, ICI and University of Durham Surface Mass Spectrometry

1995

March 1	Dr. M. Rosseinsky, Oxford University
	Fullerene Intercalation Chemistry
April 26	Dr. M. Schroder, University of Edinburgh
	Redox Active Macrocyclic Complexes
May 3	Prof. E. W. Randall, Queen Mary & Westfield College
	New Perspectives in NMR Imaging
October 4	Prof. D. Tuck, University of Windsor, Ontario
	Electron Transfer Processes in Main Group Chemistry
October 11	Prof. P. Lugar, University of Berlin
	Low Temperature Crystallography
November 17	Prof. D. Bergbreiter, Texas A&M
	Design of Smart Catalysts, Substrates and Surfaces
November 22	Prof. I. Soutar, Lancaster University
	A Water of Glass? Luminescence Studies of Water Soluble
	Polymers
December 8	Prof. M. Reetz, Mullheim
	Size Selective Synthesis of Metal Clusters

1996

January 10	Dr. B. Henderson, Waikato University
	Electrospray Mass Spectrometry - A New Technique
January 17	Prof. J. W. Emsley, Southampton University
	Liquid Crystals: More than Meets the Eye

January 31	Dr. G. Penfold
	Soft Soap and Surfaces
February 14	Prof. R. Nolte
	Design Strategies for Supramolecular Architectures
March 6	Dr. R. Whitby, University of Southampton
	New Approaches to Chiral Catalysts
March 12	Prof. V. Balzani, University of Bologna
	Supramolecular Photochemistry

EXAMINED LECTURE COURSES

Oct. - Dec. 1993	Organometallics (Prof. V. Gibson)
Oct. 1993 - Jan. 1994	General Laboratory Techniques (Dr. D. P. Hampshire)
	Electron Microscopy (Dr. K. Durose)
	Spectroscopy (Dr. D. P. Halliday)